# Natural and Mixed Convection in a Horizontal Cylindrical Annulus with and without Fins on Inner Cylinder

by

# Latifa Begum

Thesis submitted to the McGill University in Partial fulfillment of the requirements for the degree of **Master of Engineering** 

Department of Mining and Materials Engineering 3610 University Street, M. H. Wong Building McGill University Montréal, Canada. H3A 2B2

> © Latifa Begum, Montréal, Canada August 2007.



Library and Archives Canada

Published Heritage Branch

395 Wellington Street Ottawa ON K1A 0N4 Canada Bibliothèque et Archives Canada

Direction du Patrimoine de l'édition

395, rue Wellington Ottawa ON K1A 0N4 Canada

> Your file Votre référence ISBN: 978-0-494-51446-7 Our file Notre référence ISBN: 978-0-494-51446-7

#### NOTICE:

The author has granted a non-exclusive license allowing Library and Archives Canada to reproduce, publish, archive, preserve, conserve, communicate to the public by telecommunication or on the Internet, loan, distribute and sell theses worldwide, for commercial or non-commercial purposes, in microform, paper, electronic and/or any other formats.

The author retains copyright ownership and moral rights in this thesis. Neither the thesis nor substantial extracts from it may be printed or otherwise reproduced without the author's permission.

## AVIS:

L'auteur a accordé une licence non exclusive permettant à la Bibliothèque et Archives Canada de reproduire, publier, archiver, sauvegarder, conserver, transmettre au public par télécommunication ou par l'Internet, prêter, distribuer et vendre des thèses partout dans le monde, à des fins commerciales ou autres, sur support microforme, papier, électronique et/ou autres formats.

L'auteur conserve la propriété du droit d'auteur et des droits moraux qui protège cette thèse. Ni la thèse ni des extraits substantiels de celle-ci ne doivent être imprimés ou autrement reproduits sans son autorisation.

In compliance with the Canadian Privacy Act some supporting forms may have been removed from this thesis.

While these forms may be included in the document page count, their removal does not represent any loss of content from the thesis.

Conformément à la loi canadienne sur la protection de la vie privée, quelques formulaires secondaires ont été enlevés de cette thèse.

Bien que ces formulaires aient inclus dans la pagination, il n'y aura aucun contenu manquant.



## **ABSTRACT**

Determination of the heat transfer coefficients for natural and mixed convection in horizontal annuli is important for designing double pipe heat exchangers and for energy storage systems. In part one and two of this study, the 2D numerical solution of the laminar natural convection of water in six internally finned horizontal annuli has been obtained. The fins are attached to the external surface of the inner cylinder. Only the symmetrical half of the horizontal annulus with three equally spaced longitudinal divergent solid and porous fins are considered. The parameters of the problem are Rayleigh number, fin height, permeability and porosity of the porous fin, etc. The above parameters are suitably varied to ascertain their effects on fluid flow and heat transfer. The results show that traditional solid fins provide much higher heat transfer rates compared to the porous fins. Part three of this work deals with mixed convective heat transfer (laminar natural and forced convections) of water in a vented annulus. The forced flow conditions are imposed by providing an inlet at the top and an outlet at the bottom. For various parameters of the problem, the average and local Nusselt numbers along the inner cylinder are calculated for water for both aiding and opposing flows. The fourth part of this study deals with numerical modeling of natural convection of nanofluids in a horizontal cylindrical annulus. Simulations are carried out for Cu-water nanofluids. The results, in general, show that nanoparticles systematically decrease the natural convective heat transfer coefficient on the inner cylinder. Practical and useful correlations are provided for calculating average heat transfer rates from the inner cylinder in the form of average equivalent thermal conductivity and average Nusselt number for all of the four cases discussed above. These correlations are new and will be helpful in designing heat exchangers.

## Résumé

Déterminer les coefficients du transfert de chaleur de la convection naturelle et mixte dans les cylindres annulaires horizontaux est important lorsqu'on fait la conception d'échangeurs de chaleur à canalisation double et aussi pour les dispositifs de stockage d'énergie. Dans la partie une et deux de cette étude, la solution numérique en 2D de la convection naturelle laminaire de l'eau dans la partie intérieure d'un cylindre annulaire horizontal a été obtenue. Les ailettes sont fixées à la surface externe du cylindre intérieur. Seulement la moitié symétrique du cylindre annulaire horizontal avec trois ailettes longitudinales divergentes solides et poreuses espacées de manière égale a été considérée. Les paramètres du problème sont le nombre de Rayleigh, la taille de l'ailette, la perméabilité et la porosité de l'ailette, etc. Les paramètres ci-dessus sont modifiés de manière appropriée pour vérifier leurs effets sur la coulée et le transfert de chaleur. Les résultats montrent que les ailettes solides traditionnelles amènent un taux de transfert de chaleur plus élevé comparativement aux ailettes poreuses. La troisième partie de ce travail porte sur les transferts de chaleur mixtes (naturel laminaire et par convection forcée) de l'eau dans un espace annulaire ventilé. Les conditions d'écoulement forcé sont imposées en fournissant une admission par au dessus et une évacuation par en bas. Pour les paramètres divers du problème, les nombres de Nusselt moyens et locaux le long du cylindre intérieur sont calculés pour l'eau des écoulements, aidants et opposés, à la fois. La quatrième partie de cette étude porte sur la modélisation numérique de la convection naturelle des nanofluides dans un cylindre annulaire horizontal. Les simulations sont exécutées pour les nanofluides Cu-water. Les résultats, en général, démontrent que les nanoparticules réduisent systématiquement le coefficient de transfert de chaleur de la convection naturelle dans le cylindre intérieur. Des corrélations pratiques et utiles sont fournies pour le calcul de la moyenne des taux de transfert de chaleur du cylindre intérieur sous la forme de la moyenne équivalente de conductivité thermique et de la moyenne du nombre de Nusselt pour les quatre escemples traités ci-dessus. Ces corrélations sont nouvelles et seront utiles dans la conception d'échangeurs de chaleur.

## **ACKNOWLEDGEMENTS**

I would like to express my deep appreciation to my thesis supervisor, Professors M. Hasan for his guidance and constant encouragement during the course of this work. His valuable suggestions which arose from discussions throughout the course of this research and time spent in reviewing the manuscript are well acknowledged.

This work could not have been completed without the understanding, cooperation and patience of my only daughter, Tasnim Tabassum. Her sacrifices were great and my gratitude is profound. My mother provided me with love, admiration and continuous mental support during my study period. Without her continuous inspiration it would have been almost impossible for me to pursue an M.Eng degree at McGill University. My father gave me courage and strength to follow my dream.

# **Contents**

Abstract	ii	į
Résumé	ii	i
Acknowledge	mentsiv	,
Table of conte	entsv-v	⁄ii
List of Figures	sviii-x	ii
List of Tables	xii	i
Nomenclature	xiv-x	vi
Introductory N	Notexvi	i
Chapter '	<b>1</b> Convection in Horizontal Cylindrical Annulus with Equally Space	ced
Longitudir	nal Solid Fins	1
1.1 A	bstract	2
1.2 In	ntroduction	2
1.3 D	escription of the problem	5
1.4 M	Iathematical Formulation	6
1.4	4.1 Boundary conditions and assumptions	8
1.5 G	overning Parameters	9
1.6 N	umerical Solution	10
1.	6.1 Convergence criteria	12
1.	6.2 Under-relaxation factor	12
1	.6.3 Code validation	13
1.	6.4 Grid dependency and Computer time	16
1.7 R	esults and Discussion	18
1.7	7.1 Definitions	19
1.7	Velocity and temperature fields	20
	I. Effects of fin heights	20
	II. Effects of Rayleigh number	29
	III. Distribution of the local equivalent thermal conductivity	29
	IV Average equivalent thermal conductivity	34

1.8	Conclusions
1.9	References37
Chapte	er 2
, <b>-</b>	
Natural	Convection in Horizontal Cylindrical Annulus with Equally Spaced
Longitu	dinal Porous Fins 40
2.1	Abstract
2.2	Introduction41
2.3 ]	Mathematical Formulation
2.4	Boundary conditions and Assumptions
2.5	Solution and validation47
2.6 1	Results and Discussions
2.0	Effects of permeability of porous media (Da=10 <sup>-6</sup> to 10 <sup>-2</sup> )
2.0	6.2 Effect of porous fin height (H/L=0.2, 0.4, and 0.6)
2.0	Effects of Rayleigh number ( $Ra=10^3$ , $10^4$ , $10^5$ , and $10^6$ )
2.0	6.4 Comparative study between solid fins and porous fins for the same
	geometric and flow conditions
2.0	Effect of porosity of porous fin
2.7	Concluding remarks
2.8 1	References
Chapte	er 3
C-1-1-1	
	ar Mixed Convention Heat Transfer in Concentric Horizontal Cylindrical
	us for Aiding and Opposing Flows 71
	Abstract
3.2	Introduction
3.3	Analysis

3	3.4	Boundary condi	tions	.76
3	3.5	Local and Avera	age Nusselt number calculations	.77
3	3.6	Results and Dis-	cussion	78
		3.6.1	Case I	.78
		3.6.2	Local Nusselt number distributions	.84
		3.6.3	Case II	87
		3.6.4	Local Nusselt number distributions	92
		3.6.5	Average Nusselt number	95
3	3.7	Conclusions		. 99
3	3.8	References		100
Chaj	pte	r 4		
Num	eric	al Investigation	of Buoyancy Driven Fow of Nanofluids in a Horizon	ntal
Cylii	ndric	cal Annulus	1	102
	4.	.1 Abstract	1	103
	4.	.2 Introduction		103
	4.	.3 Mathematical	Formulation	106
	4.	.4 Average and I	ocal Nusselt number calculation1	10
	4.	.5 Results and D	iscussion 1	.11
	4.	.6 Conclusions .		127
	4.	.7 References		128

# **List of Figures**

# Chapter 1

1.1	Flow geometry for annulus with fins
1.2	Schematic illustrations of the configuration with the boundary
	conditions9
1.3	Control volumes for the two-dimensional
	situation
1.4	Present numerical predictions versus numerically predicted data (Kuehn and
	Goldstein, 1976) for Pr=0.7, 1.0 and 5.0 at Ra=10 <sup>4</sup> and L/D <sub>i</sub> =0.8
1.5	Local equivalent thermal conductivity variations on the inner cylinder
	(without fins) for Pr=1.0, Ra=10 <sup>4</sup> , and L/D <sub>i</sub> =0.8 with number of grids as
	parameter
1.6	Sample computational grid. 18
1.7	Velocity vectors and isotherms for three different fin heights at
	Ra=10 <sup>6</sup>
1.8	Streamlines and isotherms for three different fin heights at
	Ra=10 <sup>6</sup>
1.9	Velocity vectors and isotherms for
	H/L=0.2
1.10	Velocity vectors and isotherms for H/L=0.6
1.11	Local Nusselt number variation for the case of fin height (H) at 20%, 40%,
	and 60% of radius difference (L) for Rayleigh number of 10 <sup>3</sup> to
	10 <sup>6</sup>
1.12	Comparison of Local Nusselt number variation for the case of fin height (H)
	at 20%, 40%, and 60% of radius difference (L) for Rayleigh number of 10 <sup>3</sup>
	to 10 <sup>6</sup>

	cylinder
Chapter	· 2
2.1	Numerical solutions for the flow and temperature fields, respectively, for an internally porous finned annulus. (a) a) Ra= $10^6$ , $\varepsilon = 0.4$ , H/L= $0.2$ , Da= $10^{-3}$ ; (b) Ra= $10^6$ , $\varepsilon = 0.4$ , H/L= $0.2$ , Da= $10^{-5}$ ; (c) Ra= $10^6$ , $\varepsilon = 0.4$ , H/L= $0.2$ , Da= $10^{-6}$
2.2	Local equivalent thermal conductivity at Ra= $10^6$ , $\varepsilon = 0.4$ , H/L= $0.2$ , Da= $10^{-3}$ , and Da= $10^{-6}$
2.3	Variation of average equivalent thermal conductivity for various range of Rayleigh number at $\varepsilon = 0.4$ , H/L=0.2, Da= $10^{-3}$ , Da= $10^{-5}$ , and Da= $10^{-6}$
2.4	Numerical solutions for the flow and temperature fields, respectively, for an internally porous finned annulus. (d) Ra= $10^5$ , $\varepsilon = 0.4$ ,H/L= $0.2$ , Da= $10^{-3}$ ; (e) Ra= $10^5$ , $\varepsilon = 0.4$ ,H/L= $0.4$ Da= $10^{-3}$ ; (c) Ra= $10^5$ , $\varepsilon = 0.4$ ,H/L= $0.6$ , Da= $10^{-3}$
2.5	Local equivalent thermal conductivity at Ra= $10^5$ , $\varepsilon = 0.4$ , Da= $10^{-3}$ , for H/L=0.2, 0.4 and 0.6
2.6	Variation of average equivalent thermal conductivity for various range of Rayleigh number at $\varepsilon=0.4$ , Da= $10^{-3}$ , for H/L=0.2, 0.4 and 0.6
2.7	Numerical solutions for the flow and temperature fields, respectively, for an internally porous finned annulus. (g) Da= $10^{-4}$ , $\varepsilon=0.4$ , H/L= $0.6$ , Ra= $10^{3}$ ; (h) Da= $10^{-4}$ , $\varepsilon=0.4$ , H/L= $0.6$ , Ra= $10^{4}$ ; (i) Da= $10^{-4}$ , $\varepsilon=0.4$ , H/L= $0.6$ , Ra= $10^{5}$ ; (j) Da= $10^{-4}$ , $\varepsilon=0.4$ , H/L= $0.6$ , Ra= $10^{6}$

Buoyancy effect on heat transfer from a plain and finned inner

1.13

2.8	Local equivalent thermal conductivity at Da= $10^{-4}$ , $\varepsilon = 0.4$ , H/L=0.6, for
	$Ra=10^3$ , $Ra=10^4$ , $Ra=10^5$ , and $Ra=10^6$
2.9	Variation of average equivalent thermal conductivity for various range
	Rayleigh number at $\varepsilon = 0.4$ , H/L=0.2, 0.4, and 0.6 for Da=10 <sup>-3</sup> , Da=10 <sup>-5</sup> ,
	and Da=10 <sup>-6</sup> 64
2.10	Comparison of average equivalent thermal conductivity with various regions
	of Rayleigh number between solid fin, porous fin, and without fin (k)
	H/L=0.2, Da= $10^{-6}$ , $10^{-5}$ , $10^{-3}$ , $\varepsilon = 0.4$ ; (1) H/L=0.4, Da= $10^{-6}$ , $10^{-5}$ , $10^{-3}$
	, $\varepsilon = 0.4$ ; (m) H/L=0.6, Da= $10^{-6}$ , $10^{-5}$ , $10^{-3}$ , $\varepsilon = 0.4$
2.11	Comparison of average equivalent thermal conductivity with various
	porosities ( $\varepsilon = 0.2$ to 0.8) at Rayleigh number $10^6$ for different Darcy
	values and fin heights
~-	
Chapter	• 3
3.1	Schematic diagram of two concentric cylinders with coordinate
2.1	system
3.2	Isotherms and velocity vectors and streamlines for two different Richardson
	numbers at Reynolds number Re=50
3.3	Isotherms and velocity vectors and streamlines for two different Richardson
	numbers at Reynolds number Re=200
3.4	The local Nusselt number on the inner cylinder in case of aiding flow for
	Richardson numbers (RI=0 means heat transfer without natural convection)
	at Reynolds number (e) 50, (f) 100, (g) 150, and (h) 200 for inlet angle 15 <sup>0</sup>
	and outlet angle $5^0$
3.5	Isotherms and velocity vectors and streamlines for two different Richardson
	numbers at Reynolds number Re=50
3.6	Isotherms and velocity vectors and streamlines for two different Richardson
	numbers at Reynolds number Re=20091
3.7	The local Nusselt number on the inner cylinder in case of opposing flow for
	Richardson numbers (RI=0 means heat transfer without natural convection)

	at Reynolds number (m) 50, (n) 100, (o) 150, and (p) 200 for inlet angle 15°
	and outlet angle 5°
3.8	Variation of Average Nusselt number with various Richardson numbers at
	Reynolds number 50,100,150, and 200 during aiding flow 96
3.9	Variation of Average Nusselt number with various Richardson numbers at
	Reynolds number 50,100,150,and200 during opposing flow 96
3.10	Variation of Average Nusselt number with various Reynolds number at
	Richardson number 0.1 during opposing and aiding flow
3.11	Variation of Average Nusselt number with various Reynolds number at
	Richardson number 0.5 during opposing and aiding flow
3.12	Variation of Average Nusselt number with various Reynolds number at
	Richardson number 1.0 during opposing and aiding flow 98
3.13	Variation of Average Nusselt number with various Reynolds number at
	Richardson number 2.0 during opposing and aiding flow
Chanta	r A
Chapte	1 4
4.1	Flow geometry for the physical model
4.2	Velocity and isotherms, Streamlines and isotherms for $\Phi$ =0.2: (a).
	$Ra=10^3$ , (b) $Ra=10^4$ , (c) $Ra=10^5$ , (d) $Ra=10^6$
4.3	Velocities and isotherms, Streamlines and isotherms for Ra= $10^6$ : (a) $\Phi$ =
	$0.0$ , (b) $\Phi = 5\%$ , (c) $\Phi = 10\%$ , (d) $\Phi = 15\%$
4.4	Comparison of the average Nusselt number at different volume fraction on
	the inner cylinder for various Rayleigh number
4.5	Comparison of the average Nusselt number at different volume fraction on
	the outer cylinder for various Rayleigh number
4.6	Comparison of the local Nusselt number along the inner cylinder between
	different volume fractions at Rayleigh number 10 <sup>6</sup>
4.7	Comparison of the local Nusselt number along the inner cylinder between
	different volume fractions at Rayleigh number 10 <sup>5</sup>

4.8	Comparison of the local Nusselt number along the inner cylinder between
	different volume fractions at Rayleigh number 10 <sup>4</sup>
4.9	Comparison of the local Nusselt number along the inner cylinder between
	different volume fractions at Rayleigh number 10 <sup>3</sup>
4.10	Local Nusselt number on the inner cylinder at different Rayleigh number
	for pure fluid ( $\Phi$ =0) and nanofluid at $\Phi$ =0.5
4.11	Local Nusselt number on the inner cylinder at different Rayleigh number
	for pure fluid ( $\Phi = 0$ ) and nanofluid at $\Phi = 0.2$ 126

# **List of Tables**

1.1	Comparison between numerical results at Ra=5.0X10 <sup>4</sup> and Pr=0.7	
		. 14
1.2	Comparison between numerical results of average equivalent thermal	
	conductivity for annulus width to inner cylinder diameter ratio (L/D <sub>i</sub> ) is	;
	0.8	. 16
1.3	Effect of grid points on mean equivalent thermal conductivity ( $ar{K_{eq}}$ )	
	(without fin)	17
1.4	Thermophysical properties of different phases	111

# NOMENCLATURE

# Symbol

# Description

$a_{ m p}$	coefficient in the discretized governing equation
$C_{\mathtt{P}}$	specific heat at constant pressure, W.m <sup>-2</sup> .0C <sup>-1</sup>
$d_{ m p}$	nanoparticle diameter.
$D_e$ , $D_w$ , $D_n$ , $D_s$	diffusive conductance
$F_e, F_w, F_n, F_s$	strength of convection
g	gravitational acceleration, m. s <sup>-2</sup>
h	convective heat transfer coefficient
Н	fin height
$k_f$	fluid thermal conductivity, W.m <sup>-1</sup> .0C <sup>-1</sup>
$k_s$	solid thermal conductivity, W.m <sup>-1</sup> .0C <sup>-1</sup>
$K_{eq}$	local equivalent thermal conductivity = $\frac{Nu_L}{Nu_o}$
$\overset{ ext{-}}{K}_{ ext{eq}_{inner}}$	Circumferential average equivalent thermal conductivity = $\frac{\bar{Nu}}{Nu_0}$
L	gap width of the annulus = $(r_0 - r_i)$ , m
$Nu_0$	Nusselt number for conduction between the annuli
$Nu_L$	Local Nusselt number
Nu Circumfere	ntial average Nusselt number based on cylinder radius
P	Pressure, Pa
Pr	Prandtl number = $\frac{v_f}{\alpha_f}$
$\mathbf{r}_{i}$	Radius of inner cylinder, m

r<sub>o</sub> Radius of outer cylinder, m

R<sub>i</sub> Dimensionless radius of inner cylinder

R<sub>o</sub> Dimensionless radius of outer cylinder

Ra Rayleigh number = 
$$\frac{g\beta_f \Delta T r_i^3 \rho}{\mu \alpha}$$

Ra\* Modified Rayleigh number = 
$$\frac{g\beta_f \Delta T (r_0 - r_i)^3 \rho}{\mu \alpha \left(\frac{r_0}{r_i} - 1\right)^3}$$

RI Richardson number = 
$$\frac{Gr}{Re^2} = \frac{r_i^3 \beta g (T_H - T_C)}{v^2 * Re^2}$$

Re<sub>D</sub> Reynolds number = 
$$\frac{\mathbf{r_i} \rho \mathbf{v_{in}}}{\mu}$$

T Temperature, K

T<sub>0</sub> Temperature on cold wall, K

T<sub>i</sub> Temperature on hot wall, K

 $\Delta T$  Temperature difference between cylinders, K

 $T_{ref}$  Reference temperature, K

$$\phi$$
 = Dimensionless temperature =  $\frac{T - T_{ref}}{T_0 - T_i}$ 

 $\phi_0$  Dimensionless temperature on cold wall.

 $\phi_i$  Dimensionless temperature on hot wall.

Pe Peclet number

Φ Transported scalar

Φ Solid volume fraction (in case of nanofluids)

u, v Interstitial velocity components along  $\theta$  and r directions respectively, ms<sup>-1</sup>

U, V Dimensionless interstitial velocity components along  $\theta$  and r directions respectively

 $\theta$  , r Polar coordinates, degree and m

## **Greek symbols**

 $\alpha$  Thermal diffusivity, m<sup>2</sup>s<sup>-1</sup>

 $\beta_f$  Coefficient of thermal expansion,  $\frac{1}{T}$ ,  $K^{-1}$ 

 $V_f$  Kinematic viscosity, m<sup>2</sup>s<sup>-1</sup>

 $\rho$  Density, kg.m<sup>-3</sup>

 $\mu$  Dynamic viscosity, kg.m<sup>-1</sup>.s<sup>-1</sup>

# **Subscripts**

e, w, n, s four surfaces of control volume centred at P

E,W,N,S,NE,NW,SE,SW eight adjacent nodes to P

nb neighbouring points in numerical molecule

P nodal point to be solved in difference equation

eff effective

f fluid

nf nanofluid

s solid

i inner cylinder

in inlet port

o outer cylinder

ref Reference value

# **Introductory Note**

This thesis deals with CFD modeling of natural and mixed convection heat transfer in water. Horizontal cylindrical annulus geometry is considered with a view to designing of heat exchangers for solar energy applications. Four distinct cases are modeled and are arranged in the form of four chapters where each chapter has its own title, abstract, problem formulation, results and discussion, conclusions and references. This format is adopted to facilitate quick submission of four papers for possible publications in the relevant journals. To the best of the author's knowledge, all the results reported in this thesis are new and obtained by the author. An extensive literature search didn't reveal similar work concerning cylindrical annulus, particularly no results for the cases which are reported in the last three chapters of this thesis could be found Chapter 1 deals with natural convention in horizontal cylindrical annulus with equally spaced longitudinal fins. Chapter 2 provides modeling results on natural convention in horizontal cylindrical annulus with equally spaced longitudinal porous fins. Chapter 3 deals with laminar mixed convection heat transfer in concentric horizontal cylindrical annulus for aiding and opposing flows. Chapter 4 is concerned with the numerical investigation of buoyancy driven flow of nanofluids in a horizontal cylindrical annulus.

# **Chapter 1**

Natural Convention in a Horizontal Cylindrical Annulus with Equally Spaced Longitudinal Solid Fins

## **ABSTRACT**

The numerical solution of the laminar natural convection of water in six internally finned horizontal annuli has been obtained. The fins are attached to the external surface of the inner cylinder. Only the symmetrical half of the horizontal annulus with three equally spaced longitudinal divergent round tip solid fins are considered. The non-dimensional thermal conductivity of the fin surface to fluid was assumed to be high. A detailed parametric study reveals that complex multiple recirculation flow patterns appear at higher Rayleigh numbers and higher fin height. Rayleigh number is based on the width of the annulus gap and the results are presented for the Rayleigh number ranging from  $10^3$ - $10^6$  for the fin height to width of annulus ratio of 0, 0.2, 0.4 and 0.6. For a fixed fin height, the heat transfer rate from the inner cylinder increases with the increase of Rayleigh number. For a fixed Rayleigh umber, heat transfer rate increases with the increase of the fin height. No natural convection heat transfer results are available in the literature for an internally finned annulus with water as the working fluid. The present computed results show a similar trend with the results reported for air in the literature for natural convection in a finned annulus. Information about the flow patterns and temperature distributions are presented through velocity vectors, streamlines, and isotherm plots. Variations of the local equivalent thermal conductivity (ratio of Nusselt numbers due to convection and conduction heat transfer from the inner cylinder) are also presented.

## Introduction

In heat transfer studies, laminar natural convection from the heated cylinder is an important problem. Natural convection in concentric annulus is used to simulate a wide range of engineering applications as well as it provides a better insight into more the complex systems of heat transfer problems. So far extensive research has been performed on the measurements and predictions of the flow and associated heat transfer coefficients for natural convection between horizontal concentric cylinders with isothermal boundary conditions. Such flow configurations are found in the cooling of electronic equipment, aircraft cabin insulation, thermal energy storage devices, concentrating solar collectors, and

in some aspect of the design of nuclear reactors. The horizontal concentric cylinder geometry is also used in pressurized-gas underground electric transmission cables (Pedersen, Doepken & Bolin 1971).

It is well known that the heat transfer in a horizontal annulus is limited by the area of the inner cylinder. As a result, fins are used to increase the heat transfer area, leading to an increase in the heat transfer between the cylinders. Actually, at the fins root there is no heat transfer. Along the fin the heat transfer rate increases and at the tip it is the greatest and then it decreases. The natural convention currents near the inner cylinder surface due to fins are enhanced and as a result the heat transfer from the cylinder to the surrounding fluid increases. For a fixed geometry and working fluid, the net enhancement of the heat transfer rate depends on the combinations of the number of fins, fin height, and Rayleigh number. The presence of internal fins alters the flow patterns and temperature distributions and as a consequence the Nusselt number of the configuration increases with the buoyancy effect.

Compared to the bare annulus, a comparatively little work on natural convection heat transfer in horizontal finned annuli has been reported in the open literature. The increase in complexity, caused by the strong interaction between the boundary layer and adjacent fluid, makes it difficult to obtain a numerical solution of the problem of natural convection in a geometrically complicated finned annulus.

Natural convection between horizontal concentric isothermal cylinders was first studied experimentally by Beckmann (1931) for calculating overall heat-transfer coefficients. His working fluid was air, hydrogen and carbon dioxide. A similar investigation using air was made by Voigt & Krischer (1932). Kraussold (1934) extended these results for higher Prandtl number fluids which were water, transformer oil and machine oil. He developed a correlation for the overall heat-transfer coefficient, including also the data from Beckmann. Liu et al. (1961) measured the overall heat-transfer and radial temperature profiles of air, water and a silicone fluid. The qualitative flow descriptions were given for each fluid in their study. Bishop & Carley (1966) and Bishop et al. (1968) presented the photographs of flow patterns in air using smoke. Powe et al. (1969) investigated different flow regimes depending on the Grashof number and diameter ratio. Kuehn and Goldstein (1976 and 1978)

presented comprehensive numerical and experimental results on natural convection for horizontal concentric and eccentric cylinders over a wide range of Rayleigh number, Prandtl number, diameters and eccentricity ratio. Other researchers reported a number of experimental and numerical studies for a variety of configurations (positive and negative vertical eccentricities, and diameter ratios [Glapke et al, 1986; Projahn et al, 1981], boundary conditions (isothermal) [Tsui and Tremblay, 1984], constant heat flux [Kumar, 1987], and mixed boundary conditions [Ho et al, 1989], fluid properties (Prandtl number and variable properties) [Yang et al, 1988; Hessami et al, 1984; Charrier-Mojtaba et al, 1979; Nieckele and Patankar, 1985], and transient responses [Van de Sande and Hamer, 1979]. In 1990, Soliman and co-workers delineated the influence of internal fins on mixed convection in the fully developed region in horizontal tubes. Results were presented for tubes with two, four and sixteen fins, and for a variety of modified Grashof numbers. Internal fining was found to retard the onset of significant free convective effects and suppress the enhancement in friction factor and increase the Nusselt number compared to the smooth tubes. Hu and Chang (1973) gave results for optimal fin number for the best heat transfer rate. Masliyah and Nandakumar (1976) studied the importance of the fin geometry over the Nusselt number and Soliman et al. (1980) considered the thickness of the cylindrical walls.

Chai and Patankar (1993) studied the flow and heat transfer for an annulus with six radial fins arranged in two different configurations. It was observed that the orientation of the internal fins has no important effect on the average Nusselt number prediction, but the blockage due to the fins has significant effect on the flow and temperature fields and therefore on the rate of heat transfer. Marie et al. (1997) showed the fin geometry does not affect the rate of heat transfer but the best efficiency is associated with the fin with a round tip compared with the sharp and divergent tips. Eckert et al. (2000) wrote a paper where a more extensive review of the literature on natural convection can be found. Abu-Hijleh (2000) studied laminar natural convection and entropy generation from a horizontal cylinder with multiple, equally spaced, low conductivity baffles on its outer surface. It was shown that short baffles slightly increase the heat transfer rate at small values of Rayleigh number while there was up to 72% reduction in the value of the average Nusselt number depending

on the number and height of baffles as well as the Rayleigh number. Abu-Hijleh (2001) reported that the heat transfer rate actually decreases with the increase of Rayleigh number for the placement of uniformly spaced solid fins beyond a certain number on the cylinder surface.

On the basis of the above literature review, the objectives of this work are to evaluate numerically the circumferential average and the local Nusselt numbers round the inner cylinder wall. The outer surface of the inner cylinder is attached with six equally spaced, high conductivity solid divergent fins with round tips. This geometry has potential applications in heat exchangers. The circumferential average Nusselt number has direct applications to the heat exchanger design engineers. The local Nusselt number, which is difficult to obtain experimentally, is presented to gain a clear insight of the heat transfer processes. To the best of author's knowledge, there are no published data investigating the effect of equally spaced divergent solid round tip fins on heat transfer in laminar natural convection in a horizontal annular geometry where water is the working fluid.

The remainder of this paper is divided into three main sections. In the next section, the physical situation, the mathematical formulation of the problem considered and code validation are presented along with a brief description of the numerical procedure. This section is followed by a presentation of results and discussion. Finally, some conclusions are stated.

# Description of the problem

The physical model of the problem is illustrated schematically in Figure 1. The radius of the inner cylinder is denoted by  $r_i$  while that of the outer cylinder is denoted by  $r_o$ . Six divergent solid fins of height H with round tip are equally spaced around the inner cylinder. The inner and outer cylinders are considered to be of aluminum and their wall thickness is equal to one grid size. The inner and outer cylinders are maintained at temperatures  $T_i$  and  $T_0$  ( $T_0 < T_i$ ), respectively. The cylinders are assumed to be long enough that a two dimensional analysis can be applied. The fluid under consideration is water. The buoyancy

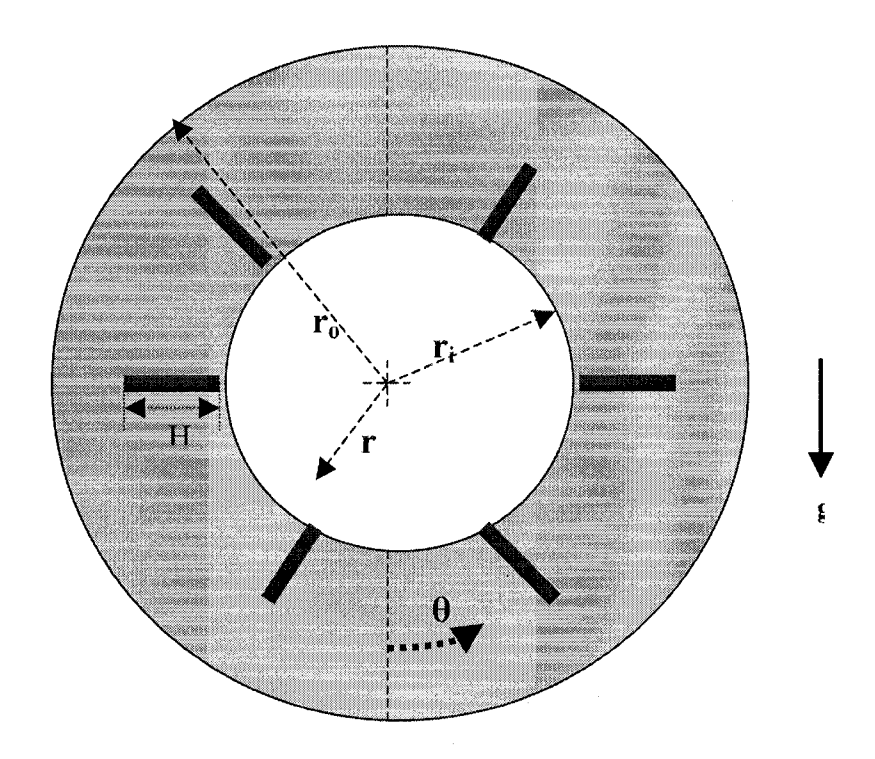


Figure 1: Flow geometry for annulus with fins.

driven fluid flow resulting from the temperature difference of the cylinders is assumed to be steady and the flow is laminar. Due to symmetry, the computations are carried for only half of the physical domain by making use of the vertical symmetry plane passing through the center of the cylinder. The number of fins located herein is that on one half of the annulus. No fins are placed at the vertical symmetry plane. The thermo-physical properties of the fluid are temperature-independent, except for the density, for which the Boussinesq approximation is applicable. Viscous dissipation, compressibility effects and radiation are neglected.

## **Mathematical formulation**

The steady-state, laminar two-dimensional conservation equations of mass, momentum and energy for a Newtonian fluid in the conservative form in cylindrical co-ordinates, including the Boussinesq approximation, are given as follow:

Using Boussinesq approximation, the density term is given by

$$\rho = \rho_{ref} \left[ 1 - \beta \left( \mathbf{T} - \mathbf{T}_{ref} \right) \right] \qquad (1)$$

Continuity:

$$\frac{1}{r}\frac{\partial(\rho_r r v)}{\partial r} + \frac{1}{r}\frac{\partial(\rho_r u)}{\partial \theta} = 0$$
 (2)

U-momentum equation:

$$\frac{1}{r}\frac{\partial}{\partial r}(\rho_{r}ruu) + \frac{1}{r}\frac{\partial}{\partial \theta}(\rho_{r}uv) = \frac{1}{r}\frac{\partial}{\partial r}\left(\mu r\frac{\partial u}{\partial r}\right) + \frac{1}{r}\frac{\partial}{\partial \theta}\left(\frac{\mu}{r}\frac{\partial u}{\partial \theta}\right) - \frac{1}{r}\frac{\partial p^{*}}{\partial \theta} + 2\frac{\mu}{r^{2}}\frac{\partial v}{\partial \theta} - \mu\frac{u}{r^{2}} - \rho_{r}\frac{uv}{r} + \rho_{r}g_{\theta}\beta(T - T_{ref})\sin\theta - \dots$$
(3)

V-momentum equation:

$$\frac{1}{r}\frac{\partial}{\partial r}(\rho_{r}ruv) + \frac{1}{r}\frac{\partial}{\partial \theta}(\rho_{r}vv) = \frac{1}{r}\frac{\partial}{\partial r}\left(\mu r\frac{\partial v}{\partial r}\right) + \frac{1}{r}\frac{\partial}{\partial \theta}\left(\frac{\mu}{r}\frac{\partial v}{\partial \theta}\right) - \frac{\partial p^{*}}{\partial r} - 2\frac{\mu}{r^{2}}\frac{\partial u}{\partial \theta} - \mu\frac{v}{r^{2}} - \rho_{r}\frac{u^{2}}{r} - \rho_{r}g_{r}\beta(T - T_{ref})\cos\theta - \dots$$
(4)

Energy equation:

In the fin surface, the conductive heat transfer is described by

$$\frac{1}{r}\frac{\partial}{\partial r}\left(\frac{K_s}{C_{P_F}}r\frac{\partial T}{\partial r}\right) + \frac{1}{r}\frac{\partial}{\partial \theta}\left(\frac{K_s}{C_{P_F}}\frac{1}{r}\frac{\partial T}{\partial \theta}\right) = 0$$
 (6)

The equations in the fluid domain are cast in dimensionless conservative form by introducing the following dimensionless variables:

For the coordinate system shown in Figure 1, the non-dimensionalized, conservative form of the governing equations in the flow region can be written as:

Continuity:

$$\frac{1}{R}\frac{\partial(RV)}{\partial R} + \frac{1}{R}\frac{\partial U}{\partial \theta} = 0 \qquad (8)$$

U-momentum equation:

$$\frac{1}{R} \frac{\partial}{\partial R} (RUU) + \frac{1}{R} \frac{\partial}{\partial \theta} (UV) = \Pr \frac{1}{R} \frac{\partial}{\partial R} \left( R \frac{\partial U}{\partial R} \right) + \Pr \frac{1}{R} \frac{\partial}{\partial \theta} \left( \frac{1}{R} \frac{\partial U}{\partial \theta} \right) - \frac{1}{R} \frac{\partial P^*}{\partial \theta} + 2 \frac{\Pr}{R^2} \frac{\partial V}{\partial \theta} - \Pr \frac{U}{R^2} - \frac{UV}{R} + Ra \Pr \phi \sin \theta \qquad (9)$$

V-momentum equation:

$$\frac{1}{R}\frac{\partial}{\partial R}(RUV) + \frac{1}{R}\frac{\partial}{\partial \theta}(VV) = \Pr \frac{1}{R}\frac{\partial}{\partial R}\left(R\frac{\partial V}{\partial R}\right) + \Pr \frac{1}{R}\frac{\partial}{\partial \theta}\left(\frac{1}{R}\frac{\partial V}{\partial \theta}\right) - \frac{\partial P^*}{\partial R} - 2\frac{\Pr}{R^2}\frac{\partial U}{\partial \theta} - \Pr \frac{V}{R^2}$$

$$-\frac{U^2}{R} - Ra\Pr \phi \cos \theta - \dots \qquad (10)$$

Energy equation:

On the solid fin wall the energy equation is:

$$\frac{K_S}{K_E} \frac{1}{R} \frac{\partial}{\partial R} \left( R \frac{\partial \phi}{\partial R} \right) + \frac{1}{R} \frac{\partial}{\partial \theta} \left( \frac{1}{R} \frac{\partial \phi}{\partial \theta} \right) = 0 \quad ----- \quad (12)$$

# **Boundary conditions and assumptions**

The geometry (the right half of the annuli is chosen as the solution domain) and the boundary conditions corresponding to this problem are presented in Figure 2. The dimensionless boundary conditions are given by

- 1. On the inner cylinder surface, i.e.,  $R_i = 1.0$ ; U=V=0.0;  $\phi = 1.0$
- 2. On the outer cylinder surface, i.e.,  $R_o = 2.6$ ; U=V=0.0;  $\phi = 0.0$
- 3. Lower plane of symmetry; i.e.,  $\theta = 0$ ; U=0.0;  $\frac{\partial V}{\partial \theta} = \frac{\partial \phi}{\partial \theta} = 0.0$
- 4. Upper plane of symmetry; i.e.,  $\theta = \pi$ ; U=0.0;  $\frac{\partial V}{\partial \theta} = \frac{\partial \phi}{\partial \theta} = 0.0$
- 5. On the solid fin surface, i.e., U=V=0.0;  $\frac{K_s}{K_F}$  = 647.0

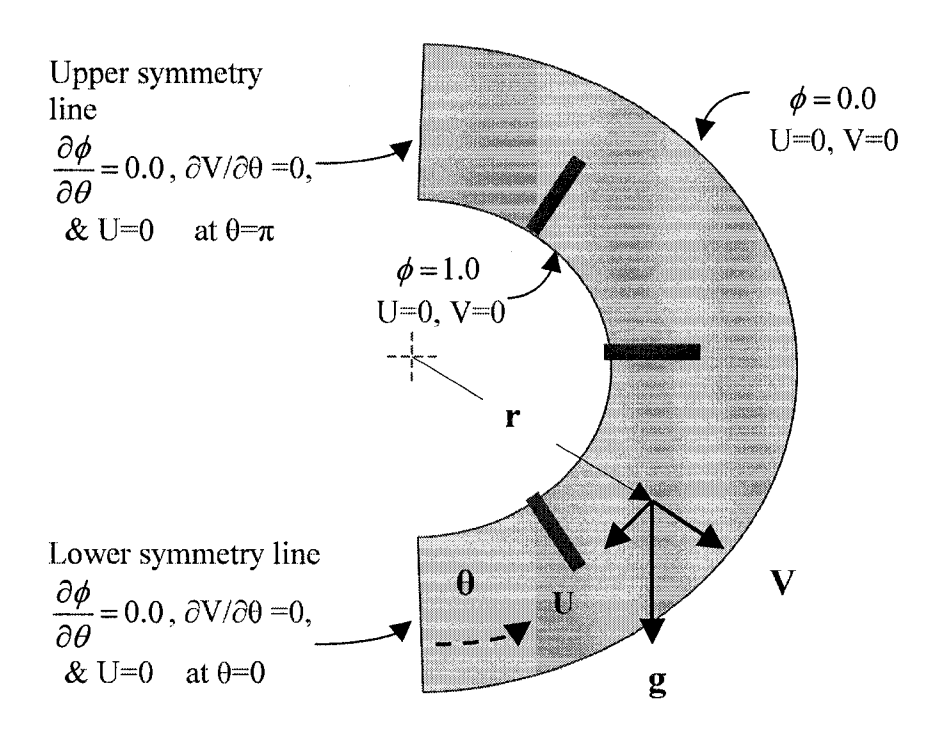


Figure 2: Schematic illustrations of the configuration with the boundary conditions.

## Assumptions are:

- The thickness of the inner and outer cylinders coincides with one grid spacing.
- The flow of the working fluid (water) is laminar and axisymmetric.
- No-slip conditions are applicable for the velocity components at the boundary.
- Uniform but different temperatures for the inner and outer cylinders.
- The angular gradient of the temperature and the angular gradient of radial velocity and angular velocity are zero at the axis of symmetry.
- The Boussinesq approximation is valid.

# Governing parameters

The governing parameters of the problem are the number of fins, the orientation of fins, the fin conductance, the ratio of fin height to the annulus gap, Rayleigh number, Prandtl number, and the ratio of the outer radius to the inner radius.

The first two governing parameters have been selected from the open literature, which were found by others [Marie-Isabelle & coworkers, 1997] to be the best option so far the natural convective heat transfer is concerned for the inner cylinders. The dimensionless conductance

of fin to fluid, and Prandtl number are assigned a value of 647.0, and 6.78, respectively. The working fluid is water. The ratio of the outer radius to the inner radius is assigned a value of 2.6, which is also reported to be the best geometry for obtaining the maximum heat transfer rate. It is seen from the literature that a lower radius ratio leads to multiple solutions and for a greater radius ratio of more than 2.6 the importance of the outer cylinder is diminished so far the natural convection heat transfer is concerned. The remaining two parameters are varied over a wide range of values. One is the Rayleigh number which is assigned fixed values of  $10^3$ ,  $10^4$ ,  $10^5$ , and  $10^6$ . Other parameter is the ratio of fin height to the annulus gap which is assigned a value of 0, 0.2, 0.4 and 0.6.

## **Numerical solution**

The first step in numerical solution is to provide the algebraic form of transport equations at appropriately chosen grid points. This operation is termed 'discretization'. Discretization equations are derived by integration of the partial differential equations over each control volume of the domain. To solve the discretized transformed governing equations, a program based on the control volume finite difference (CVFD) was written. Patankar's SIMPLER algorithm (1980) was used to resolve the pressure-velocity coupling in the momentum equations. The general form of the algebraic governing equations obtained from the discretization can be written in the general form as follows:

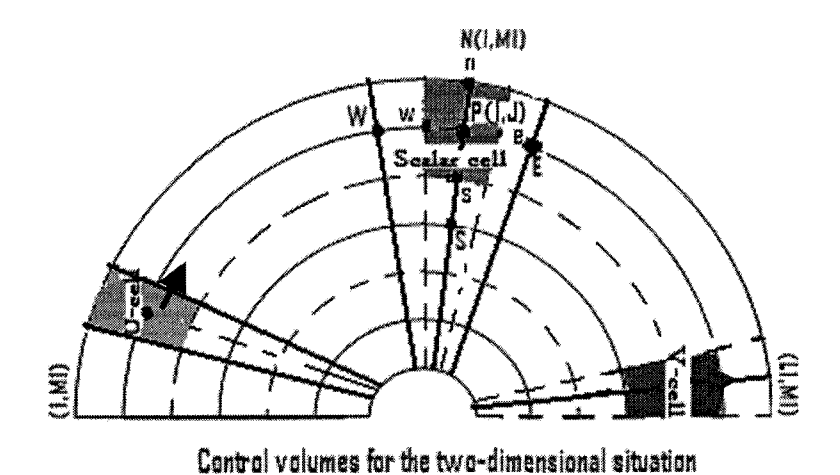
$$a_{\rm P}\Phi_{\rm P} = a_{\rm E}\Phi_{\rm E} + a_{\rm W}\Phi_{\rm W} + a_{\rm N}\Phi_{\rm N} + a_{\rm S}\Phi_{\rm S} + b_{\rm \Phi}$$
 -----(13)

Here,  $a_{\rm E}$ ,  $a_{\rm W}$ ,  $a_{\rm N}$ ,  $a_{\rm S}$  are the coefficients of neighboring nodes and  $b_{\rm \Phi}$  is the source term. With this computational procedure the whole domain is described by a displaced or staggered grid system as shown in Figure 3. Such a displaced grid for the velocity components was first used by Harlow and Welch (1965) in their MAC method and has been used in other methods developed by Harlow and co-workers. It also formed the basis of the SIMPLER procedure of Patankar and Spalding (1972).

The scalar quantities (P, T) are located at the middle of the scalar control volume shown by the farm line, while the velocity components (U and V) are located at the faces of the scalar control volumes and their control volumes are presented by dotted lines.

The advantages of the staggered grid are twofold: firstly, the mass flow rates across the control volume faces can be calculated without any interpolation from adjacent velocities and secondly, the pressure difference between two adjacent grid points becomes the natural driving forces for the velocity components located between these grid points.

The variable U denotes the velocity in the  $\theta$ -direction at the 'e' and 'w' locations of the east and west faces. Similarly, the variable V denotes the velocity in the r-direction at the 'n' and 's" locations of the north and south faces. Integration of convective diffusion equations over the control volume involves approximating the value of  $\Phi$  at the control volume surfaces. The approximation can be done using different schemes. Here power-law scheme [Patankar, 1980] was used to discretize the convective derivatives in the main flow direction.



The generalized formula for the neighbor point coefficients for each schemes are as follows:

Figure 3

$$\begin{split} a_E &= D_e A \big( \! \left| \operatorname{P} e_e \right| \big) + \left\| -\operatorname{F}_{\mathrm{e}} , 0 \right\| \\ a_W &= D_w A \big( \! \left| \operatorname{P} e_w \right| \big) + \left\| -\operatorname{F}_{\mathrm{w}} , 0 \right\| \\ a_N &= D_n A \big( \! \left| \operatorname{P} e_n \right| \big) + \left\| -\operatorname{F}_{\mathrm{n}} , 0 \right\| \\ a_S &= D_s A \big( \! \left| \operatorname{P} e_s \right| \big) + \left\| -\operatorname{F}_{\mathrm{s}} , 0 \right\| \end{split}$$

Here,  $D_e$  is diffusion conductance at interface e between P and E, and  $D_w$ ,  $D_n$  and  $D_s$  are similar values in w, n, and s interfaces, respectively.  $F_e$  denotes the strength of convection at interface e between P and E and  $F_w$ ,  $F_n$  and  $F_s$  are similar values in w, n, and s interfaces, respectively. Pe is Peclet number defined by the ratio of strength of convection to diffusion conductance. The operator  $\|a, b\|$  is equivalent to AMAX (A,B) in FORTRAN.

For power-law difference scheme the formula for the function  $A(|Pe_e|)$  is given by [Patanker,1980]. The general form of linearized source term is:  $S_{\Phi} = S_C + S_P \Phi_P$  where,  $S_C$  becomes the contributor to b and  $S_P$  a contributor to  $a_P$  in the discretized equation. An in-house CFD code developed over the years by Professor Hasan's group at

McGill University was modified to solve the problems presented in this thesis.

## Convergence criteria

The termination of an iteration loop depends on the values of the residuals for U, V,  $\Delta P$  and T. The residual is defined by the general variable  $\Phi$  as follows:

Residual= 
$$\frac{\Phi^{k+1} - \Phi^k}{\Phi_{Max}^k}$$

where, k is the number of iteration. The convergence was achieved when the maximum absolute value of the residuals were less than 10<sup>-4</sup>. A block correction procedure (Patankar, 1980) was used to enhance the convergence of the solution procedure.

## **Under-relaxation factor**

The nonlinearity and inter-linkage of the governing equations may appreciably change the results from iteration to iteration. These rapid changes influence the magnitude of the coefficients of the tri-diagonal matrix which then generally yields to the divergence. To prevent the program from divergence under-relaxation parameters were introduced for velocities and temperature. Use of the implicit form of under-relaxation before solution of the algebraic equations, changes the coefficients of these equations as follows:

$$\frac{a_{\rm p}}{\alpha_{\rm \phi}}\Phi_{\rm p} = \sum_{nb} a_{nb}\Phi_{nb} + b_{\rm \phi} + (1-\alpha_{\rm \phi})\frac{a_{\rm p}}{\alpha_{\rm \phi}}\Phi_{\rm p}^{\bullet} - \cdots$$
 (14)

where,  $\alpha_{\Phi}$  is the under relaxation factor for the general variable  $\Phi$ . The suitable values of the relaxation factor were found by experience since they depend upon a number of factors (grid resolution, Rayleigh number, etc.). In the present study, much effort has been paid to find the relevant under-relaxation factors. Various combinations of under-relaxation factors were examined and after numerous runs the following under-relaxation factors were selected for the production runs:

$$\alpha_{\nu} = 0.5$$
;  $\alpha_{\nu} = 0.5$ ; and  $\alpha_{\tau} = 0.5$ .

## Code validation

In this part, the accuracy of the present numerical results was investigated by computing natural convection in concentric horizontal annular region without fin. Various authors have studied this configuration in detail and established to an extent that is used as a source of comparison for validating the numerical codes. Here, the present numerical code is extensively validated against the experimental and numerical results of Kuhen and Goldstien (1976) and numerical results of Hessami et al (1984), Yang et al (1988), Marie-Isabelle et al (1997). Table 1 presents a comparison between the present numerical results with the available experimental results of Kuhen and Goldstien (1976) and numerical results of others. The values of the dimensionless parameters were chosen exactly the same as others so as to facilitate the comparison with the available experimental and numerically predicted data. An equivalent thermal conductivity K<sub>eq</sub> on the outer surface of the inner cylinder and inner surface of the outer cylinder was used to compare the accuracy of the present computations. This parameter is defined as the ratio of actual heat flux to the heat flux that would have occurred due to pure conduction without the convective motion of the working fluid. Many authors have used the value of K<sub>eq</sub> on the inner and outer cylinders as a suitable criterion for the accuracy of their numerical procedures. This choice may yield an error in computing the actual heat transfer rate since various authors have used various expressions for calculating conductive heat transfer rate. In this study, one dimensional conduction

equation was solved to compute the heat flux without fluid motion [defined in Eqn. 15]. It can be seen in Table 1 that the numerical results are in very good agreement with the experimental results of Kuhen and Goldstien (1976) for Rayleigh number  $5x10^4$ , Pr number 0.7 and non-dimensional diameter ratio 2.6. The percentage of error was calculated with respect to the experimental results presented by Kuehn & Goldstein. The difference between the experimental and the present numerical results for Nusselt numbers is less than 1.5% for the inner and about 2.2% for the outer cylinder. The errors in the numerical result may arise from the constant-property assumption, the finite number of nodes, the convergence level of the solution, etc. The numerical analysis has the advantage of obtaining and observing the velocity field which is difficult to obtain experimentally. In addition, an overall energy balance was made, i.e., the integrated heat transfer rate through the inner cylinder must be equal to that of the outer cylinder. The discrepancy between the heat transfer rates was found to be less than 3.6%.

Table 1: Comparison between numerical results at Ra=5.0X10<sup>4</sup> and Pr=0.7

	Kuehn &	Kuehn &	Hessami	Yang	Marie	Present
	Goldstein	Goldstein	et al	et al	et al	numerical
	exp. (1976)	num. (1976)	num. (1984)	num. (1988)	num. (1997)	computation
Ra <sub>L</sub>	4.7X10 <sup>4</sup>	5.0X10 <sup>4</sup>	5.0X10 <sup>4</sup>	4.7X10 <sup>4</sup>	$5.0X10^4$	$5.0X10^4$
Pr	0.706	0.7	0.7	0.7	0.7	0.7
	3.0	3.024	3.26	2.943	2.955	3.044
$\overset{-}{K}_{^{eq_{\mathit{inner}}}}$ on inner cylinder						
Percent of error	0.0%	0.8%	8.7%	1.9%	1.5%	1.5%
$\overset{-}{K}_{^{eq_{outer}}}$ on outer cylinder	3.0	2.973	3.05	2.901	2.955	2.935
Percent of error	0.0%	0.9%	1.7%	3.3%	1.5%	2.2%

Figure 4 shows the comparison between the present numerically predicted data and Kuhen and Goldstien's (1976) numerically predicted local equivalent thermal conductivities along the inner and outer cylinders for Pr numbers 0.7, 1.0 and 5.0;  $L/D_i=0.8$ ; all for a fixed Rayleigh number of  $10^4$ . These results were obtained using a uniform 42X42 (r- $\theta$ ) grid system. It is observed from Fig. 4 that a solution similar to the one presented by Kuhen and

Goldstien was obtained. These authors published results of averaged equivalent thermal conductivity for the same conditions and these results are compared in Table 2. There is an excellent agreement between the present results and the results from Kuhen and Goldstien; the average equivalent conductivities differ by less than 05%. This small difference may be due to the lower convergence criterion used by Kuhen and Goldstien which was 10<sup>-3</sup> and in the present simulation study a ten-fold lower convergence criterion (10<sup>-4</sup>) was used. Besides this, Kuhen and Goldstien used an arbitrary set of non-uniform grids while in the present numerical simulation a higher density uniform grid system was used.

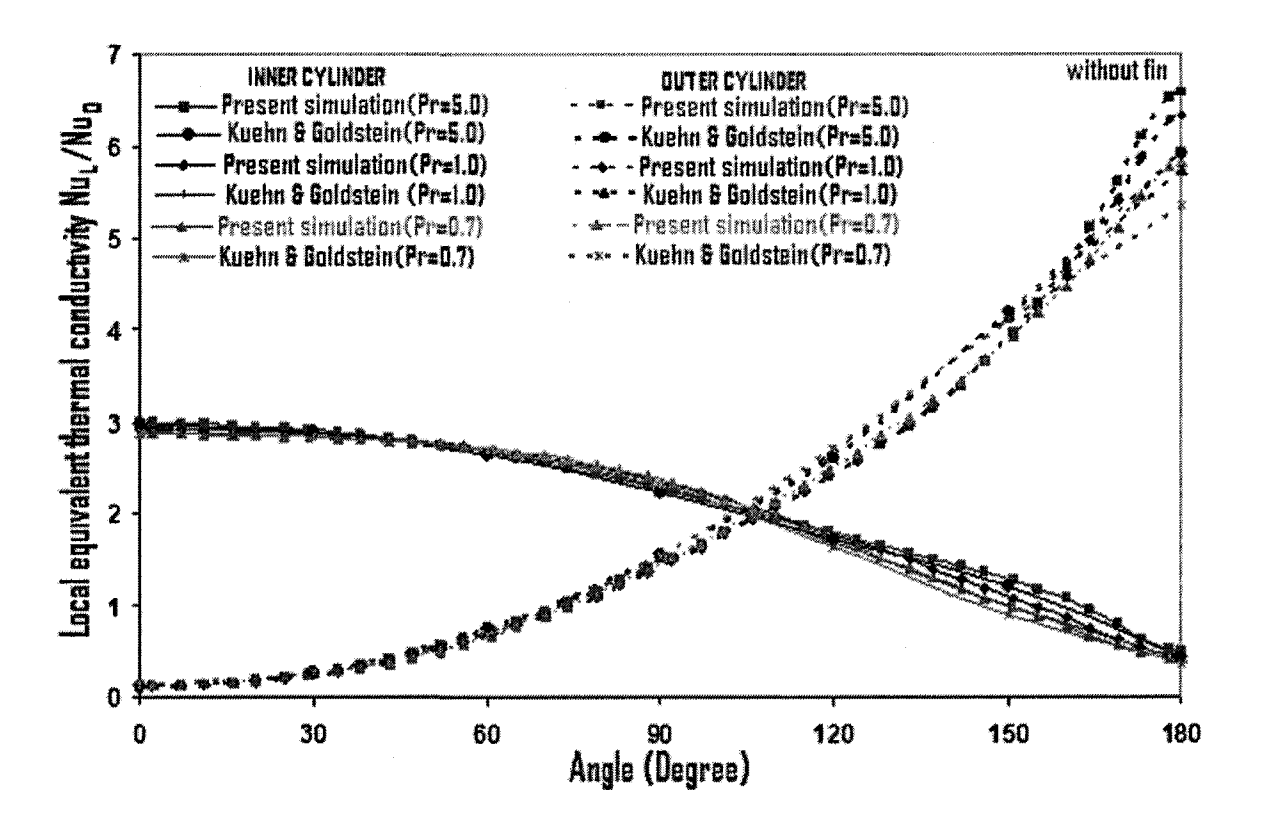


Figure 4: Present numerical predictions versus numerically predicted data of Kuehn and Goldstein, 1976 for Pr= 0.7, 1.0 and 5.0 at Ra=10<sup>4</sup> and L/D<sub>i</sub>=0.8

Table 2: Comparison between numerical results of average equivalent thermal conductivity for annulus width to inner cylinder diameter ratio (L/D<sub>i</sub>) 0.8

	Kuehn & Goldstein num. (1976))	Present numerical computation	Kuehn & Goldstein num. (1976)	Present numerical computation	Kuehn & Goldstein num. (1976)	Present numerical computation
Ra <sub>L</sub>	104	10 <sup>4</sup>	$10^4$	104	$10^{4}$	10 <sup>4</sup>
Pr	5.0	5.0	1.0	1.0	0.7	0.7
$\overset{-}{K}_{{}^{eq}_{inner}}$ on	2.069	2.119	2.038	2.089	2.010	2.05
inner cylinder						
Percent of error	0.0%	2.42%	0.0%	2.50%	0.0%	1.99%
$\overset{-}{K}_{_{eq_{outer}}}$ on outer cylinder	2.066	1.994	2.039	1.951	2.005	1.933
Percent of error	0.0%	3.48%	0.0%	4.32%	0.0%	3.59%

# **Grid Dependency and Computer time**

As mentioned earlier, in the present work the grid distribution in the r- $\theta$  coordinates was uniform. The selection of the number of grid points used in the present computation was reasoned based on equivalent thermal conductivity prediction along the inner cylinder. To obtain grid independent results four different numbers of grid distributions were tested. The computations were carried out with 42x42, 62x62, 82x82 and 102x102 grid design for a Prandtl number of 1.0, annulus gap-based Rayleigh number of 10<sup>4</sup> and outer to inner cylinder diameter ratio of 2.6. Table 3 shows the effect of number of grid points on mean equivalent thermal conductivity ( $ar{K_{eq}}$ ) for the inner cylinder of a horizontal cylindrical annulus without fins. As is observed from the Table 3, the difference among the mean equivalent thermal conductivity obtained for 82x82 grid points and those computed with other number of grid points is not very significant (an error of less than 7.0%). The effect of grid points on local equivalent thermal conductivity predictions is also investigated. Figure 5 represents the results of the local equivalent thermal conductivity variation along the inner cylinder for the above stated conditions. This figure shows that the local equivalent thermal conductivity prediction along the inner cylinder for 82x82 grid points nearly correspond to those obtained from 42x42 and 62x62 grid points, while the difference with 102x102 grid points is significant. The number of iterations required to obtain converged solution was presented in Table 3. In view of the above results, for getting accurate predictions and for the sake of computational economy all production runs were performed with the 82x82 grid system which was uniform in both directions, except near the walls where non-uniformity was due to the employment of B-type staggered grids.

Table 3: Effect of grid points on mean equivalent thermal conductivity ( $K_{eq}$ ) (without fin)

Grid points	42x42	62x62	82x82	102x102
$ar{K_{eq}}$ on inner	2.1	2.14	2.18	2.33
cylinder				
Percent of error	3.7%	1.84%	0.0%	6.88%
No. of iterations	1056	1742	2701	2804
for convergence				

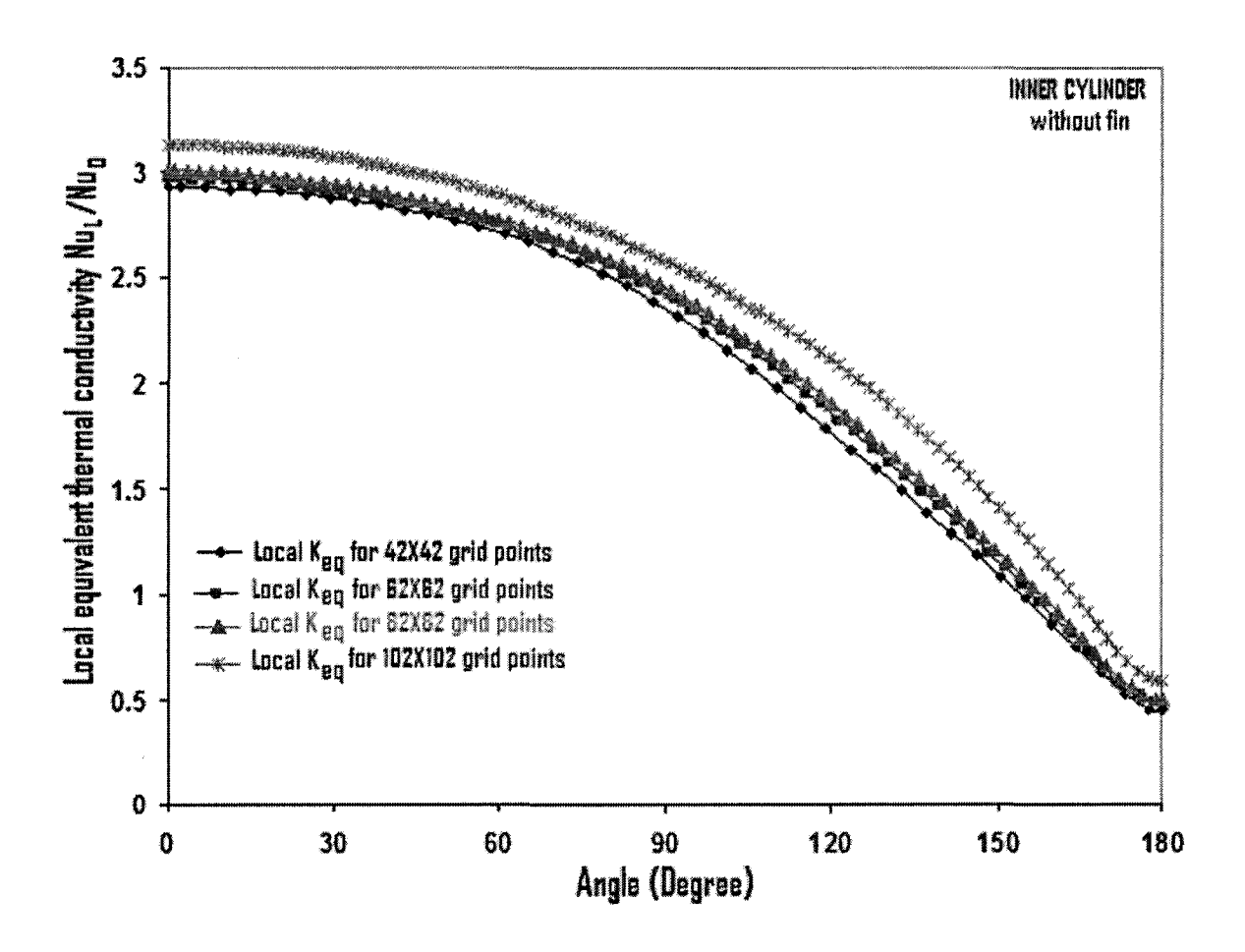


Figure 5: Local equivalent thermal conductivity variations on the inner cylinder (without fins) for Pr=1.0, Ra= 10<sup>4</sup> and L/D<sub>i</sub>=0.8 with number of grids as parameter

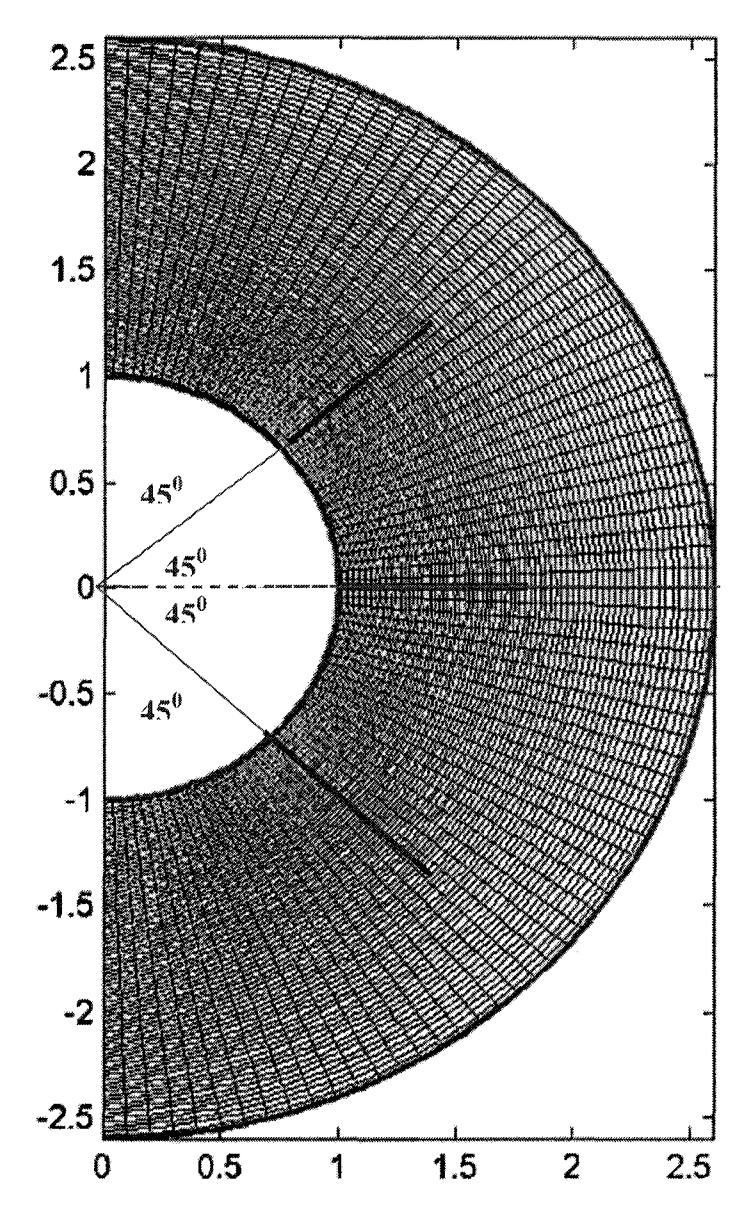


Figure 6: Sample computational grid

# **Results and Discussion**

Figure 1 shows the geometry considered in this study. All computations were carried out for a radius ratio of 2.6 and with water (Pr=6.78) as the working fluid. Dimensionless temperatures for the inner and outer cylinders were selected as one and zero and ratio of the

thermal conductivity of solid and fluid was considered as 647.0. These values were chosen so as to facilitate a comparison with the available numerical and experimental data.

This section is divided into four subsections, namely, definitions of related variables, discussion on the velocity and temperature fields, the variation of local equivalent thermal conductivity along the inner wall, and finally, the average equivalent thermal conductivity on the inner cylinder.

#### **Definitions**

For presenting the results two quantities are used. These are circumferential average equivalent thermal conductivity ( $\bar{K}_{eq_{inner}}$ ) and local equivalent thermal conductivity  $K_{eq}$  along the inner cylinder.

$$\overline{K}_{eq_{inner}} = \frac{\overline{Nu_{avg}}}{Nu_0}$$
 and  $K_{eq} = \frac{Nu_L}{Nu_0}$ 

 $\overline{Nu_{avg}}$  = circumferential average Nusselt number based on cylinder radius, is calculated as

$$\overline{Nu}_{avg} \underset{\text{at } r=r_i}{\text{at } r=r_i} = \frac{\int_0^L \int_0^\pi (Nu_L)_{r=r_i} r_i d\theta dZ}{\int_0^L \int_0^\pi r_i d\theta dZ}; \text{ and } Nu_{L \text{ at } r=r_i} = \frac{h(\theta)r_i}{k}; \text{ where, } h(\theta) = \frac{q_w}{T_w - T_{ref}};$$

$$q_{w \text{ at } r=r_i} = -k \frac{\partial T(r_i, \theta)}{\partial r}$$

 $Nu_0$  = Nusselt number for conduction between the annuli. The subscript o indicates Nusselt number for conduction heat transfer in the annulus. This is obtained by solving the one-dimensional conduction equation at steady state which is given by

$$\frac{1}{r}\frac{\partial}{\partial r}\left(kr\frac{\partial T}{\partial r}\right) = 0 \quad (15)$$

The Nusselt number for conduction is evaluated as

$$Nu_0 = \frac{1}{\ln \frac{R_0}{R_i}}$$

A Lagrangien interpolation scheme was used to calculate the local Nusselt number results because of the non-uniform grid distributions near the walls. To calculate the average Nusselt number, the Nusselt number along the fin surfaces was also considered.

The local Nusselt number at the fin, based on radius, is given by:

$$Nu_{f}(\theta_{f}) = \int_{1}^{fin} \frac{1}{R} \left[ \frac{\partial \phi(R, \theta_{f})}{\partial \theta} \Big|_{TOP} + \frac{\partial \phi(R, \theta_{f})}{\partial \theta} \Big|_{BOTTOM} \right] dR - - - - - - - - - - - (16)$$

The effective average Nusselt number, including the effect of the fin(s) is given by:

$$\overline{Nu_{AV}} = \int_{0}^{\pi} Nu_{L \text{ at } R=R_{I}}(\theta) d\theta + \sum_{i}^{N_{f}} Nu_{f}(\theta_{f}) - \cdots$$
 (17)

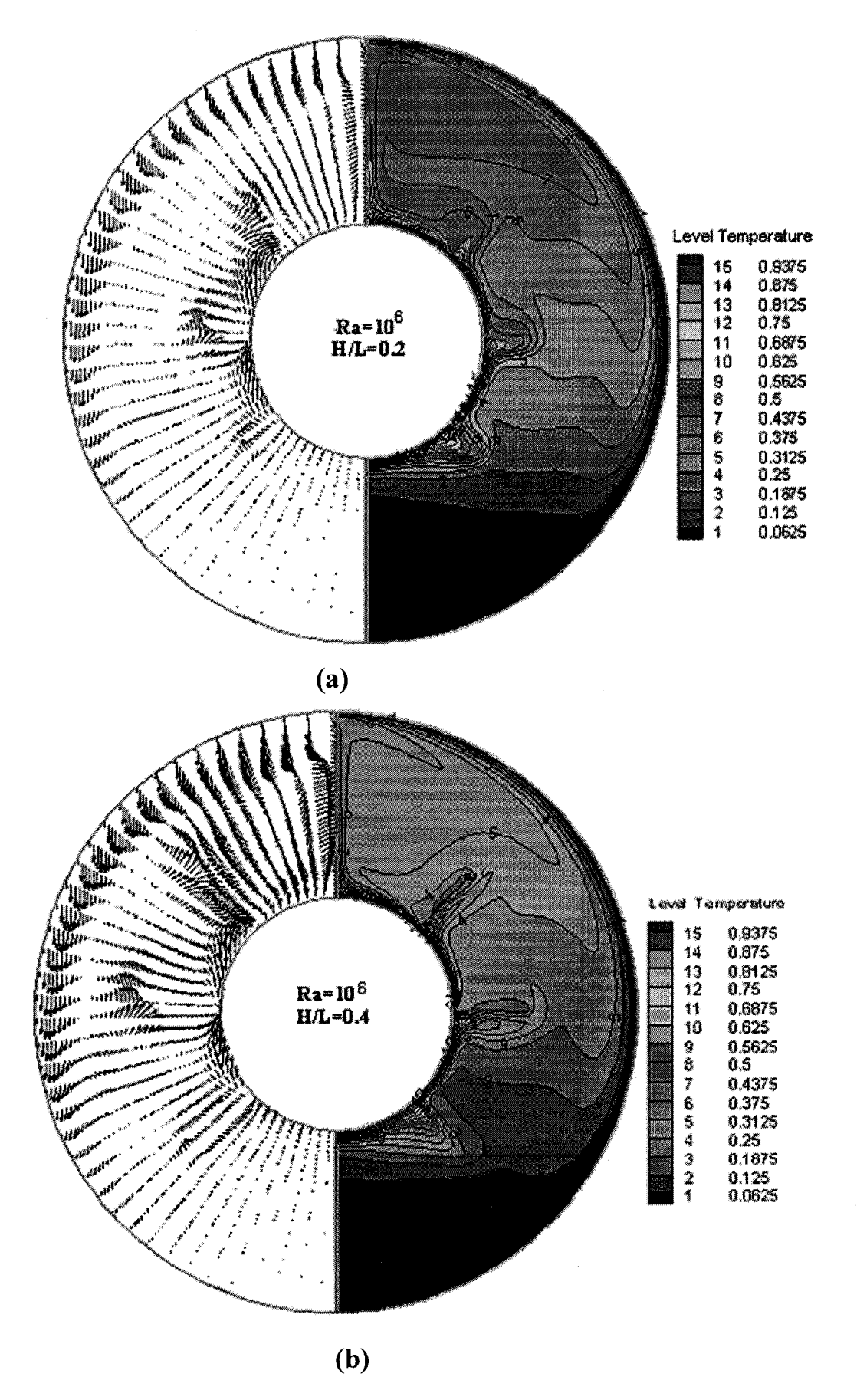
The average Nusselt number on the inner cylinder surface is obtained by integrating the local Nusselt number over the inner cylinder, which was obtained by using the Simpson integration rule. The average Nusselt number thus consists of the average Nusselt number on the inner cylinder and the effective average Nusselt number on the three fin surfaces.

# Velocity and temperature fields

Effects of fin height: This section represents the results obtained for an annulus with longitudinal divergent fin(s) which are the main part of the present study. As mentioned before, fin(s) height is preferred as 20%, 40%, and 60% of radius difference for the selected geometry. Flow and temperature fields in the form of velocity vectors and isotherms are shown in Figs. 7(a), 7(b), and 7(c) and in the form of streamlines and isotherms are shown in Figs. 8(d), 8(e), and 8(f) for different fin heights at Ra= 10<sup>6</sup>. There are a lot of differences between the velocity vectors/streamlines and isotherms for different fin heights. Results represent remarkable differences in contours especially in the upper part of the annulus and near the fins top and bottom surfaces and fins tips. Fluid starts to move upward into the domain with an angular velocity around the inner cylinder. The fluid then approaches to the bottom fin, the fluid (water) gains heat and flows downwards along the fin then follows the contour of the annulus until it reaches the second fin. In this region, the fluid is forced to

bend and concentrate at the bottom of the fin on the inner cylinder. The continuous heating of the downward moving water creates an upward force, causing the acceleration of the upward motion. Thus, the momentum of the upward flow, which continues into the regions between the bottom and second fin, is greater in the long fin annulus. This is because the resistance force created by the heating of the downward fluid acts smaller in the long-fin situation. The water continues to rise until it reaches the third fin. In the long-fin geometry, most of the fluid flows into the gap between the bottom and second fin, while the remaining fluid continues to move in the direction parallel to the fin before joining the cold water moving down along the outer cylinder. In the short-fin annulus, small amount of the flow is guided parallel to the fin. Thus, the flow between the second and third region forms an "almost closed" circulating bubble. It may be noticed that near the upper symmetry plane, the flow changes its direction. Most of the flow near the inner cylinder follows anticlockwise angular direction and rest of the angular component converted to a tangential one in downward direction in the annulus. While at a higher fin height, the velocity adjacent to the fins is higher. This is mainly due to the smaller stagnant zone by the low fin in the short-fin annulus, helping faster water flow from gap to gap, which can not accelerate the heat transfer rate. The streamlines adjacent to the inner cylinder are wavy in shape as the flow bends near the tip of the fins and more convention cells are observed for the long-fin geometry.

The heat transfer between the two cylinders depends on the flow velocity, the surface area, and the flow patterns. So, higher velocity leads to higher heat transfer, and larger surface area also enhances the heat transfer rate. In the annulus geometry, the hot upward flow at the top of the inner cylinder gets cold upon impingement on the cold outer wall. The local heat transfer rate is high at this region of impingement. The region of impingement enlarges in case of long-fin geometries. Besides this, the stagnant zone due to the fins is remarkably efficient for the long-fin geometry. Due to blockage, fluid can contact closely with the outer wall of the inner cylinder, thus fluid can take away more heat for long-finned annulus. The upward motion of the hot fluid causes the isotherms to be packed densely at the top of the outer and lower portions of the inner cylinder, respectively.



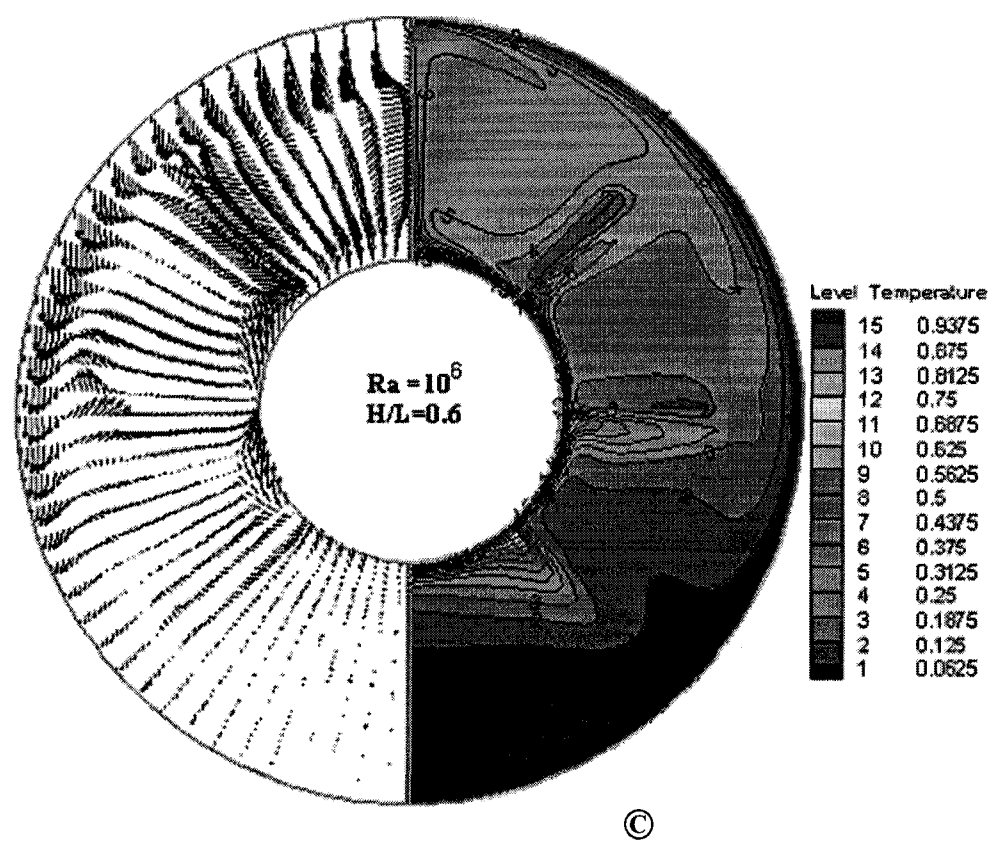
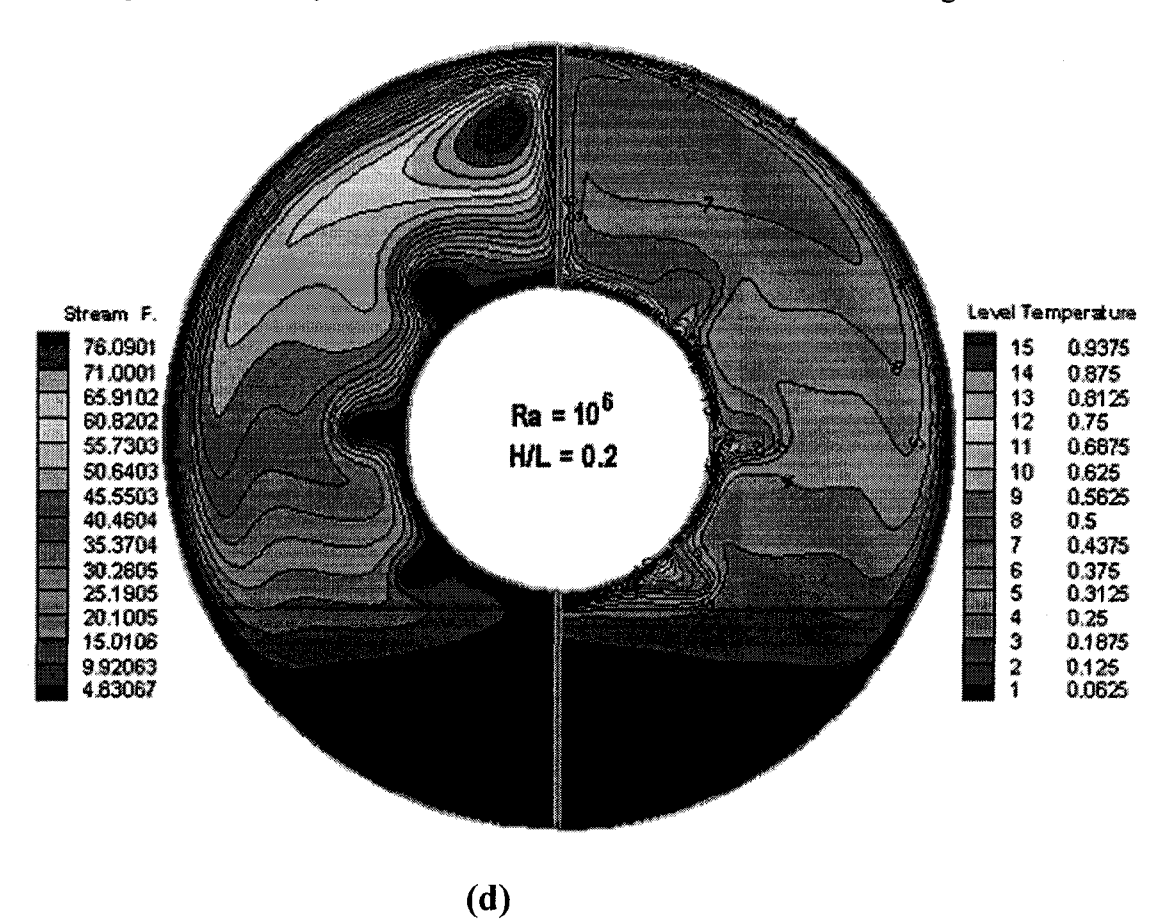


Figure 7: Velocity vectors and isotherms for three different fin heights at Ra=10<sup>6</sup>



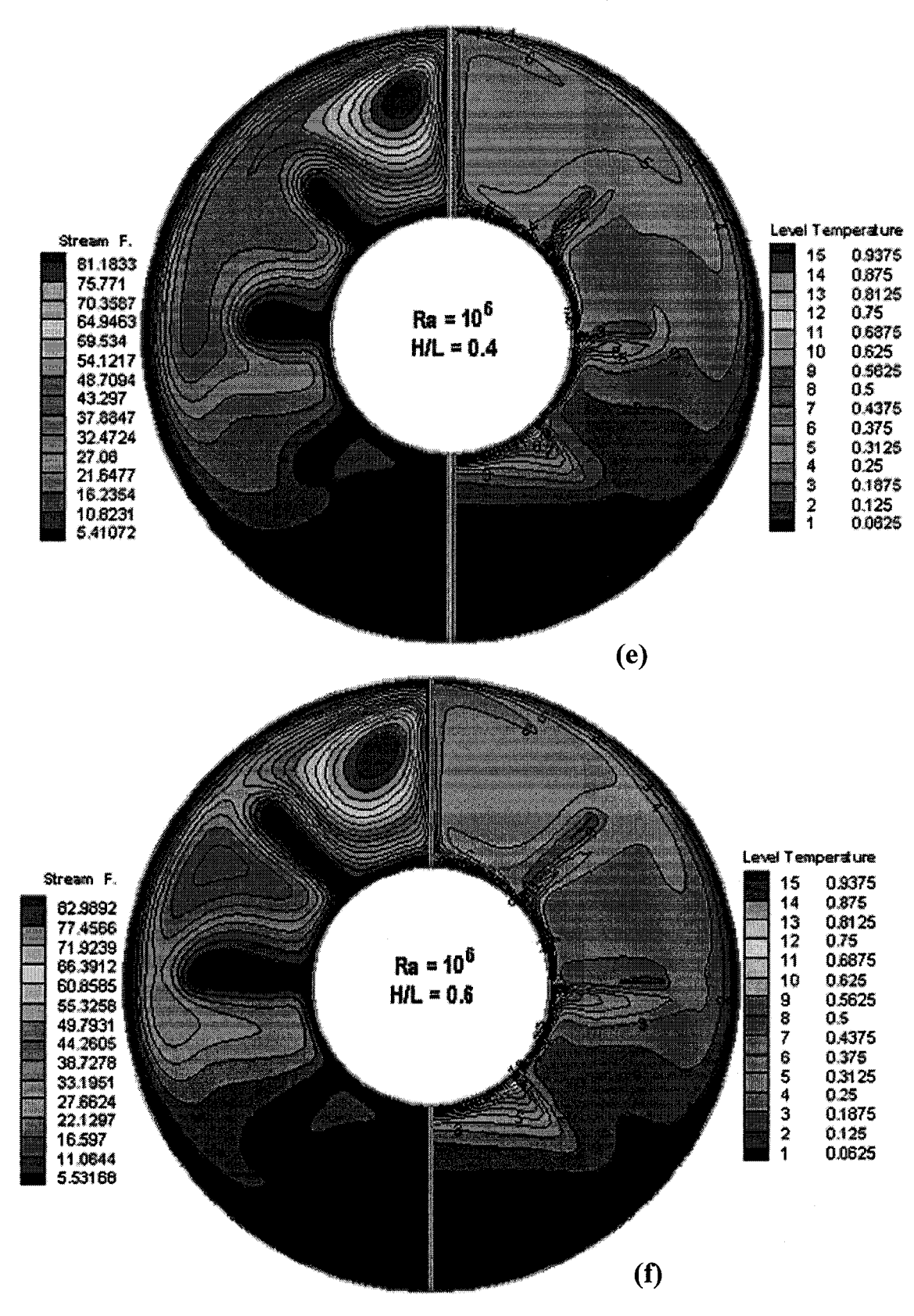
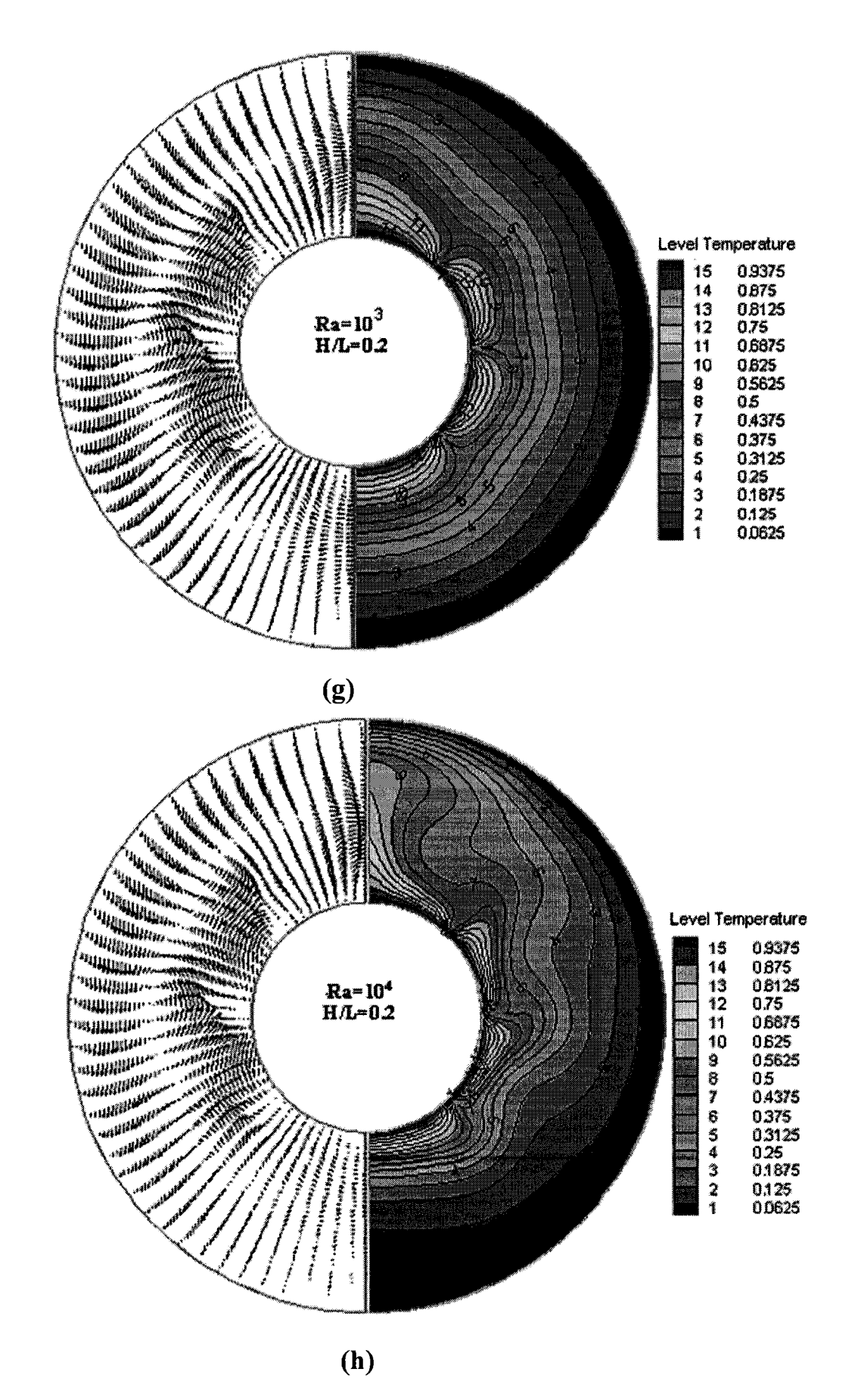


Figure 8: Streamlines and isotherms for three different fin heights at  $Ra=10^6$ 



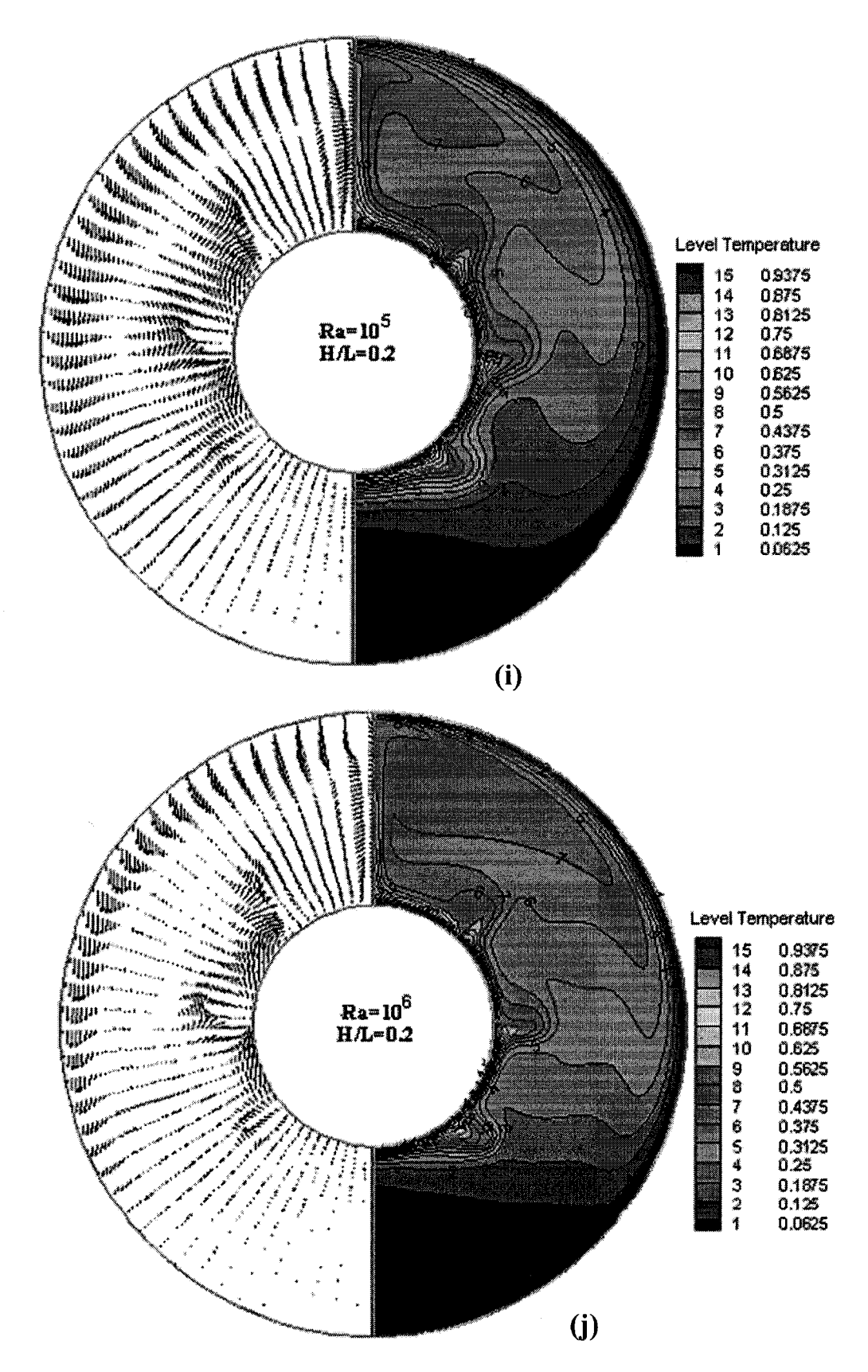
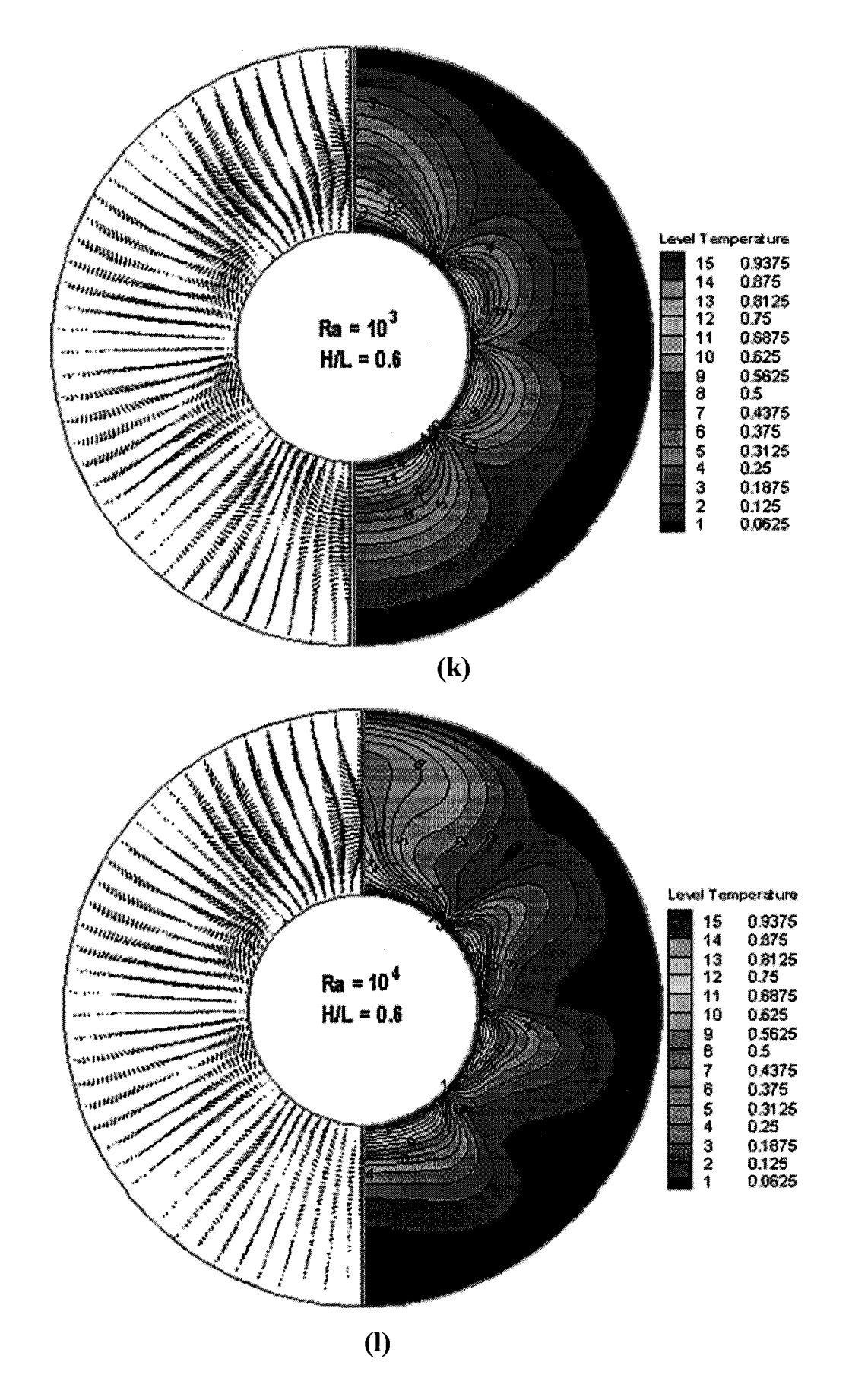


Figure 9: Velocity vectors and isotherms for H/L=0.2



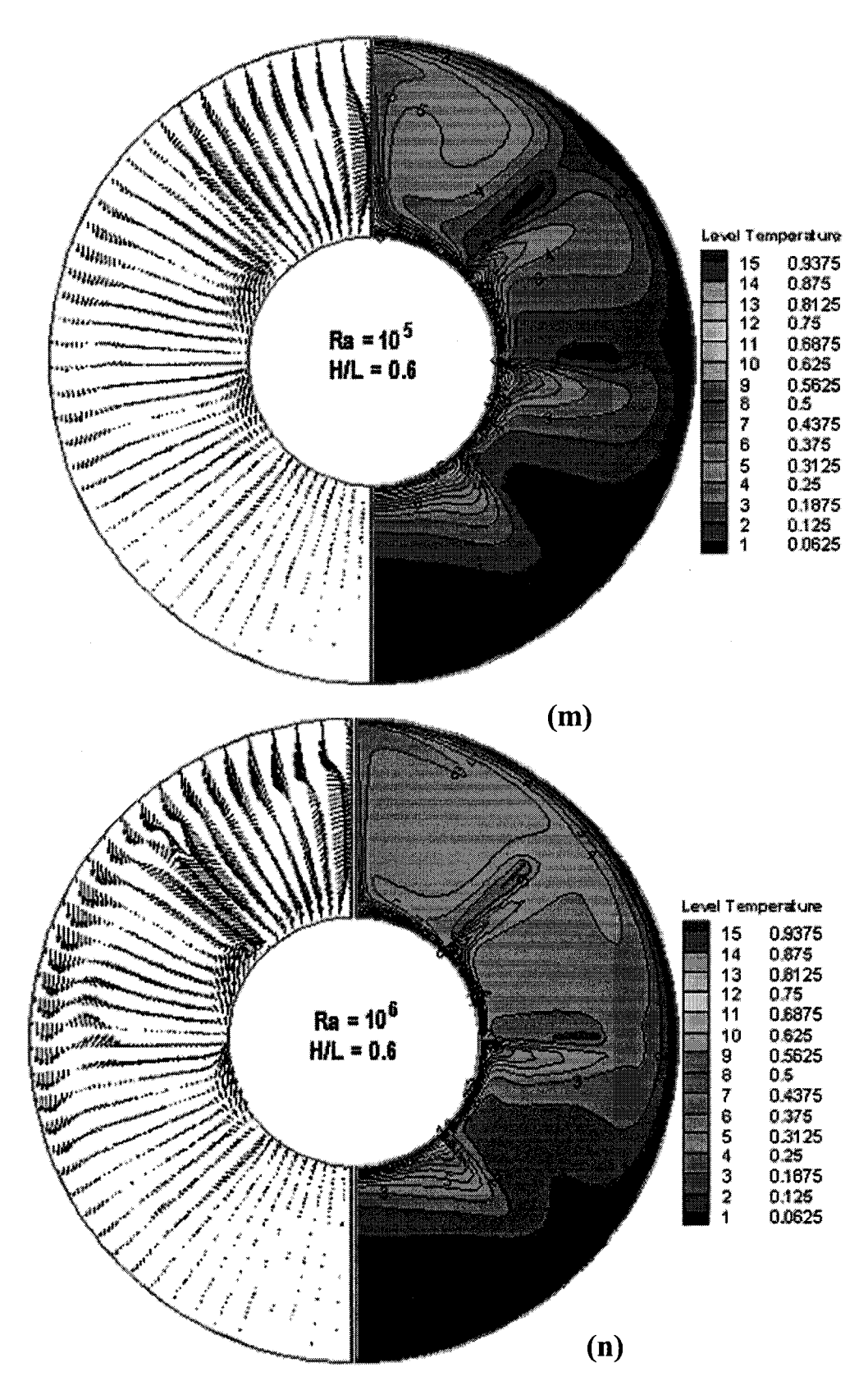


Figure 10: Velocity vectors and isotherms for H/L=0.6

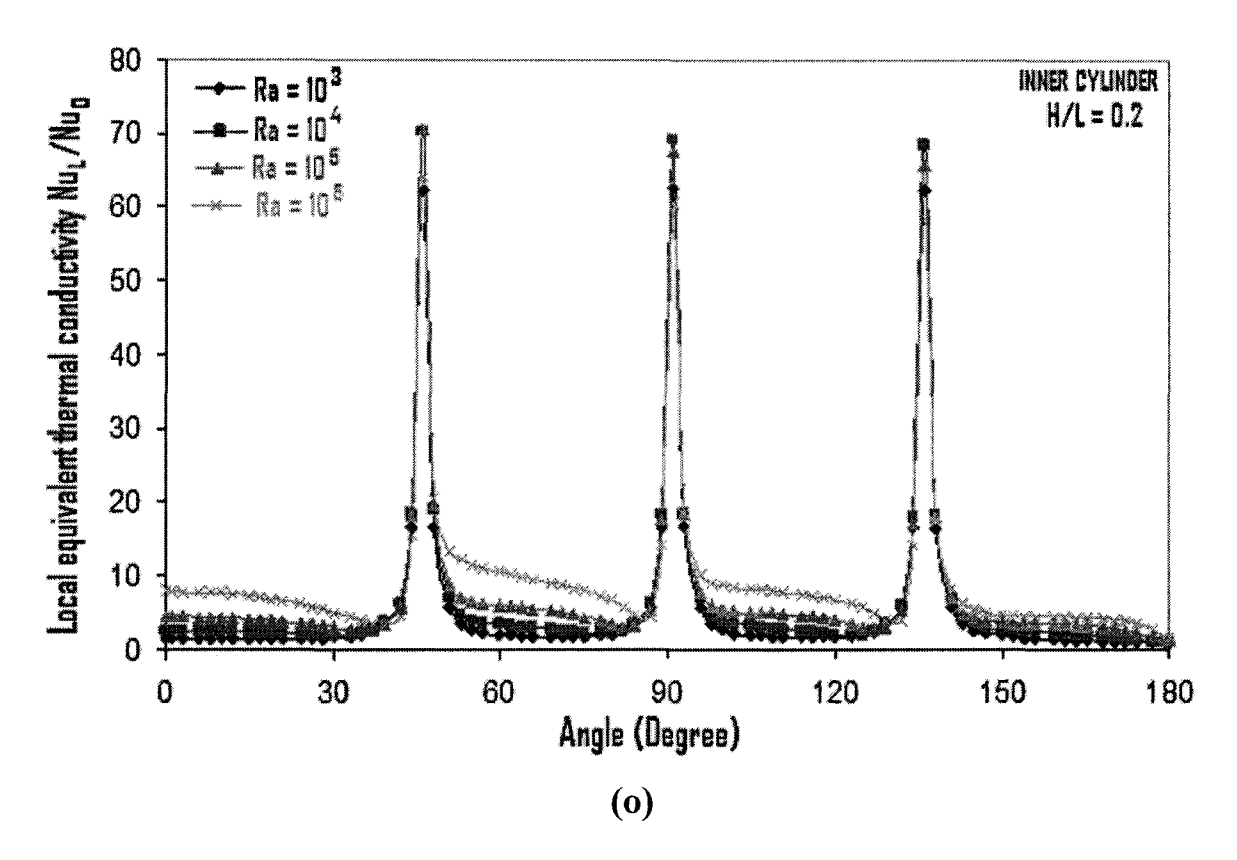
#### Effects of Rayleigh number:

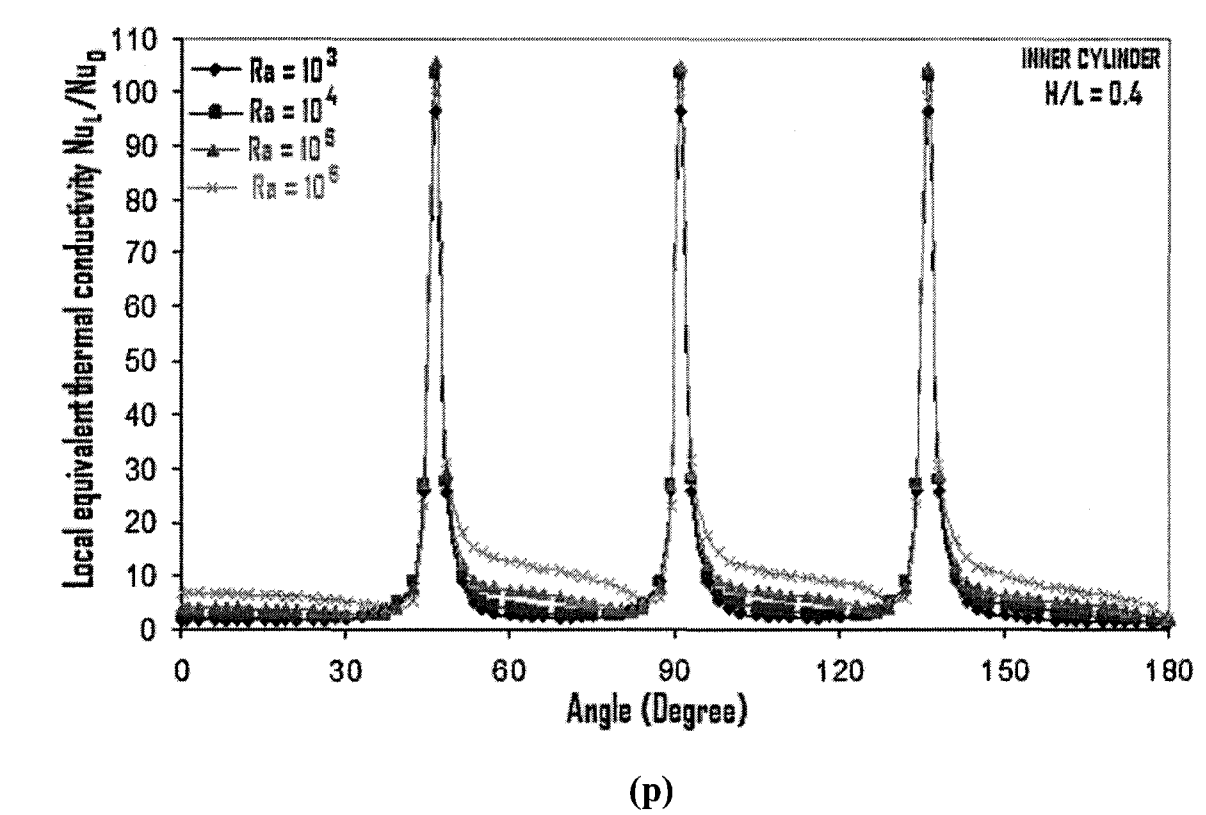
Figures 9(g)-9(j) and Figs. 10(k)-10(n) present the flow patterns and temperature distributions inside the annulus for H/L of 0.2 and 0.6 for Ra varying from 10<sup>3</sup> to 10<sup>6</sup>. These figures represent that the flow recirculation increases with the increase of Rayleigh number and are consistent with the physics of the problem. In the short-fin case, the fins are too short to block the flow between the two gaps of the fins. Besides this, only small impingements are observed at the tip and at the base of the fins. When the Rayleigh number increases, the isotherms follow the contour of the outer cylinder more closely and the isotherms move toward the outer wall of the inner cylinder. This movement is more pronounced near the lower part of the inner cylinder; thus distorting the symmetric nature of the isotherms when Rayleigh number increases. This indicates that the local heat transfer coefficient becomes non-uniform with the increase of Ra. Again, the flow blockage due to the fins can be seen in the long-fin geometry, especially at high Rayleigh numbers.

#### Distribution of the local equivalent thermal conductivity:

The local equivalent thermal conductivity is presented in Figures 11(o)-11(q) for the inner cylinder for H/L of 0.2, 0.4, and 0.6 when the non-dimensional radius ratio is 2.6. These figures provide the values of the local equivalent thermal conductivity of internally attached finned geometry on the inner cylinder for  $10^3 \le Ra \le 10^6$ . These figures show a trend which is similar to the trend of the figures for an internally finned horizontal annulus available in the literature. For comparison purposes, the local heat transfer results for fin height to annulus width of 0.2, 0.4, and 0.6 and for Ra of  $10^4$  to  $10^6$  are given in Figs. 12(R)-12(t). A careful inspection shows that for a given fin height, local equivalent thermal conductivity increases with the increase of the Rayleigh number except in the case of fin height to annulus width of 0.2 for which it shows a non-monotonic behavior against Rayleigh numbers. For Ra= $10^4$ , a maximum value of local equivalent thermal conductivity is observed at the fin tips, which deceases with the increase of Ra at the fin-tips. This behavior indicates the existence of the optimal fin height when the number of fins is specified. It is observed that the circulation at Ra= $10^3$  is very weak for all fin heights, leading to a

temperature distributions similar to the conduction situation. The pattern of local equivalent thermal conductivities with respect to angular movement for H/L of 0.2, 0.4, and 0.6 is similar. Here, the local equivalent thermal conductivity starts from a higher value for top of the fin-tip at the bottom and decreases much faster to nearly zero at the base of the fin. From the base of the lower fin surface to the base of the upper fin surface there is an increase and decrease in local equivalent thermal conductivity for every fin up to 180 degrees. This behavior of the local equivalent thermal conductivity can be explained as follows: In regions near the base of the fins, the flow is virtually stagnant due to the resistance imposed on the flow by the fin wall. The fluid in this part attains or nearly attains the temperature of the inner cylinder and fin walls, reducing the transfer of heat. This leads to a near-zero local equivalent thermal conductivity. As fluid moves away from the base, it gains momentum, leading to continuous increase in the velocity. The increase in the velocity removes heat from the wall more effectively. As a result, the heat transfer rate increases as one move towards the tip. And another reason for increasing the heat transfer rate, as we move away from the base of the fin, is the impingement of water on the fin surface which is clearly noticeable at Ra=10<sup>6</sup> in Figs. 7 and 8. The impingement of cold fluid on the hot fin at the fin-tip creates a region of high rate of heat transfer. For all fin heights, in this region a highest heat transfer rate is observed which reveals through the densely packed isotherms at the fin tips as seen in Figs. 9 and 10. Local equivalent thermal conductivity then decreases as it approaches the upper part of the inner cylinder. This is because the heated fluid gradually gets detached from the inner cylinder wall. This region is ordinarily known as the plume region. Figures 12(R), 12(s) and 12(t) show the comparison of the local equivalent thermal conductivity for different ratios of fin height to radius difference at Ra=10<sup>4</sup>, 10<sup>5</sup>, and 10<sup>6</sup>. The local equivalent thermal conductivity increases with the increase of the fin height no matter what the Rayleigh number is except at the fin-tip for H/L=0.4 and 0.6 and  $Ra=10^6$ .





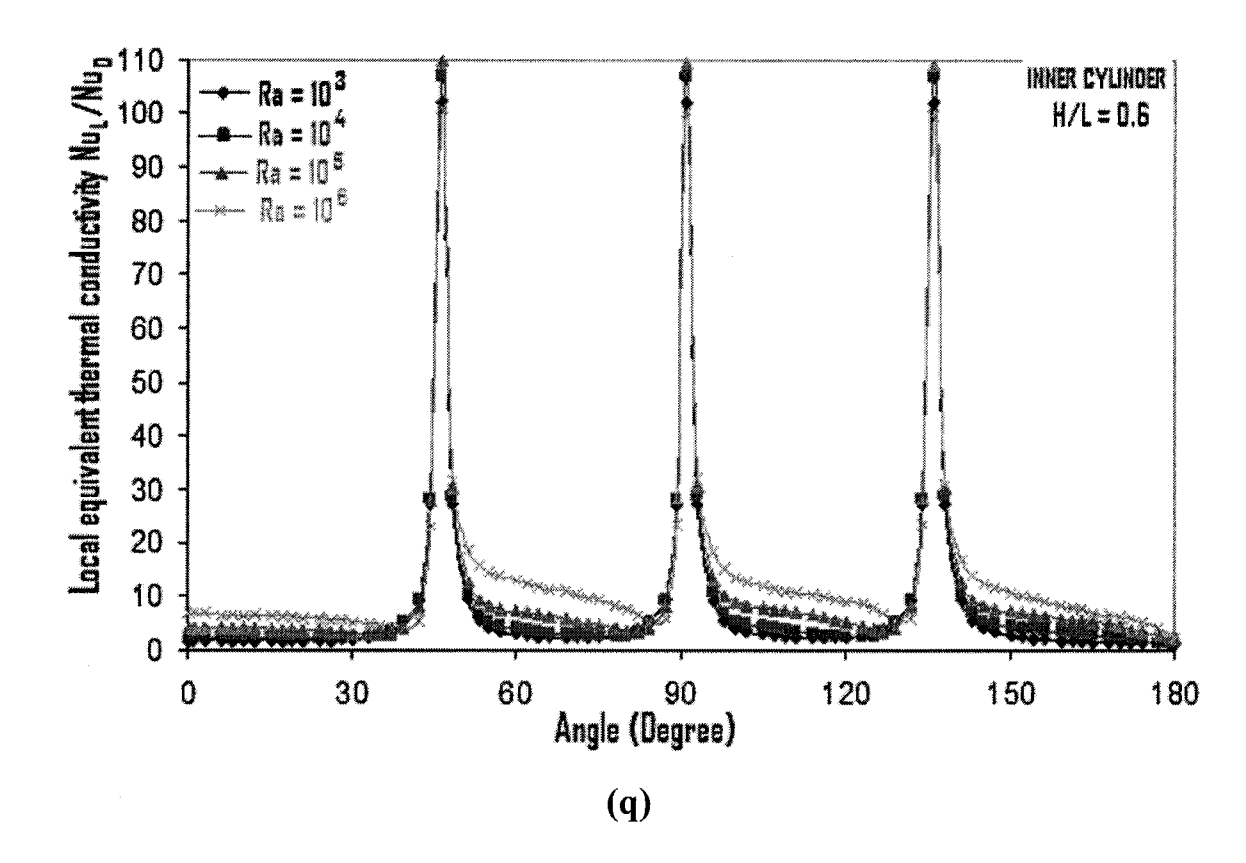
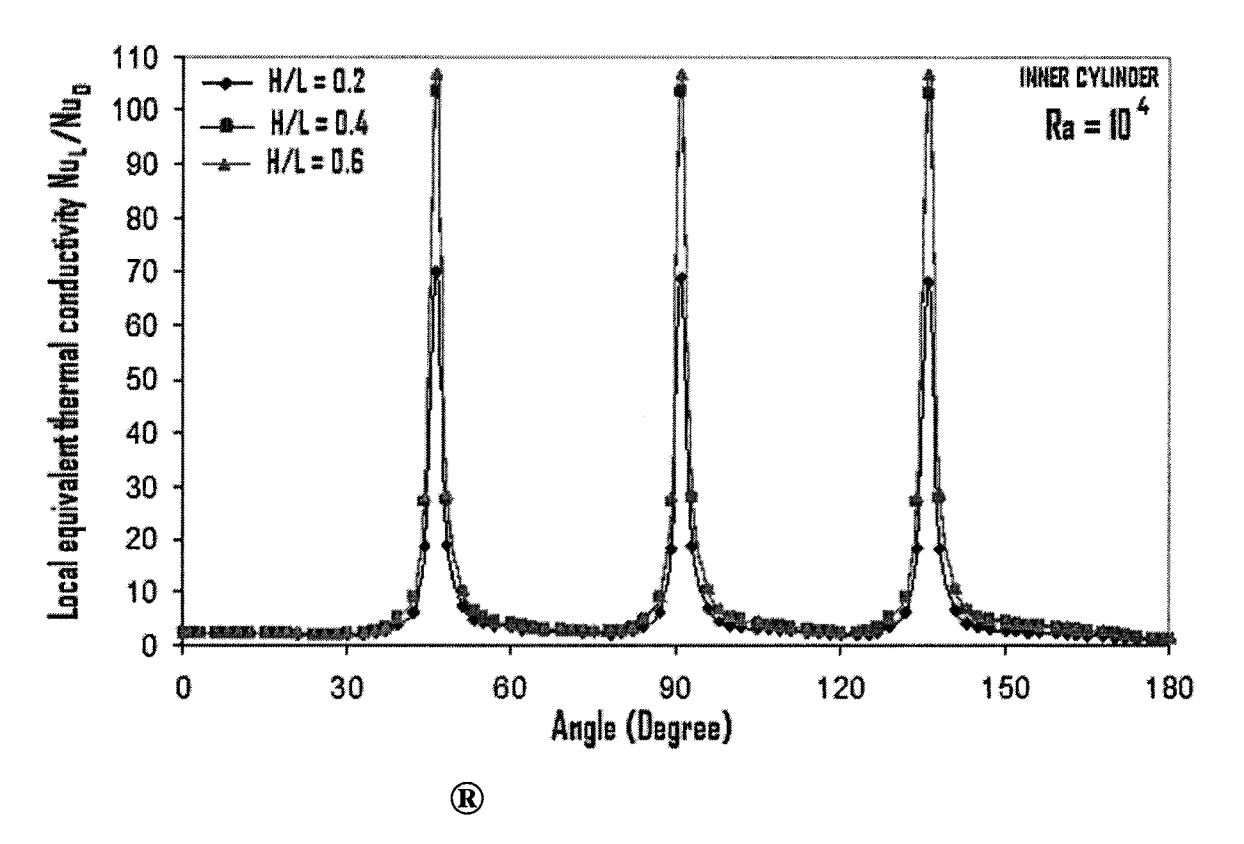


Figure 11: Local Nusselt number variation for the case of fin height (H) at 20%, 40%, and 60% of radius difference (L) for a Rayleigh number of  $10^3$  to  $10^6$ 



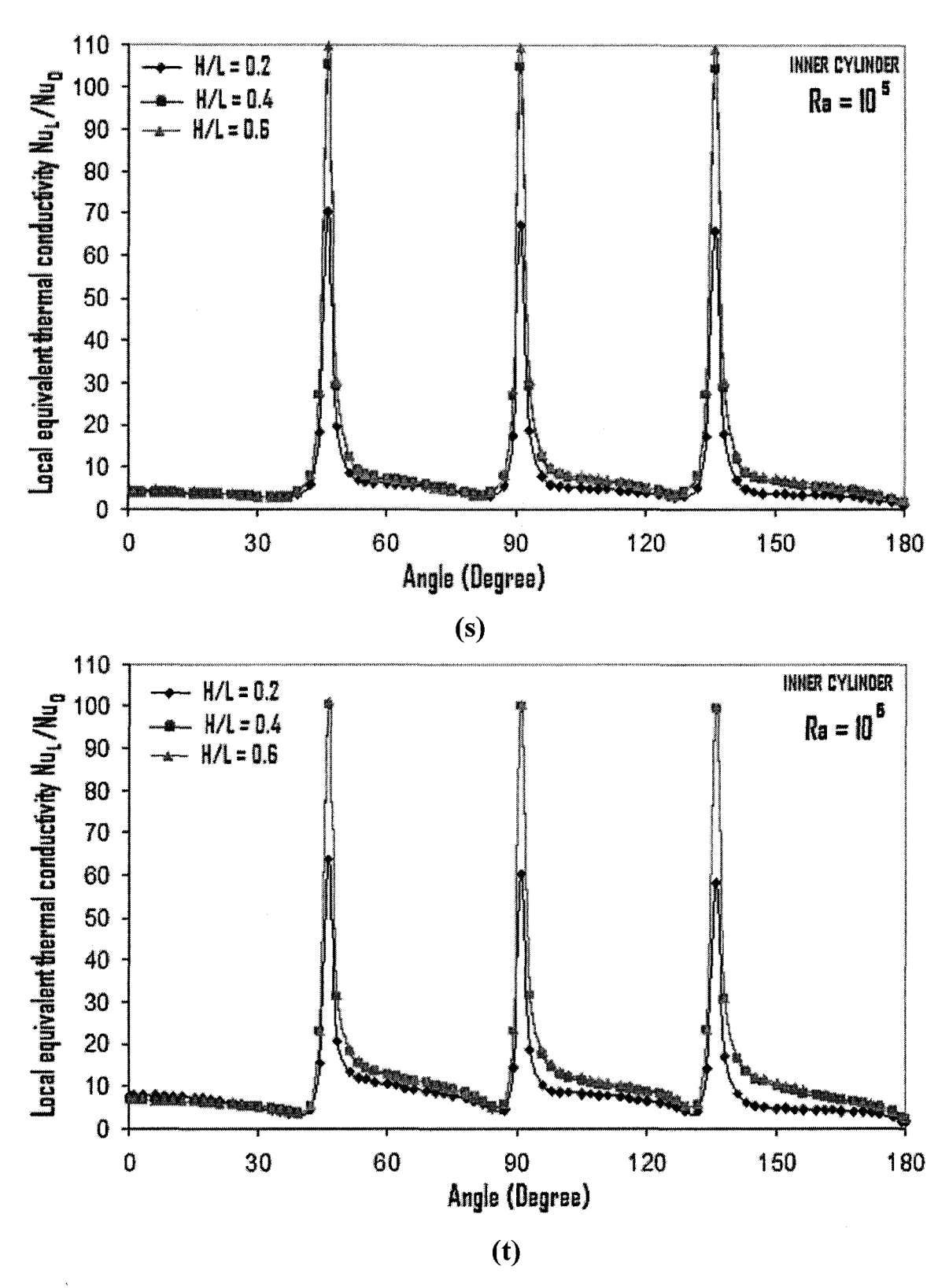


Figure 12: Comparison of Local Nusselt number variation for the case of fin height (H) at 20%, 40%, and 60% of radius difference (L) for a Rayleigh number of  $10^3$  to  $10^6$ 

# Average equivalent thermal conductivity:

Figure 13 shows the average equivalent thermal conductivity for three values of H/L as a function of Ra for the horizontal annulus with no fins. As discussed earlier, Fig. 7 provides the flow patterns and isotherms for different fin heights. We can easily see that the highest fin generates a flow that has the highest stagnant zone (at the bottom of the geometry), as well as it accelerates more convective flow within the fins gap which contributes more to the heat transfer. The highest fin therefore uses the surface area more efficiently and produces the highest heat transfer rate.

The heat transfer data for water are correlated using a least-squares regression analysis and are expressed below:

$$\overline{K}_{eq_{inner}} = 0.2695 \text{ Ra}^{0.2272}, \quad 10^3 \le \text{Ra} \le 10^6, \text{ for plain cylinder}; \quad R^2 = 99.9\%$$
 (18)

$$\overline{K}_{eq_{inner}} = 2.8602 \text{ Ra}^{0.0946}, \quad 10^3 \le \text{Ra} \le 10^6, \text{ for H/L} = 0.2; \quad \text{R}^2 = 99.1\%$$
 (19)

$$\overline{K}_{eq_{inner}} = 4.5322 \text{ Ra}^{0.0858}, \quad 10^3 \le \text{Ra} \le 10^6, \text{ for H/L} = 0.4; \quad R^2 = 99.3\%$$
 (20)

$$\overline{K}_{eq_{inner}} = 4.8448 \text{ Ra}^{0.0833}, \quad 10^3 \le \text{Ra} \le 10^6, \text{ for H/L} = 0.6; \quad R^2 = 99.1\%$$
 (21)

From the above correlations, it is evident that, as the fin height increases, the Rayleigh number exponent decreases and the value of the constant multiplying factor increases. The decrease in the exponent illustrates that the fin makes the flow less global. This means that when the fin height increases the communication in the cavity decreases and leads to the formation of small convection cells through partitioning the flow. The adequacy of the regression model listed is above 99% for all three fin heights. For Ra=10<sup>6</sup>, three fins of dimensionless height to annulus width ratio 0.6 increase the average equivalent thermal conductivity by 154% over its value for the plain cylinder, whereas the corresponding increase for three fins of dimensionless height to annulus width ratio 0.2 and 0.4 are 77% and 147%, respectively, indicating it is better to use higher fin height.

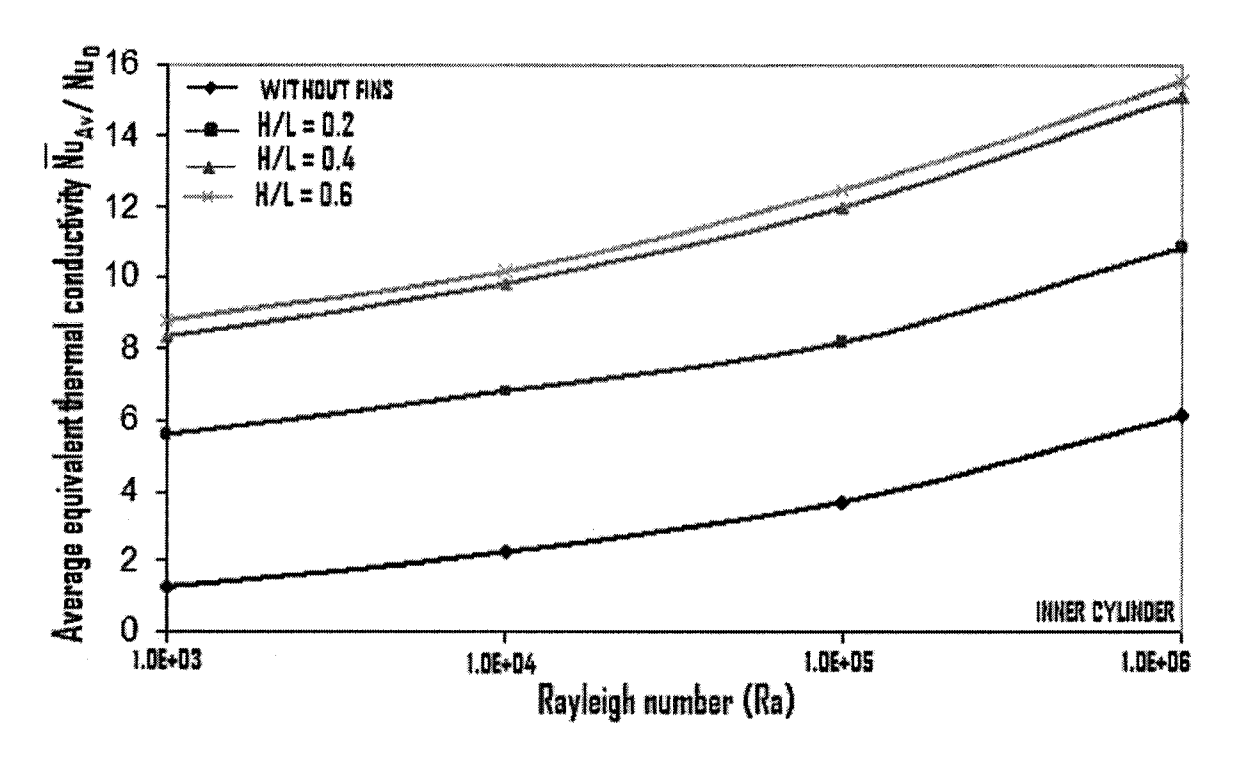


Figure 13: Buoyancy effect on heat transfer from a plain and finned inner cylinder

## **Conclusions**

The problem of laminar natural convection in a horizontal concentric finned annulus is studied numerically. The inner cylinder of the annulus geometry is fitted with six internal longitudinal divergent round tip fins positioned at an equal angular spacing. The flow and heat transfer between concentric horizontal cylinders have been studied for Ra up to  $10^6$ , a fin length up to 0.6 times the radius difference of the cylinders with water as the working fluid. The heat transfer results for the plain cylinder (without fins) are found to be in good agreement with the published experimental and numerical data in the open literature. The following major conclusions can be drawn from this study:

- > For all fin heights, results indicate that heat transfer increases with an increase in Rayleigh number.
- Larger fin height has the highest stagnant zone, there is less communication in the cavity and increased partitioning of the flow into small convection cells occurs. The

highest fin has more surface area. All of the above factors lead to enhance the heat transfer rate between two concentric cylinders in natural convection. It is predicted that heat transfer rate increases with the increasing fin height. Heat transfer results are presented in the form of several correlations to facilitate the design of heat exchangers.

# References

- [1] A. W. Date, "Numerical prediction of natural convection heat transfer in horizontal annulus", Int. J. Heat Mass Transfer, Vol.29, pp.1457-1464, 1986.
- [2] Abu-Hijleh, B. A/K, "Natural Convection and Entropy Generation From a Cylinder with high Conductivity Fins", J. Numer. Heat Transfer, Vol.39, pp. 405-432, 2001.
- [3] Beckmann, W. "Die Warmeubertragung in zylindrischen Gasschichten bei naturlicher Konvektion" Forsch. Geb. d. Ingenieurwesen, Vol. 2(5), pp.165-178, 1931.
- [4] Bishop, E.H. & Carley, C.T. "Photographic studies of natural convection between concentric cylinders" Heat Transfer Fluid Mech. Inst. pp.63-78, 1966.
- [5] Chai JM, Patankar SV, "Laminar natural convection in internally fined horizontal annuli", Numerical Heat Transfer Pt A-Appl, Vol.24, pp.67-87, 1993.
- [6] Charrier-Mojtabi MC, Mojtabi A, Caltagirone JP, "Numerical solution of a flow due to natural convection in horizontal cylindrical annulus", J. Heat Transfer, Vol.101, pp.171-173, 1979.
- [7] Eckert, E. R. G., Goldstein, R.J., Ibele, W. E., Patankar, S.V., Simon, T.W., Kuehn, T.H., Strykowski, P.J., Tamman, K.K., Bar-Cohen, A., Heberlein, J. V. R., Davidson, J. H., Bischof, J., Kulacki, F. A., Kortshagenm, U., and Garrick, S., "Heat Transfer-A Review of 1997 Literature", Int. J. Heat Mass Transfer, Vol.43, pp.2431-2528, 2000.
- [8] Glapke EK, Watkins B jr, Cannon JN, "Constant heat flux solutions for natural convection between concentric and eccentric horizontal cylinders", Numerical Heat Transfer, Vol.10, pp.279-295, 1986.
- [9] Hessami MA, Pollard A, Rowe RD, "Numerical calculation of natural convective heat transfer between horizontal concentric isothermal cylinders-Effects of the variation of the fluid properties", J. Heat Transfer, Vol.106, pp.668-671, 1984.
- [10] Ho Cj, Lin YH, Chen TC, "A numerical study of natural convection in concentric and eccentric horizontal cylindrical annuli with mixed boundary conditions", Int. J. Heat Fluid Flow, Vol.10, pp.40-47, 1989.
- [11] Hu. MH., Chang. YP., "Optimization of finned tubes for heat transfer in laminar flow" J. Heat Transfer, Vol.95, pp.332-338, 1973.

- [12] Kraussold, H. "Warmeabgabe von zylindrischen Flussigkeitsschichten bei naturlicher Konvektion" Forsch. Geb. d. Ingenieurwesen, Vol. 5(4), pp.186-191, 1934.
- [13] K. S. Syed. Mazhar Iqbal. N. A. Mir, "Convective heat transfer in the thermal entrance region of finned double-pipe", Heat Mass Transfer, Vol.43, pp.449-457, 2007.
- [14] Kuehn TH, Goldstein Rj, "An experimental and theoretical study of natural convection in the annulus between horizontal concentric cylinders", J. Fluid Mech, Vol.74, pp.695-719, 1976.
- [15] Kuehn TH, Goldstein Rj, "An experimental and theoretical study of natural convection heat transfer in concentric and eccentric horizontal cylindrical annuli", J. Heat Transfer, Vol.100, pp.635-640, 1978.
- [16] Kumer R, "Numerical study of natural convection in a horizontal annulus with constant heat flux on the inner wall", In: Proc 1987 ASME-ISME Thermal Engineering joint conference, Vol.2, pp.187-193, 1987.
- [17] Liu, C.Y., Mueller, W.K. & Landis, F. "Natural convection heat transfer in long horizontal cylindrical annuli", Int. Developments in Heat Transfer, A.S.M.E. pp.976-984, 1961.
- [18] Masliyah JH, Nandakumar K, "Heat transfer in internally finned tubes" J Heat Transfer, Vol.98, pp.257-261, 1976.
- [19] Marie-Isabelle Farinas, André Garon\*, Katia Saint-Louis, "Study of heat transfer in a horizontal cylinder with fins", Rev Gén Therm, Vol.36, pp.398-410, 1997.
- [20] Mohammad Rahnama\*, Mousa Farhadi, "Effect of radial fins on two-dimensional turbulent natural convection in a horizontal annulus", International Journal of thermal Sciences, Vol.43, pp.255-264, 2004.
- [21] Nieckele, AO., Patankar, SV., "Laminar mixed convection in a concentric annulus with horizontal axis" J. Heat Transfer, Vol.107, pp.902-909, 1985.
- [22] Patankar SV, Ivanovic M, Sparrow EM, "Analysis of turbulent flow and heat transfer in internally finned tubes and annuli", J. Heat Transfer, Vol.101, pp.29-37, 1979.

- [23] Pedersen, B.O., Doepken, H.C. & Bolin, P.C., Development of a compressed-gas-insulated transmission line. I.E.E.E. Winter Power Meeting, paper 71 TP 193-PWR.
- [24] Powe, R.E., Carley, C.T & Bishop, E.H. "Free convective flow patterns in cylindrical annuli" J. Heat Transfer, Vol.91, pp. 310-314, 1969.
- [25] Projahn U, Rieger H, Beer H, "Numerical analysis of laminar natural convection between concentric and eccentric cylinders", Numerical Heat Transfer, Vol.4, pp.131-146, 1981.
- [26] P. F. Hodnett, "Natural convection between horizontal heated concentric circular cylinders", Z. Angew. Math. Phys., Vol.24, pp.507-516, 1973.
- [27] Rustum LM, Soliman HM, "Numerical analysis of laminar mixed convection in horizontal internally finned tubes", Int. J. Heat Mass Transfer, Vol.33, pp.1485-1496, 1990.
- [28] Soliman HM, Chau TS, Trupp AC "Analysis of laminar heat transfer in internally finned tubes with uniform outside wall temperature", J. Heat Transfer, Vol.102, pp.598-604, 1980.
- [29] T. H. Kuehn and R. J. Goldstein, "Correlating equations for natural convection heat transfer between horizontal circular cylinders", Int. J. Heat Mass Transfer, Vol.19, pp.1127-1134, 1976.
- [30] Van de Sande. E, Hamer, BJG., "Steady and transient natural convection in enclosures between circular cylinders (constant heat flux)", Int. J. Heat Mass Transfer, Vol.22, pp.361-370, 1979.
- [31] Voigt, H. & Krischer, O. "Die Warmeubertragung in zylindrischen Luftschichten bei naturlicher Konvektion" Forsch. Geb. d. Ingenieurwesen, Vol. 3(6), pp.303-306, 1932.
- [32] Y. T. Tsui and B. Tremblay, "On transient natural convection heat transfer in the annulus between concentric, horizontal cylinders with isothermal surfaces", Int. J. Heat Mass Transfer, Vol.27, No.1, pp.103-111, 1984.
- [33] Yang, HQ., Yang, KT., Lloyd, JR. "Natural convection suppression in horizontal annuli by azimuthal baffles" Int. J. Heat Mass Transfer, Vol.10, pp.2123-2135, 1988.

# Chapter 2

Natural Convention in a Horizontal Cylindrical Annulus with Equally Spaced Longitudinal Porous Fins

#### **ABSTRACT**

Numerical simulations for natural convection are also carried out for the same cylindrical configuration discussed in Chapter 1 but for porous fins instead of solid fins. The flow and heat transfer in the porous fins are modeled based on Darcy-Brinkmann-Forschiemer equations for porous media. The non-dimensional parameters of this problem are: Rayleigh number (Ra), Darcy number and fin height. Numerical solutions are obtained for  $10^3 \le Ra \le$  $10^6$ ,  $10^{-6} \le Da \le 10^{-2}$ , and  $0.2 \le H/L \le 0.6$ . The results show that, irrespective of the Darcy number, the traditional solid fins provide much higher heat transfer rates compared to the porous fins of the same height and for an identical geometrical configuration. Although the convection current is increased near the inner cylinder for porous fins but this increase in convection is overshadowed due to the decrease in the thermal conductivity of the porous fins compared to the solid fins. For a higher Ra and H/L greater than 0.2 with the increase of Da, the heat transfer rate from the inner cylinder decreases. This might be due to the fact that with the increase of fin height the flow adjacent to the confining walls becomes of boundary-layer type over which the velocity reaches its maximum value. The thermal boundary-layer thickness near the porous fins increases with Da, as a result the heat transfer rate decreases. The average equivalent thermal conductivity decreases with the increase of porosity due to the reduction of the effective thermal conductivity of the porous fins. The latter also contributes in reducing the heat transfer in the annulus with the increase of fin height.

#### 1. Introduction

The fins industry has been trying in different ways to reduce the size and cost of fins and increase the heat transfer rate. The demand of fins is often justified by the high cost of the high-thermal-conductivity metals that are employed in the manufacture of finned surfaces. Compared to the solid fins, the porous fins offer an overall reduction of weight and the associated operating cost of the equipment also decreases which is attractive especially in airplanes, motorcycles and heat exchanger applications. Heat transfer from finned surfaces can be enhanced through accomplishments of the following techniques: (1) increasing the

surface area to volume ratio, (2) increasing the thermal conductivity of the fin, and (3) increasing the convective heat transfer coefficient between the surface of the solid fin and the surrounding fluid.

Large number of works have been conducted to find the optimum shape of fins, Duffin, [1959], Jany and Bejan [1988], Snider and Kraus [1986], Irey [1968], Lau and Tan [1973], Look [1988]. This approach is based on splitting a certain dimension of the fins in an optimal way where the total volume of the material is fixed. For example, Duffin [1959] has used variational calculus to calculate the optimum fin shape. The optimum profile shape of fins with conductivity which is dependent on temperature has been determined by Jany and Bejan [1988]. Snider and Kraus [1986] presented an overview of the fin optimum shaping issue. Look [1988] carried out the optimization process for a fin under the effect of a variable convection heat transfer coefficient.

In the present study, .the longitudinal porous fins are considered with the hope to enhance the fins thermal performance. Due to their larger effective surface area, porous fins should offer a better thermal performance compared to the performance of equal weight convectional solid fins which is the logical expectation.

In the literature, porous substrates of high thermal conductivity have been used to improve the thermal performance of various thermal systems, Alkam and Al-Nimr [1999], Al-Nimr and Alkam [1997 & 1998]. Alkam and Al-Nimr [1999] showed that porous substrates can be used to improve the performance of heat exchangers. Al-Nimr and Alkam [1998] claimed that porous substrates can improve the heat transfer performance of conventional and tubeless solar collector. Porous fins can be manufactured using Aluminum, Copper and Silver metals all of which have a high thermal conductivity.

Most of the numerical studies reported in the open literature on natural convection heat transfer in a cylindrical horizontal annulus have used solid finned annuli. Recently, Abu-Hijleh [2003] discussed the use of permeable fins on the natural convection heat transfer from a horizontal cylinder. In his study, he assumed the fins to be very thin and made of

very high thermal conductivity. In case of a laminar natural convection flow he showed that the permeable fins provide a much higher heat transfer rates compared to the more traditional solid fins for a similar cylinder configuration. But in a real situation fins will have a finite thickness and finite thermal conductivity which contradicts his assumptions. Moreover, he failed to use the porous media equations for his permeable fins. To the best of the author's knowledge, no work on natural convection heat transfer in a horizontal porous finned annulus has been reported in the open literature.

The objective of this study is to investigate numerically the performance of internal porous fins on the natural convective flow patterns, the temperature distributions and the heat transfer rates between concentric horizontal cylinders. A comparison between the performance of the porous-finned and solid finned annuli will also be conducted. In the analysis, the Darcy-Brinkman-Forscheimer model for porous media is adopted to simulate the fluid flow behavior inside the porous fins which are fitted externally to the inner cylinder.

#### 2. Mathematical formulation

Schematic of the problem, showing a case with equally spaced fin distribution is shown in Figure 1 in Chapter 1. Assuming a local thermal equilibrium between the solid and fluid and invoking Boussinesq approximation, the steady-state, two-dimensional conservation equations of mass, momentum and energy for a Newtonian fluid in the conservative form and under laminar convection in a cylindrical annulus and in porous fins are given, respectively as follows:

Using Boussinesq approximation, the density term is given by

$$\rho = \rho_{ref} \left[ 1 - \beta \left( T - T_{ref} \right) \right] \qquad (1)$$

For fluid:

Continuity:

$$\frac{1}{r}\frac{\partial(\rho_r r v)}{\partial r} + \frac{1}{r}\frac{\partial(\rho_r u)}{\partial \theta} = 0 \qquad (2)$$

U-momentum equation:

$$\frac{1}{r}\frac{\partial}{\partial r}(\rho_{r}ruu) + \frac{1}{r}\frac{\partial}{\partial \theta}(\rho_{r}uv) = \frac{1}{r}\frac{\partial}{\partial r}\left(\mu r\frac{\partial u}{\partial r}\right) + \frac{1}{r}\frac{\partial}{\partial \theta}\left(\frac{\mu}{r}\frac{\partial u}{\partial \theta}\right) - \frac{1}{r}\frac{\partial p^{*}}{\partial \theta} + 2\frac{\mu}{r^{2}}\frac{\partial v}{\partial \theta} - \mu\frac{u}{r^{2}} - \rho_{r}\frac{uv}{r} + \rho_{r}g_{\theta}\beta(T - T_{ref})\sin\theta - \dots$$
(3)

V-momentum equation:

Energy equation:

#### For porous fin:

Continuity:

$$\frac{1}{r}\frac{\partial(\rho_r r v)}{\partial r} + \frac{1}{r}\frac{\partial(\rho_r u)}{\partial \theta} = 0$$
 (6)

U-momentum equation:

$$\frac{1}{\varepsilon^{2}} \left\{ \frac{1}{r} \frac{\partial}{\partial r} (\rho_{r} r u u) + \frac{1}{r} \frac{\partial}{\partial \theta} (\rho_{r} u v) \right\} = \frac{1}{\varepsilon * r} \frac{\partial}{\partial r} \left( \mu r \frac{\partial u}{\partial r} \right) + \frac{1}{\varepsilon * r} \frac{\partial}{\partial \theta} \left( \frac{\mu}{r} \frac{\partial u}{\partial \theta} \right) - \frac{1}{r} \frac{\partial p^{*}}{\partial \theta} + 2 \frac{\mu}{\varepsilon * r^{2}} \frac{\partial v}{\partial \theta} - \frac{u u}{\varepsilon * r^{2}} - \rho_{r} \frac{u v}{\varepsilon^{2} * r} + \rho_{r} g_{\theta} \beta \left( T - T_{ref} \right) \sin \theta - \frac{u \mu_{f}}{k} - \frac{C}{\sqrt{k}} \left| u^{2} + v^{2} \right| \rho_{r} u - \dots$$
(7)

V- momentum equation:

Energy equation:

$$\frac{1}{r}\frac{\partial}{\partial r}(\rho_{r}rvT) + \frac{1}{r}\frac{\partial}{\partial \theta}(\rho_{r}uT) = \frac{1}{r}\frac{\partial}{\partial r}\left(\frac{K_{EFF}}{C_{P_{E}}}r\frac{\partial T}{\partial r}\right) + \frac{1}{r}\frac{\partial}{\partial \theta}\left(\frac{K_{EFF}}{C_{P_{E}}}\frac{1}{r}\frac{\partial T}{\partial \theta}\right) - \cdots$$
(9)

The above equations have been non-dimensionalized using the following variables:

$$R = \frac{r}{r_i} \; ; \quad U = \frac{u}{\alpha/r_i} \; ; \quad V = \frac{v}{\alpha/r_i} \; ; \quad \phi = \frac{T - T_{ref}}{T_i - T_0} \; ; \quad Ra = \frac{r_i^3 \beta g(T_i - T_0)}{v\alpha}$$
$$K_{EFF} = \varepsilon K_F + (1 - \varepsilon)K_S$$

$$p^* = \frac{\rho(r_i \operatorname{Pr})^3}{\mu^2} \left[ P + \left( \rho_{\operatorname{ref}} (1 - \beta \Gamma_{\operatorname{ref}}) - \frac{\operatorname{Pr}^2 \rho^3 \beta \Gamma_{\operatorname{ref}}}{\mu} \right) gr \cos \theta \right] - \dots$$
 (10)

For the coordinate system shown in Figure 1 (Chapter 1), the non-dimensionalized conservative form of the governing equations in the flow region and in porous fins can be written as:

#### For flow region:

Continuity:

$$\frac{1}{R}\frac{\partial(RV)}{\partial R} + \frac{1}{R}\frac{\partial U}{\partial \theta} = 0 \qquad (11)$$

U-momentum equation:

$$\frac{1}{R}\frac{\partial}{\partial R}(RUU) + \frac{1}{R}\frac{\partial}{\partial \theta}(UV) = \Pr \frac{1}{R}\frac{\partial}{\partial R}\left(R\frac{\partial U}{\partial R}\right) + \Pr \frac{1}{R}\frac{\partial}{\partial \theta}\left(\frac{1}{R}\frac{\partial U}{\partial \theta}\right) - \frac{1}{R}\frac{\partial P^*}{\partial \theta} + 2\frac{\Pr}{R^2}\frac{\partial V}{\partial \theta} - \Pr \frac{U}{R^2} - \frac{UV}{R} + Ra\Pr \phi \sin \theta$$
(12)

V-momentum equation:

$$\frac{1}{R} \frac{\partial}{\partial R} (RUV) + \frac{1}{R} \frac{\partial}{\partial \theta} (VV) = \Pr \frac{1}{R} \frac{\partial}{\partial R} \left( R \frac{\partial V}{\partial R} \right) + \Pr \frac{1}{R} \frac{\partial}{\partial \theta} \left( \frac{1}{R} \frac{\partial V}{\partial \theta} \right) - \frac{\partial P^*}{\partial R} - 2 \frac{\Pr}{R^2} \frac{\partial U}{\partial \theta} - \Pr \frac{V}{R^2} - \frac{U^2}{R}$$

$$- Ra \Pr \phi \cos \theta \qquad (13)$$
Energy equation:

#### For porous fins:

Continuity:

$$\frac{1}{R}\frac{\partial(RV)}{\partial R} + \frac{1}{R}\frac{\partial U}{\partial \theta} = 0 \qquad (15)$$

U-momentum equation:

$$\frac{1}{\varepsilon^{2}} \left[ \frac{1}{R} \frac{\partial}{\partial R} (RUU) + \frac{1}{R} \frac{\partial}{\partial \theta} (UV) \right] = \frac{\Pr}{\varepsilon} \frac{1}{R} \frac{\partial}{\partial R} \left( R \frac{\partial U}{\partial R} \right) + \frac{\Pr}{\varepsilon} \frac{1}{R} \frac{\partial}{\partial \theta} \left( \frac{1}{R} \frac{\partial U}{\partial \theta} \right) - \frac{1}{R} \frac{\partial P^{*}}{\partial \theta} + 2 \frac{\Pr}{\varepsilon * R^{2}} \frac{\partial V}{\partial \theta} - \frac{\Pr}{\varepsilon} \frac{U}{R^{2}} - \frac{UV}{\varepsilon^{2} * R} - \frac{\Pr}{Da} U - \frac{C}{\sqrt{Da}} \left( \sqrt{U^{2} + V^{2}} \right) U + Ra \Pr \phi \sin \theta - \dots (16)$$

V-momentum equation:

$$\frac{1}{\varepsilon^{2}} \left[ \frac{1}{R} \frac{\partial}{\partial R} (RUV) + \frac{1}{R} \frac{\partial}{\partial \theta} (VV) \right] = \frac{\Pr}{\varepsilon} \frac{1}{R} \frac{\partial}{\partial R} \left( R \frac{\partial V}{\partial R} \right) + \frac{\Pr}{\varepsilon} \frac{1}{R} \frac{\partial}{\partial \theta} \left( \frac{1}{R} \frac{\partial V}{\partial \theta} \right) - \frac{\partial P^{*}}{\partial R} - 2 \frac{\Pr}{\varepsilon * R^{2}} \frac{\partial U}{\partial \theta} - \frac{\Pr}{\varepsilon} \frac{V}{R^{2}} - \frac{U^{2}}{\varepsilon^{2} * R} - \frac{\Pr}{Da} V - \frac{C}{\sqrt{Da}} \left( \sqrt{U^{2} + V^{2}} \right) V - Ra \Pr \phi \cos \theta \quad (17)$$

Energy equation:

# 3. Boundary conditions and assumptions

The dimensionless boundary conditions for the right-half of the annulus are given by:

- On the inner cylinder surface, i.e., Ri=1.0; U=V=0.0;  $\phi = 1.0$
- On the outer cylinder surface, i.e., Ro=2.6; U=V=0.0;  $\phi = 0.0$
- Lower plane of symmetry; i.e.,  $\theta = 0$  ; U=0.0;  $\frac{\partial V}{\partial \theta} = \frac{\partial \phi}{\partial \theta} = 0.0$
- Upper plane of symmetry; i.e.,  $\theta = \pi$ ; U=0.0;  $\frac{\partial V}{\partial \theta} = \frac{\partial \phi}{\partial \theta} = 0.0$
- On the porous fin surface, i.e., U=V=0.0;  $\frac{K_S}{K_E}$  = 647.0

The physical significance of the parameters is given below:

- The relative buoyancy potential is given by the Rayleigh number Ra.
- The relative significance of the inertia term is given by the Prandtl number Pr.
- The relative significance of the permeability term is given by the Darcy number Da.
- The relative significance of the effective surface area is given by the term porosity (  $\varepsilon = 0.4$  ).
- The Forcheimer constant term for inertia in a porous media C = 0.55.

#### 4. Solution and validation

Equations (12)-(19) subject to the above boundary conditions are solved numerically using the control volume finite difference (CVFD) scheme. Patankar's SIMPLER algorithm is used to resolve the pressure-velocity couplings in the momentum equations. A uniform grid net 82x82 and the under relaxation technique are applied. The same convergence criterion reported in Chapter-1 is considered. The procedure of calculation for the average equivalent

(  $K_{eq_{inner}}$  ) and local thermal conductivities on the inner cylinder is described in Chapter-1.

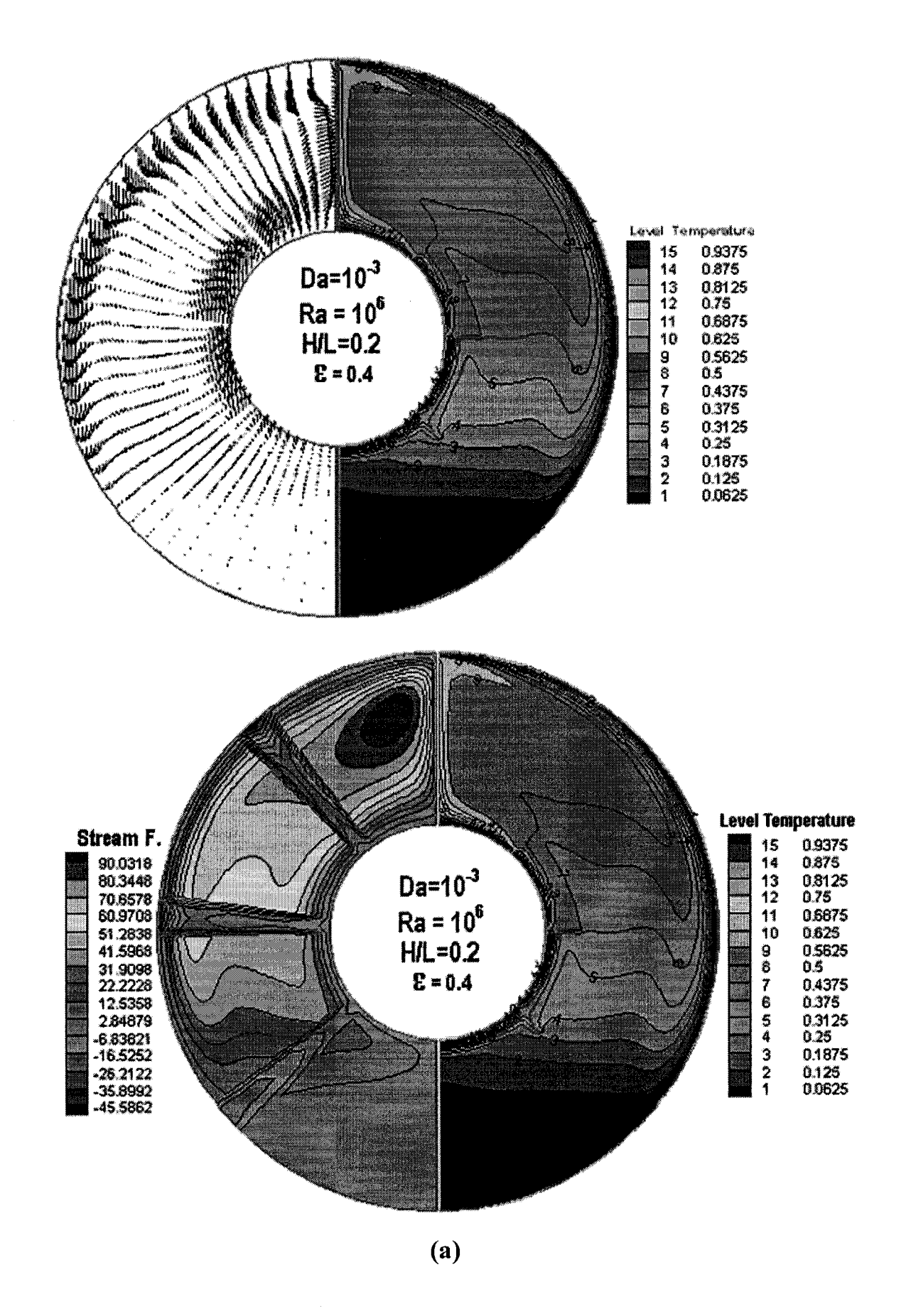
## 5. Results and Discussion

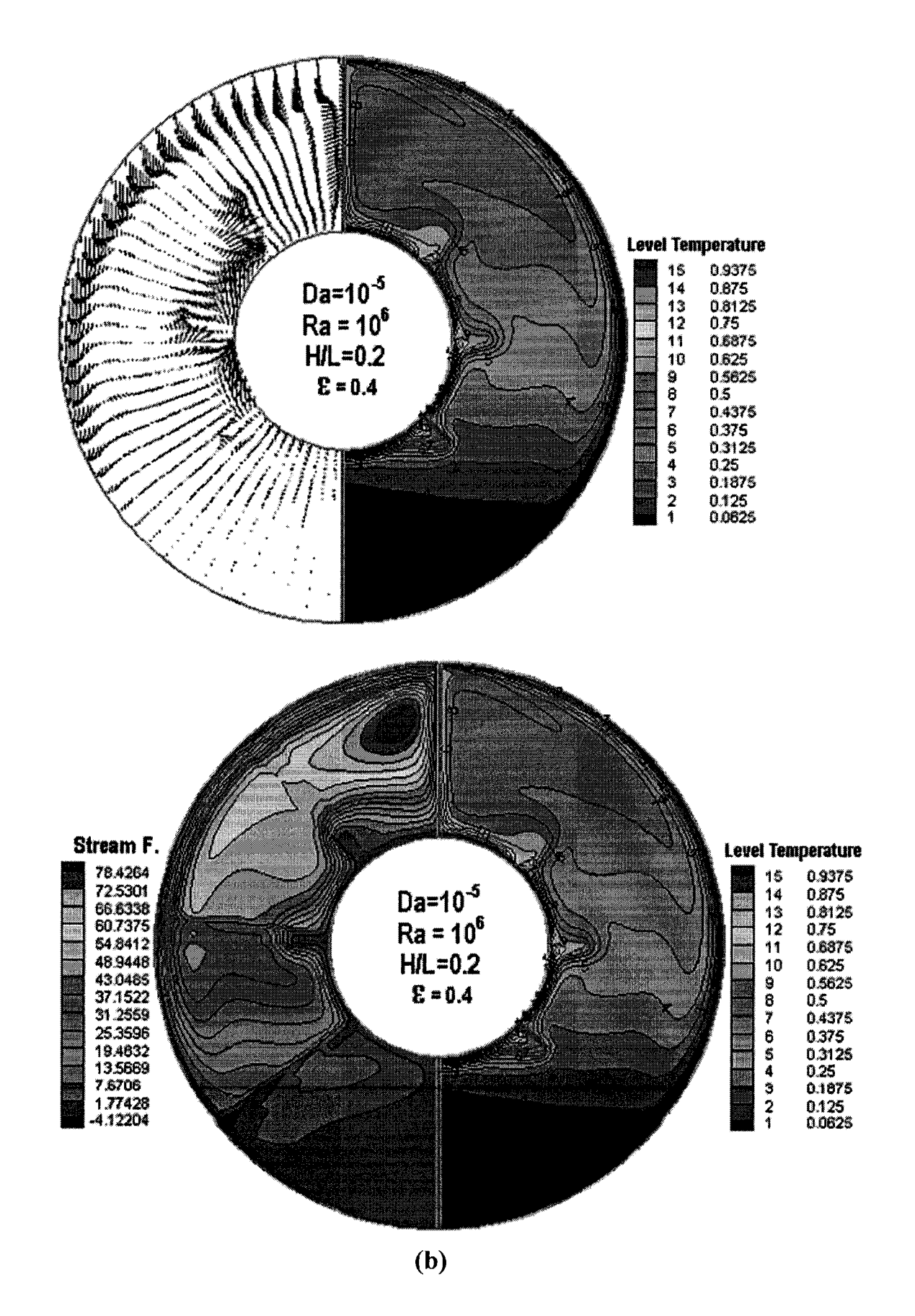
In this section, some representative results are presented to illustrate the effects of various controlling parameters on natural convection heat transfer in a finned, horizontally placed cylindrical annulus. First, the case of permeability of porous medium (represented in the form of Darcy number) is examined. Second, the importance of the internally placed porous fin length effects on the heat transfer is discussed. The buoyancy effect for a range of Rayleigh numbers is also presented in this study. Next, a comparative study between the solid finned cylinder and porous finned cylinder is shown for the same cylinder/fin configuration and flow conditions. Finally, the effect of fin porosity on heat transfer rate is discussed.

# Effect of permeability of porous medium ( Da=10<sup>-6</sup> to 10<sup>-2</sup> )

Typical numerical results are presented in Figures 1a-1c for the case of internally placed porous finned annulus. For a ratio of fin height to annulus width of 0.2, Ra= $10^6$ , porosity  $\varepsilon = 0.4$ , and Da= $10^{-3}$ , the velocity vectors and isotherms, and streamlines and isotherms are presented in Figure 1a. For lower Darcy numbers the evolution of the flow structure in the annulus can be observed from Figs. 1b and 1c, which correspond to Da= $10^{-5}$ , and Da= $10^{-6}$ , respectively. For a fixed porosity of 0.4, Figure 2 illustrates the effect of the angular distance on local equivalent thermal conductivity for Ra= $10^6$  and Darcy varying from  $10^{-6}$  to  $10^{-2}$ . As expected, for a given porosity, the permeability effects are maximum

when Da=10<sup>-2</sup>, i.e., when the flow resistance is minimum. As the value of Da decreases, the flow resistance within the porous fins increases, as a consequence the heat transfer rate reduces. Thus, Figure 2 indicates that heat transfer increases with the increase of Darcy values. Variation of average equivalent thermal conductivity against Rayleigh number at  $\varepsilon = 0.4$ , H/L=0.2, for various Darcy numbers for the present system and for the plain annulus are illustrated in Fig. 3. The trend of this figure is expected, since for a porous finned annulus the rate of heat transfer is expected to increase compared to the plain annulus. For a small fin height, the average equivalent thermal conductivity is enhanced with increasing Darcy values at high Rayleigh numbers. Figure 9 shows that for a fixed porous fin length of 0.2 and Ra  $\geq 10^5$ , with the increase of Da the heat transfer rate increases but for Ra < 10<sup>5</sup>, with the increase of Da, an insignificant change in heat transfer is observed. For a fixed porous fin length of 0.4 and Ra  $\geq 10^5$ , with the increase of Da the heat transfer rate decreases but for Ra < 105, an anomalous behavior in heat transfer rate is observed with the increase of Da. When the porous fin length is 0.6 and Ra  $\geq 10^5$ , heat transfer rate decreases with the increase of Da, but for Ra < 105, with the increase of Da, there is a relatively small change in heat transfer. At lower fin heights, heat transfer rate is enhanced with increasing Darcy values. It is shown that since at increased fin height the flow adjacent to the confining walls becomes of boundary-layer type, with a very thin sublayer over which the velocity reaches its maximum value, then as long as the contribution of the higher Darcy values prevail, the reduction in the heat transfer rate is seen. For this situation the effects of permeability theory is inapplicable, there is no reason to expect that the resulting flow field, within internally porous finned annulus should be parallel for any fin height.





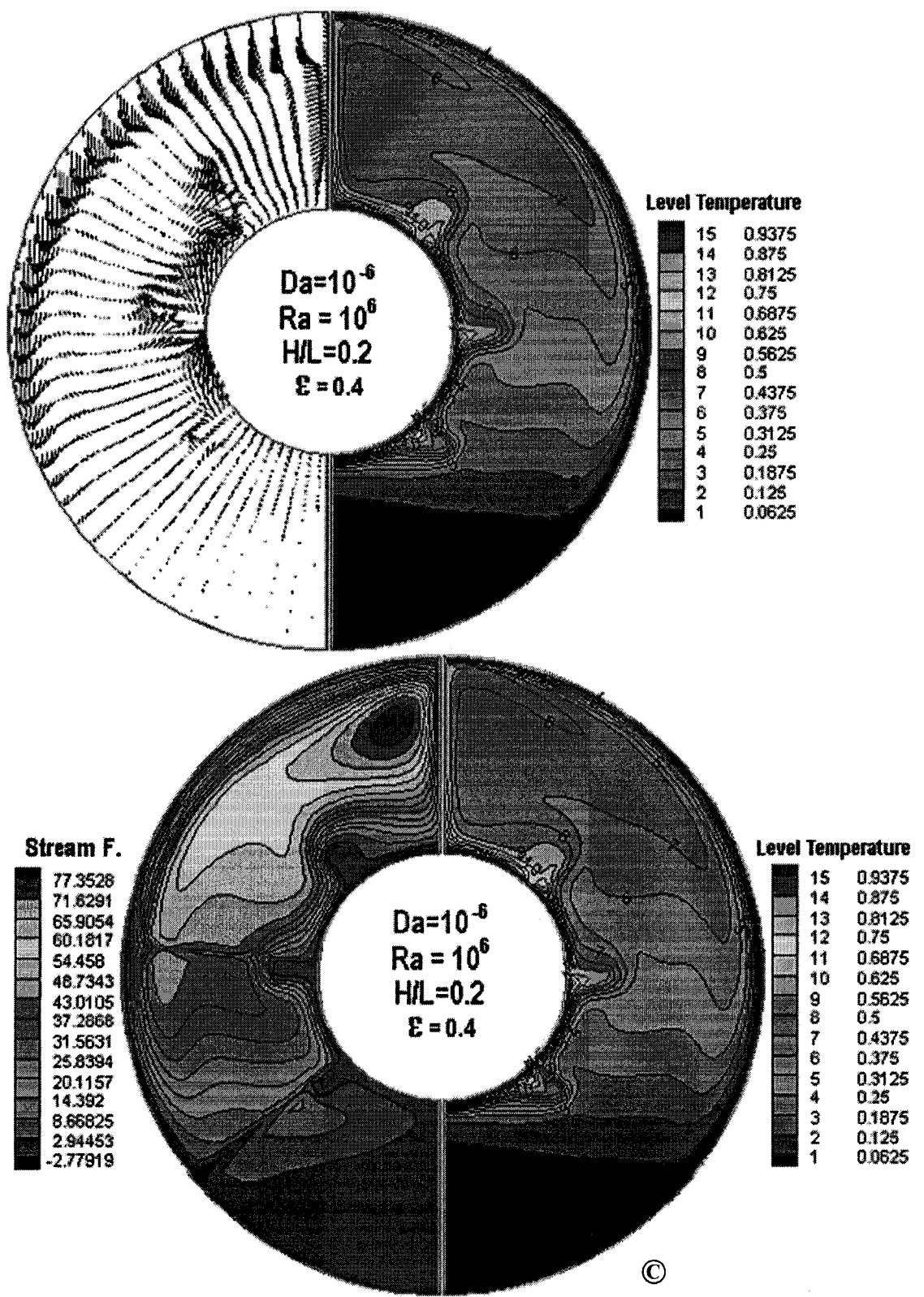


Figure 1: Numerical solutions for the flow and temperature fields, respectively, for an internally porous finned annulus. (a) Ra= $10^6$ ,  $\varepsilon = 0.4$ ,H/L=0.2, Da= $10^{-3}$ ; (b) Ra= $10^6$ ,  $\varepsilon = 0.4$ ,H/L=0.2, Da= $10^{-6}$ 

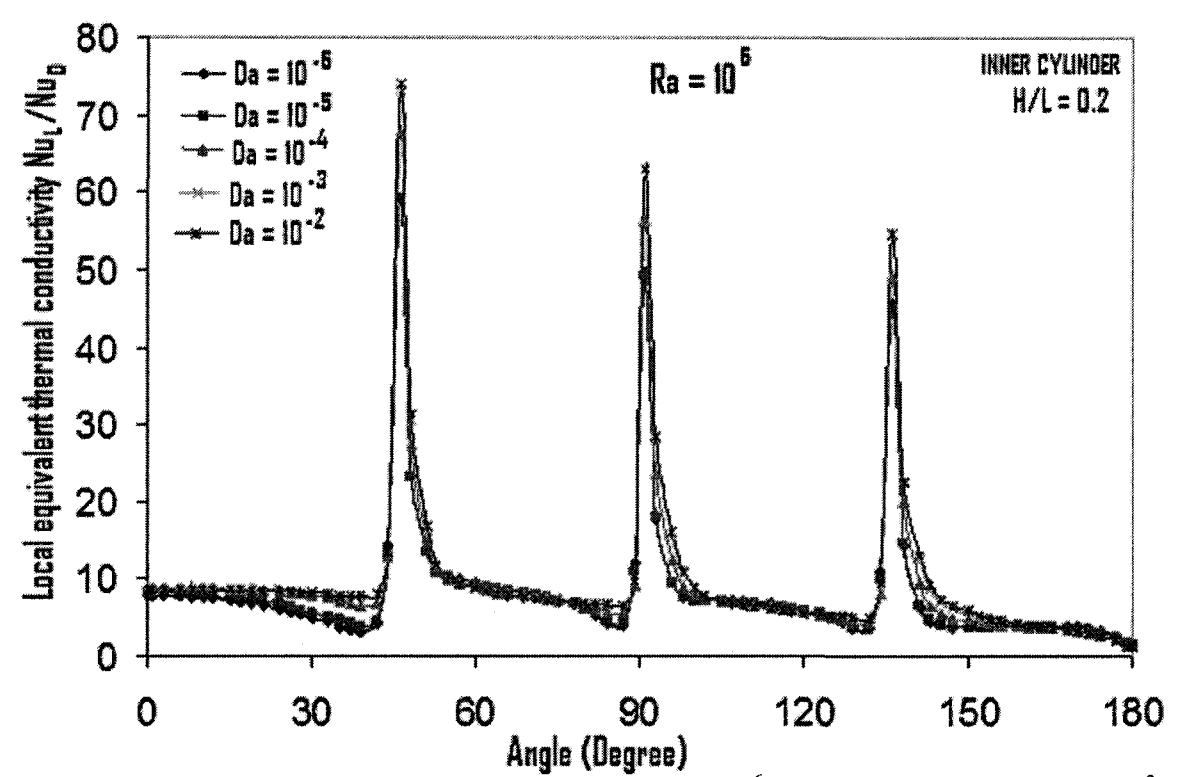


Figure 2: Local equivalent thermal conductivity at Ra= $10^6$ ,  $\varepsilon = 0.4$ , H/L=0.2, for Da= $10^{-3}$ , Da= $10^{-5}$ , and Da= $10^{-6}$ .

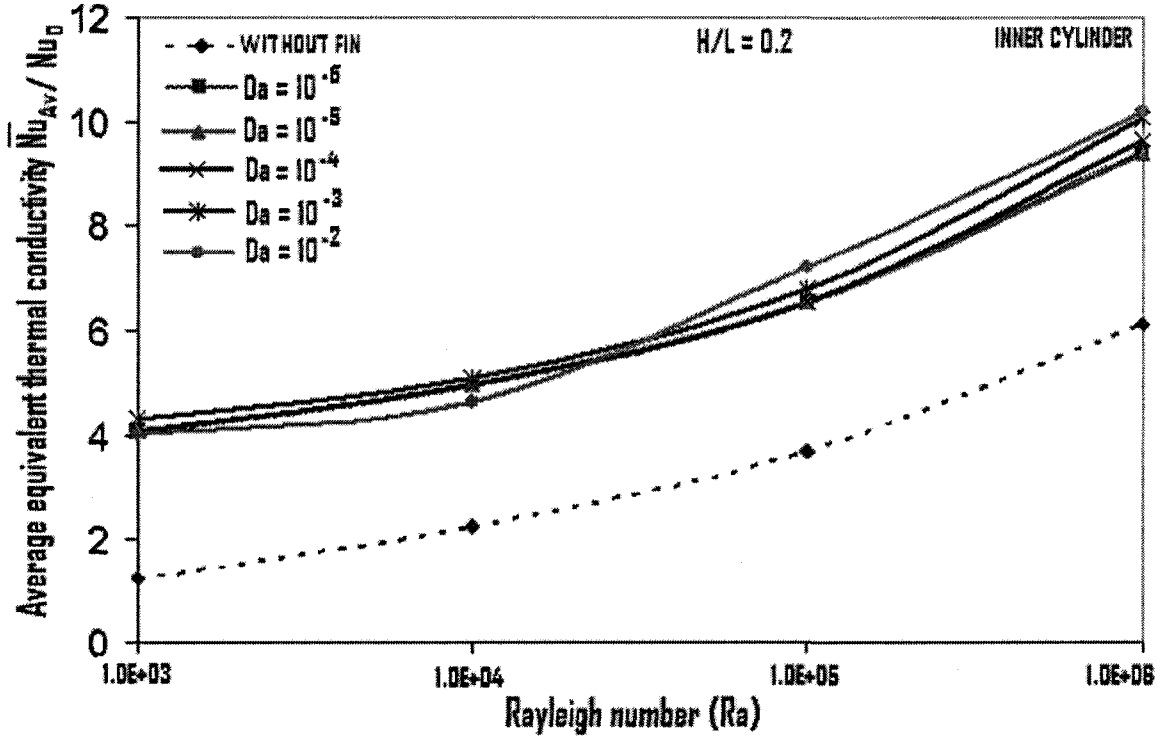
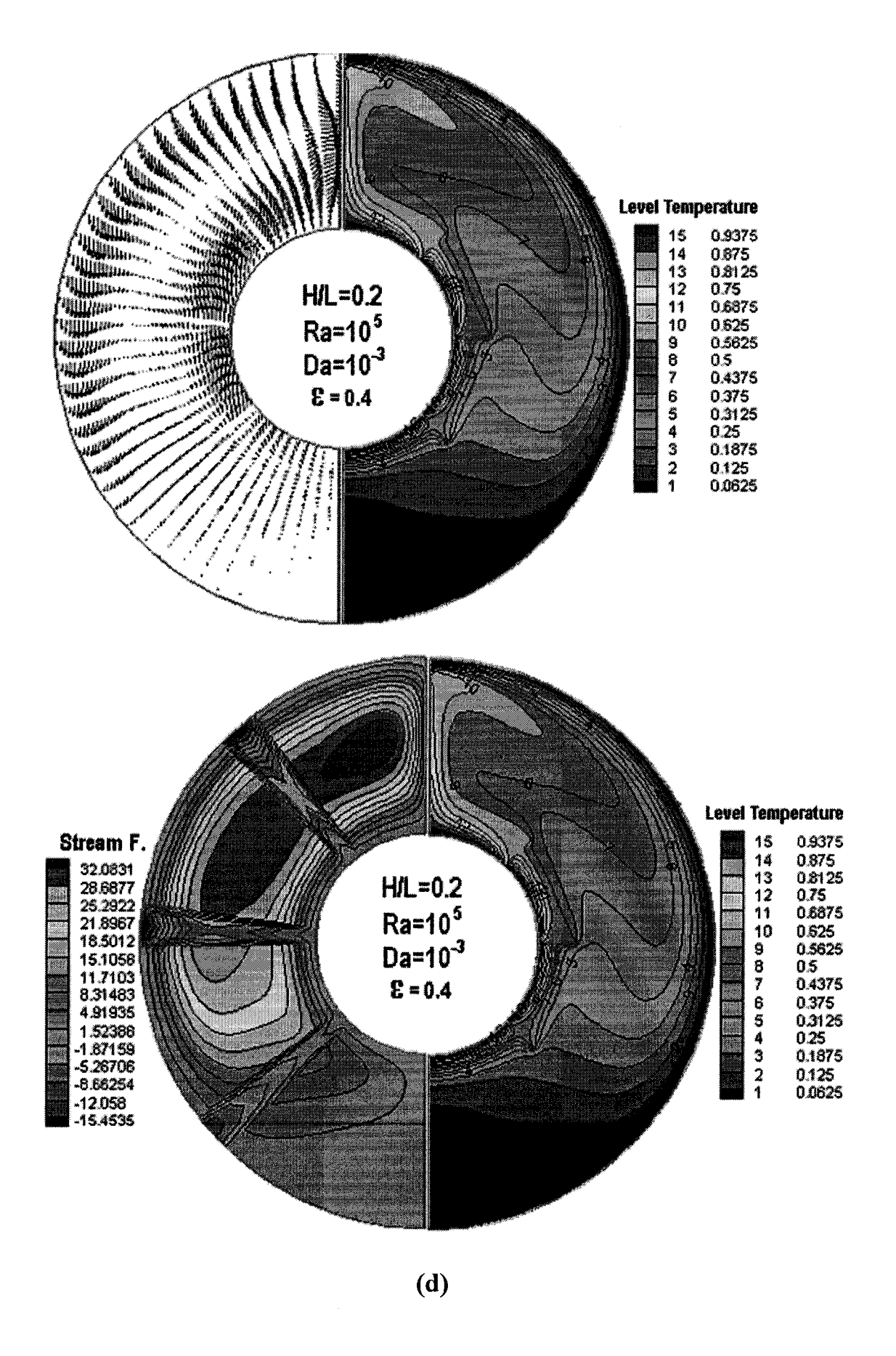
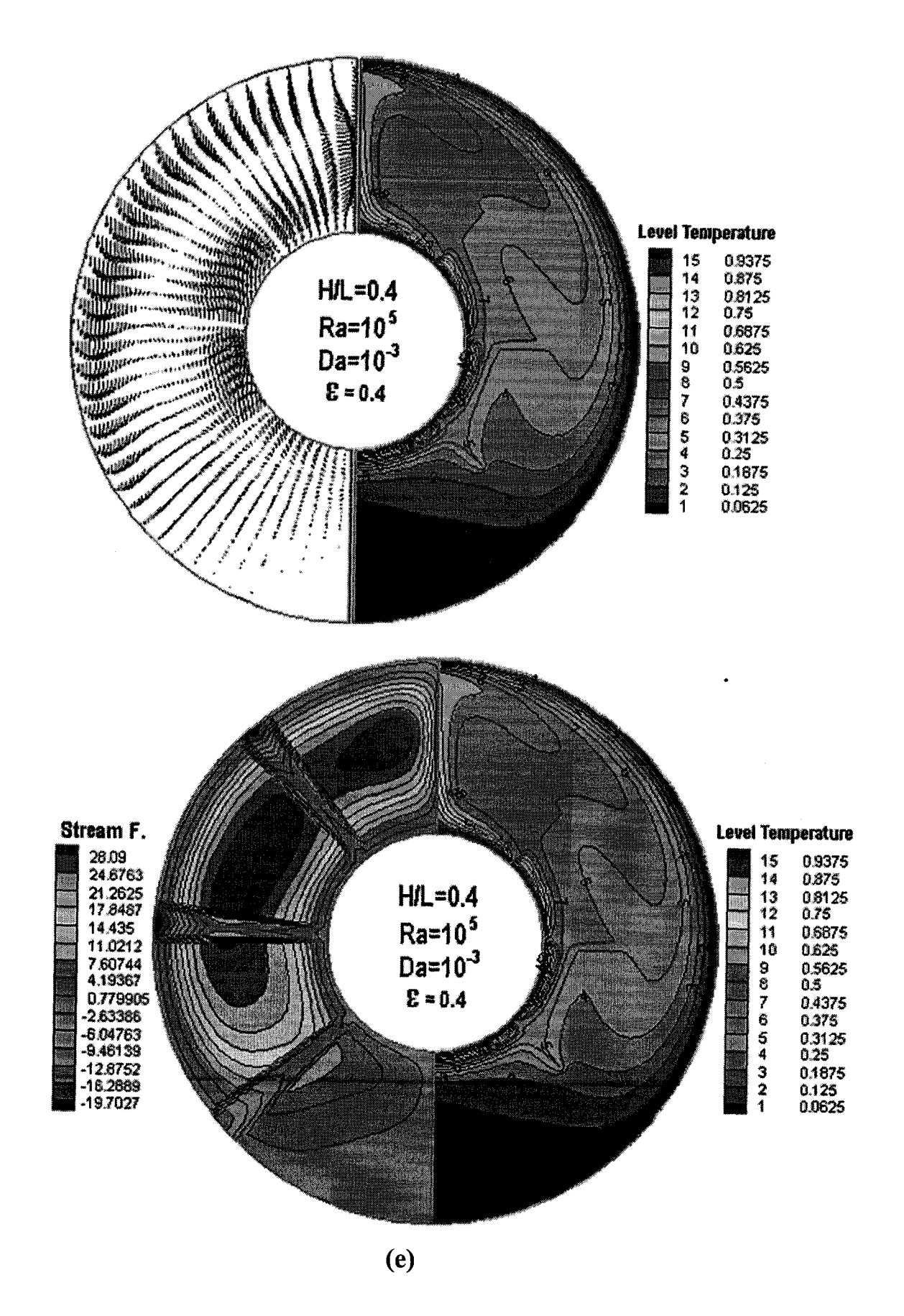


Figure 3: Variation of average equivalent thermal conductivity for various range of Rayleigh number at  $\varepsilon = 0.4$ , H/L=0.2, for Da= $10^{-3}$ , Da= $10^{-5}$ , and Da= $10^{-6}$ 

# Effect of porous fin height (H/L=0.2, 0.4, and 0.6)

The heat transfer between the two cylinders depends on the flow velocity, the surface area (means porosity), permeability (i.e., Darcy number), and the flow patterns. Figure 4(d)-4(f) show the velocity vectors and isotherms, and streamlines and isotherms at Ra=10<sup>5</sup> for internally porous finned annulus (Da=10<sup>-3</sup>, porosity =0.4) with various fin height to annulus width. In the long-fin geometry, the fins blocked the flow between the fins gap. This is clearly shown in the third fin, where the flow impinges on the outer surface before joining the descending fluid. It is also noticed the adverse pressure gradient causes the flow to separate at the lower portion of the outer cylinder at higher Rayleigh number. The transport of cold fluid from the outer cylinder into the porous fin for a low Darcy value of 10<sup>-6</sup> causes the isotherms more distorted which is clearly observed in Figs. 1(c). The guided (by the third fin) impingement on the outer cylinder can also be observed through the densely packed isotherms near the outer cylinder. The upward motion of the hot fluid causes the isotherms to be packed closely at the top of the outer, lower portion of the inner cylinders, and in between the fins gap on the inner cylinder, respectively. Effect of fin height on the local equivalent thermal conductivity corresponding to the parameters shown in Figure 4 is presented in Figure 5. In general, the local Nusselt number increases monotonically with the increase of fin height. This is due to the increase of the blockage effect on the flow and thermal fields between the fins for larger fin heights. The increase of the blockage with fin height makes the flow and heat transfer more localized and results in a higher heat transfer. The numerical results for average equivalent thermal conductivity on the inner cylinder obtained for Da=10<sup>-3</sup> and fin height of 20%, 40%, and 60% of the annulus gap are presented in Figure 6. Figure 6 indicates that compared to the bare inner cylinder, heat transfer rate is increased when porous fins are attached to the inner cylinder. The present numerical solution, based on the Darcy-Brinkman-Forschheimer law for porous fin, correctly predicts the expected heat transfer trend.





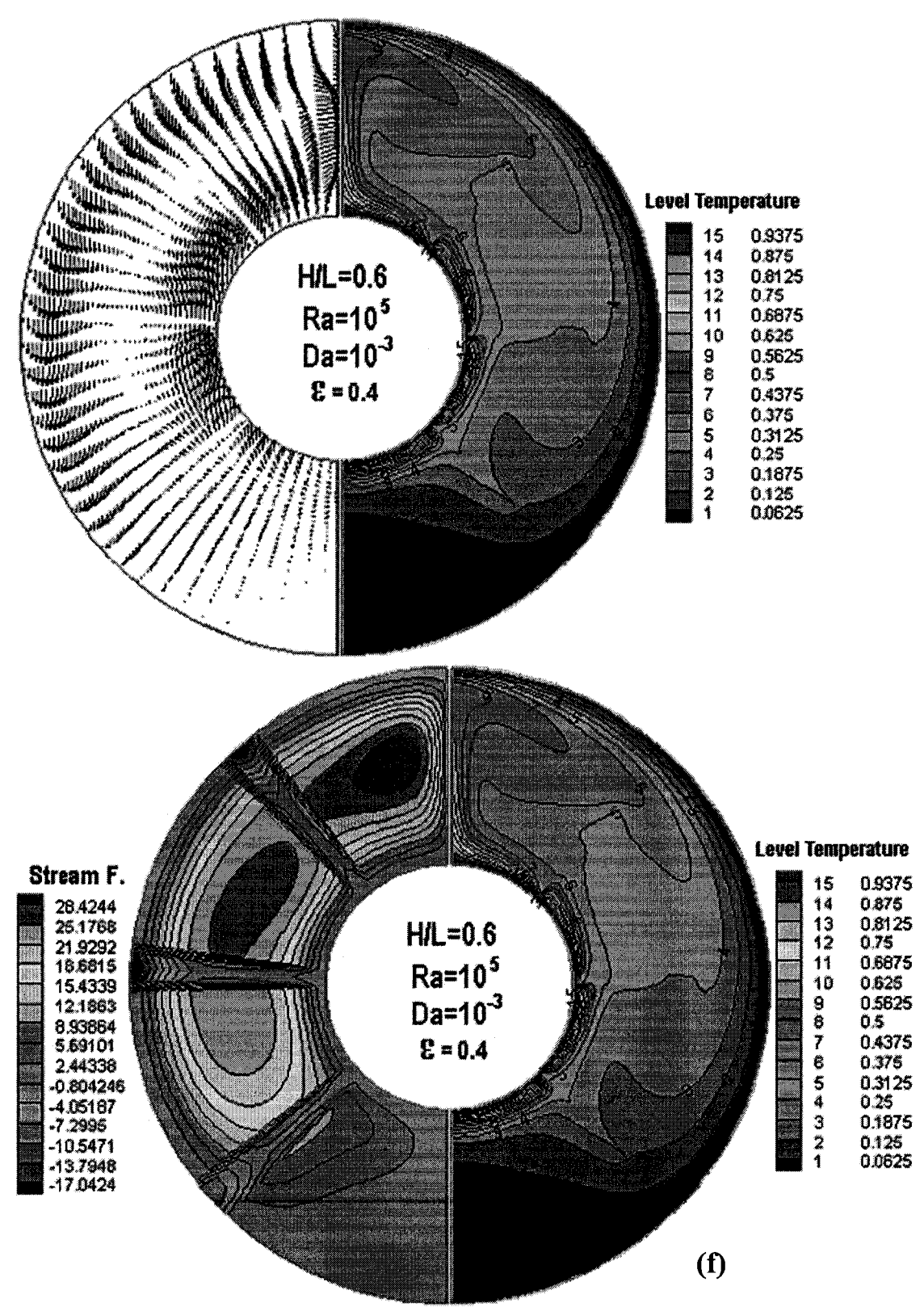


Figure 4: Numerical solutions for the flow and temperature fields, respectively, for an internally porous finned annulus. (d) Ra= $10^5$ ,  $\varepsilon=0.4$ , Da= $10^{-3}$ , H/L=0.2; (e) Ra= $10^5$ ,  $\varepsilon=0.4$ , Da= $10^{-3}$ , H/L=0.4; (f) Ra= $10^5$ ,  $\varepsilon=0.4$ , Da= $10^{-3}$ , H/L=0.6.

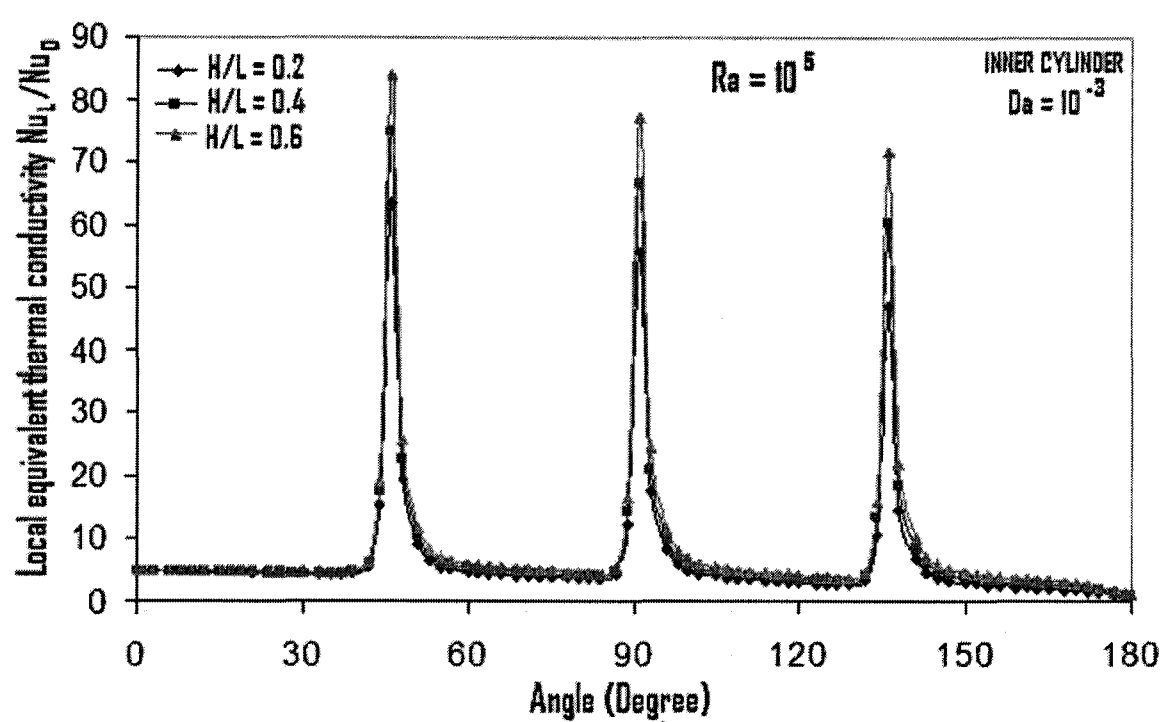


Figure 5: Local equivalent thermal conductivity at  $Ra=10^5$ ,  $\varepsilon=0.4$ ,  $Da=10^{-3}$ , for H/L=0.2, 0.4, and 0.6

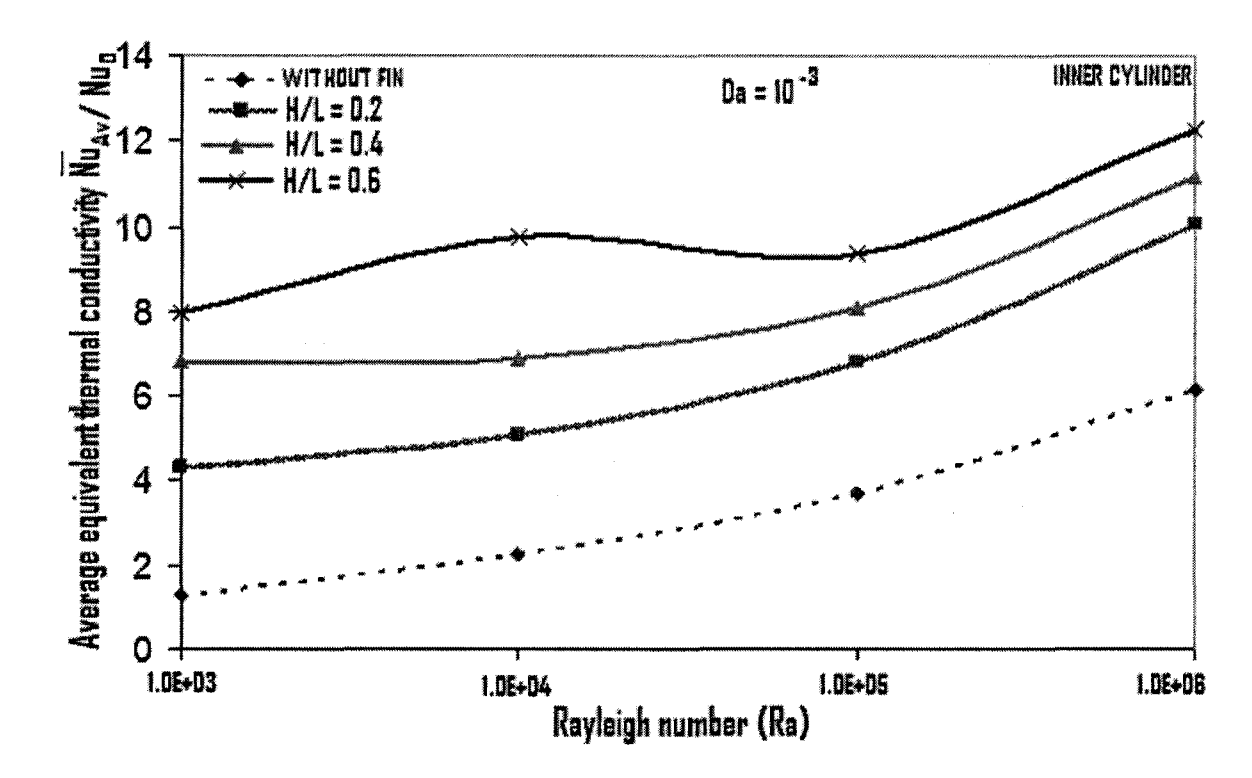


Figure 6: Variation of average equivalent thermal conductivity for various range of Rayleigh number at  $\varepsilon = 0.4$ , Da= $10^{-3}$ , for H/L=0.2, 0.4, and 0.6

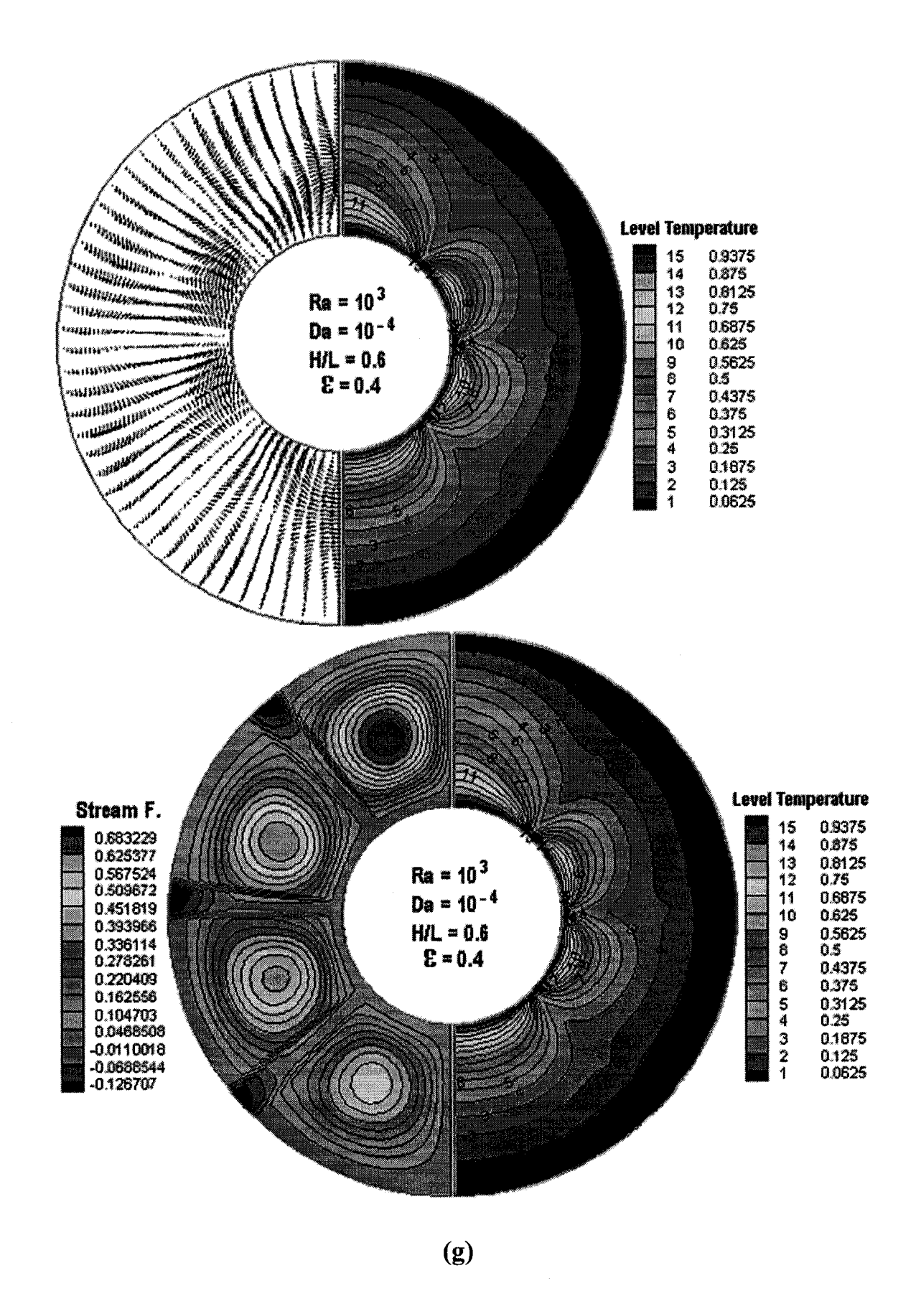
# Effect of Rayleigh number (Ra=10<sup>3</sup>, 10<sup>4</sup>, 10<sup>5</sup>, and 10<sup>6</sup>)

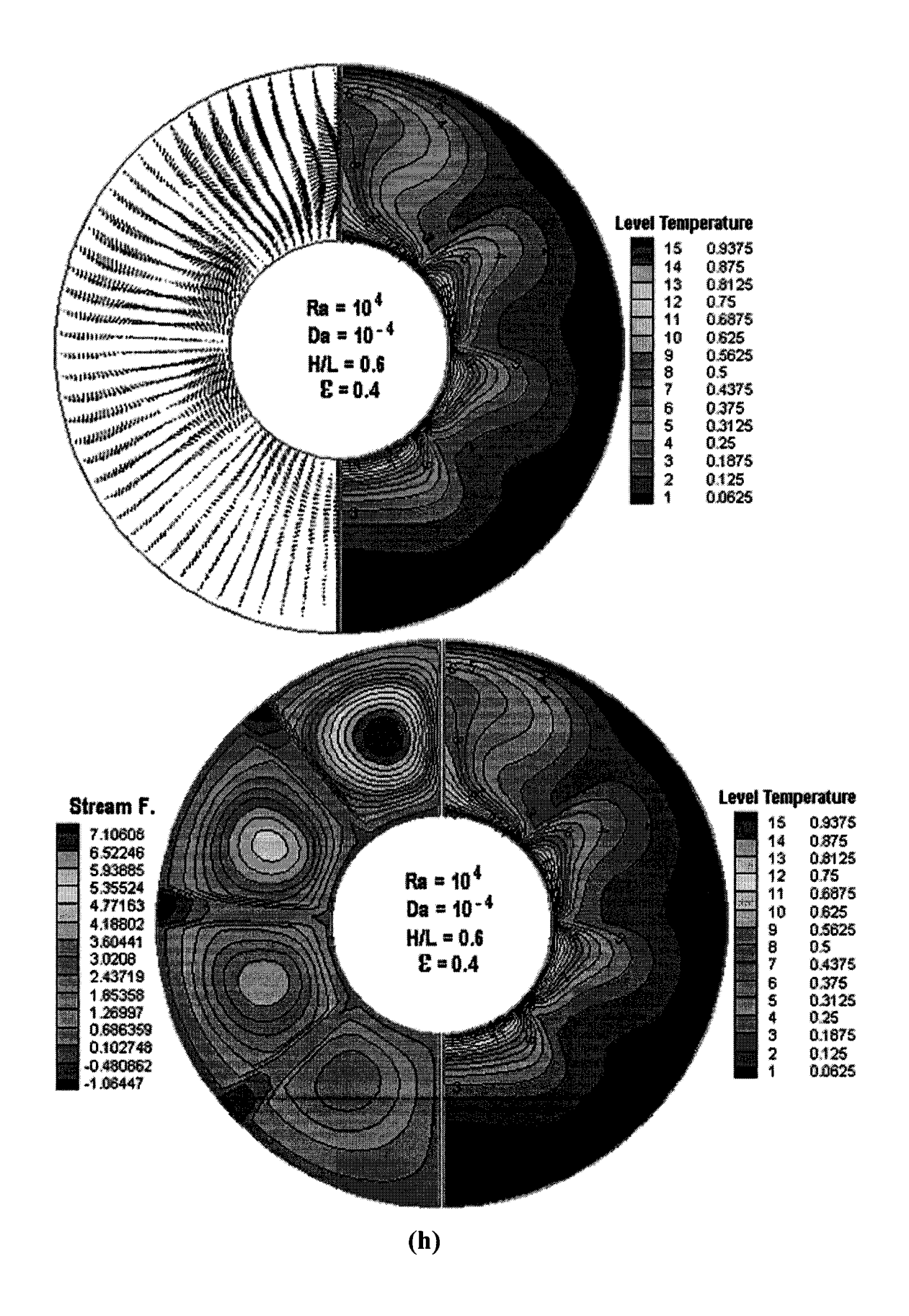
When the Rayleigh number increases, the isotherms follow the contour of the outer cylinder more closely (Figures 7(g)-7(j)). This leads to more uniform heat transfer coefficients on the outer wall. The isotherms also move toward the inner cylinder with increasing Rayleigh number. This movement is more pronounced in the lower part of the inner cylinder and in between the gaps of the fins on the inner cylinder surface, thus distorting the symmetric nature of the isotherms as Rayleigh number increases. Once again, the flow blockage due to the fins can be seen in the long-fin geometry, especially at the high Rayleigh numbers. The overall behavior of the local Nusselt number variations for various Rayleigh numbers at Darcy number 10<sup>-4</sup>, and fin height to width ratio 0.6 is similar. For four Rayleigh numbers Figure 8 shows the similarity in the behavior, that is, the reduction of local Nusselt number along the outer surface of the inner cylinder and increasing and decreasing of the local Nusselt number on the fin's bottom and top surfaces, respectively. It is expected that the initial reduction rate of local Nusselt number would be much higher for higher Rayleigh numbers. It is shown in this figure that the qualitative behavior of local Nusselt number for every Rayleigh number is exactly same as expected, but at the fin tip it differs, where for Ra=10<sup>4</sup> it reaches the maximum value. The reason could be that for Ra=10<sup>4</sup>, the fluid comes in contact with the fin tips more compared with other Rayleigh values. In Fig. 9 the average equivalent thermal conductivity versus Rayleigh number is plotted for different fin heights and for various Darcy numbers. It is observed in this figure that the mean equivalent thermal conductivity increases with increasing Rayleigh number for higher fin heights However, a comparison with Darcy values of Fig. 9 shows a slight dependence on Darcy number for each fin height. In most of the natural convection flows, there is an enhancement in average Nusselt number with the increase in Rayleigh number and Darcy number. For a fin to annulus width of 0.6, the average equivalent thermal conductivity first increases, then decreases and then again increases for Da=10<sup>-3</sup> and this pattern is remarkable. It is observed that there is almost no difference in equivalent thermal conductivity values for Da= 10<sup>-6</sup> and Da=10<sup>-5</sup> in the range of Rayleigh numbers 10<sup>3</sup>-10<sup>6</sup> for the cases of three fin to annulus width ratios. At higher Darcy values, the heat transfer increases for non-dimensional fin height of 0.2, but for 0.4 and 0.6 the heat transfer rate decreases at higher Rayleigh numbers (Fig. 9).

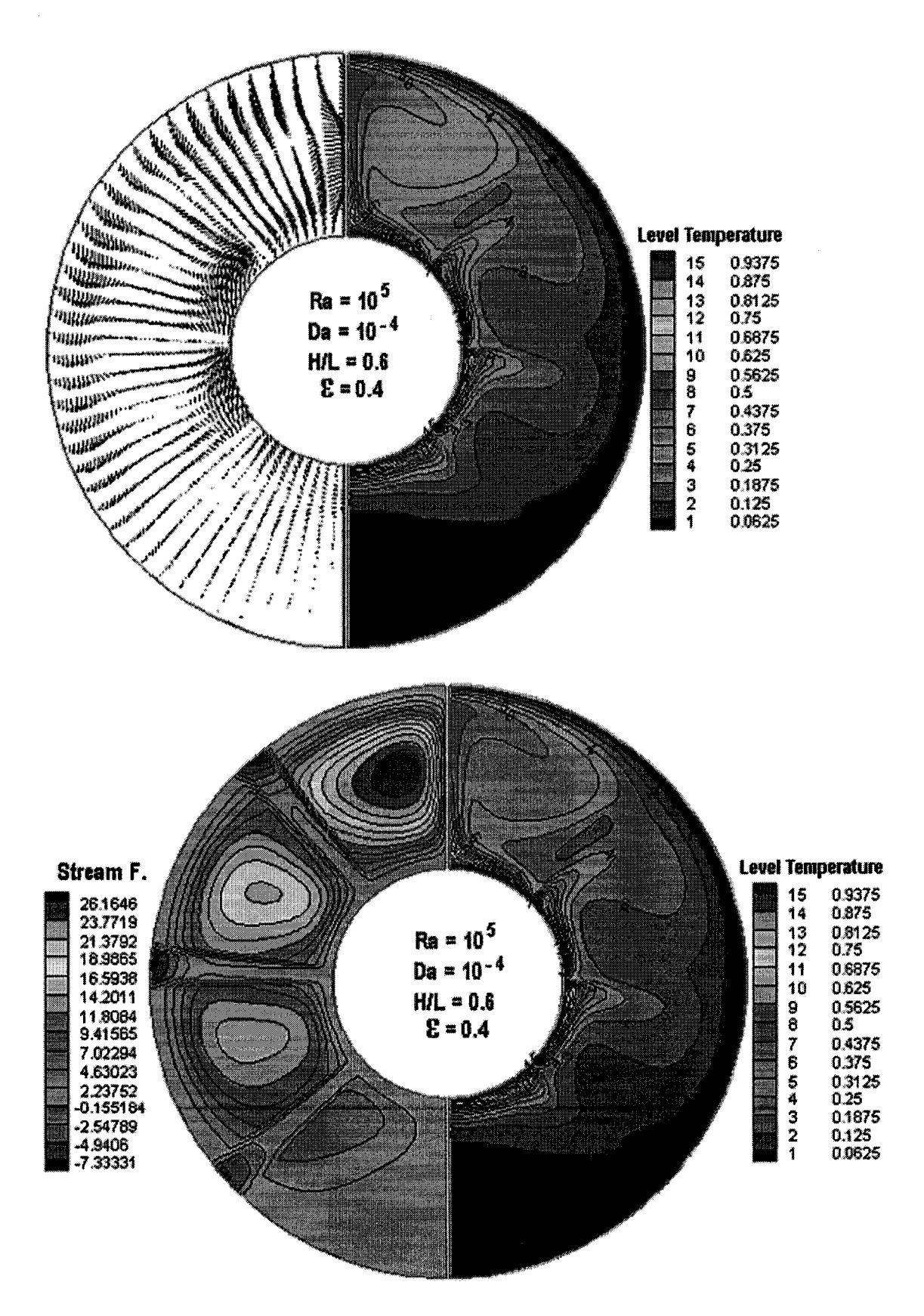
For design purposes, the correlation associated with the porous fin geometry is given below along with the ranges of the validity of the parametric values:

$$\overline{K_{eq_{inner}}} = 4.22(Ra)^{0.101}(Da)^{-0.008} \left(\frac{H}{L}\right)^{0.476} \qquad (19)$$
where,  $10^3 \le Ra \le 10^6$ ;  $10^{-6} \le Da \le 10^{-2}$ ;  $0.2 \le \frac{H}{L} \le 0.6$ ;  $\varepsilon = 0.4$ ;

The adequacy of the regression model used in the correlation is 93.4%. By looking at the exponent on Da, it can be observed that the absolute value of the exponent is low which signifies that the correlation is weekly dependent on Da. In general, the above correlation predicts that with the decrease of Da, more heat transfer will take place from the inner cylinder, whereas with the increase of Ra and fin height, a greater average equivalent thermal conductivity can be obtained.







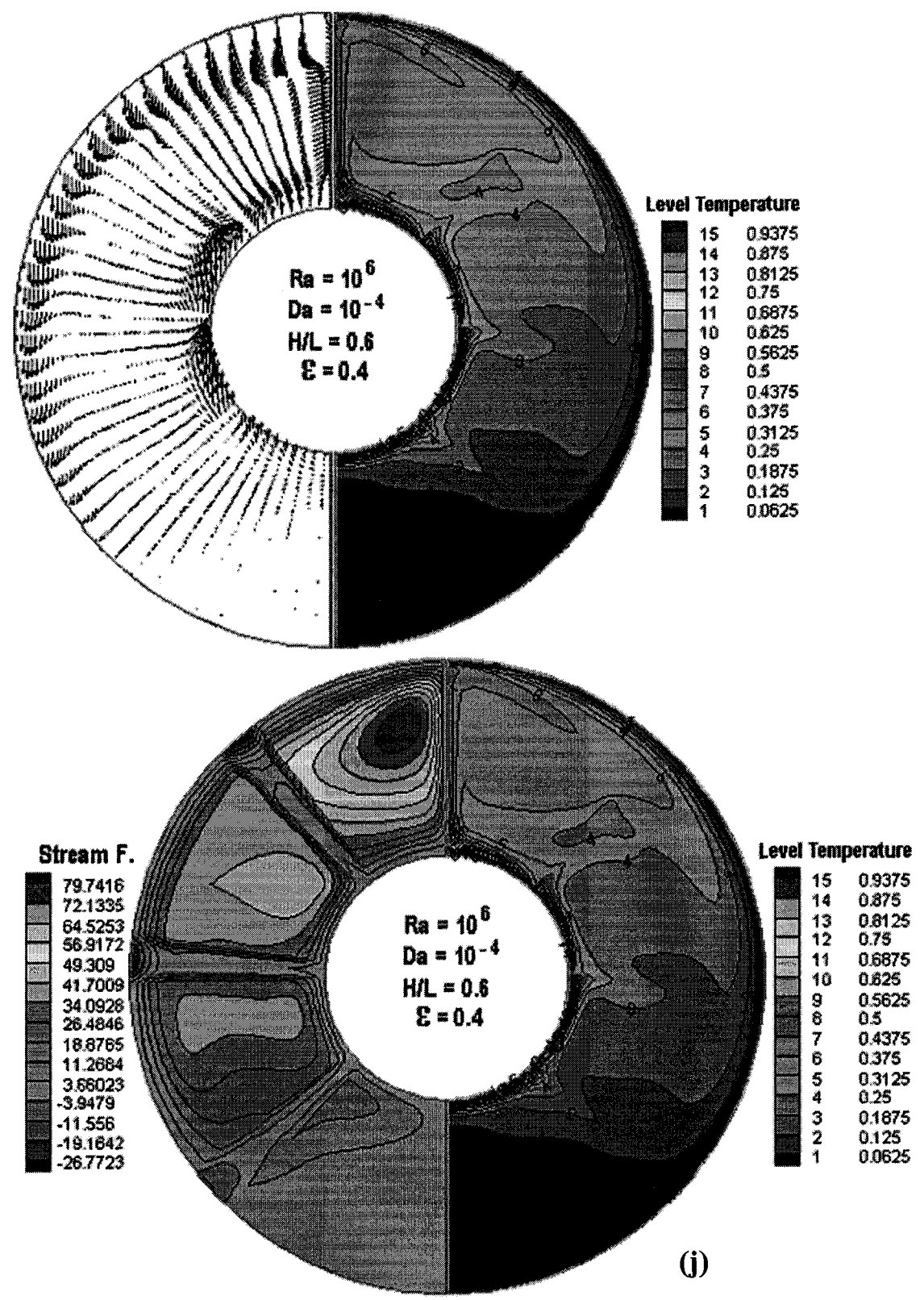


Figure 7: Numerical solutions for the flow and temperature fields, respectively, for an internally porous finned annulus. (g)  $Da=10^{-4}$ ,  $\varepsilon=0.4$ , H/L=0.6,  $Ra=10^{3}$ ; (h)  $Da=10^{-4}$ ,

 $\varepsilon = 0.4 \,,\, H/L = 0.6,\, Ra = 10^4;\, (i)\,\, Da = 10^{-4},\,\, \varepsilon = 0.4 \,,\, H/L = 0.6,\, Ra = 10^5;\, (j)\,\, Da = 10^{-4},\,\,\, \varepsilon = 0.4 \,,\, H/L = 0.6,\, Ra = 10^6$ 

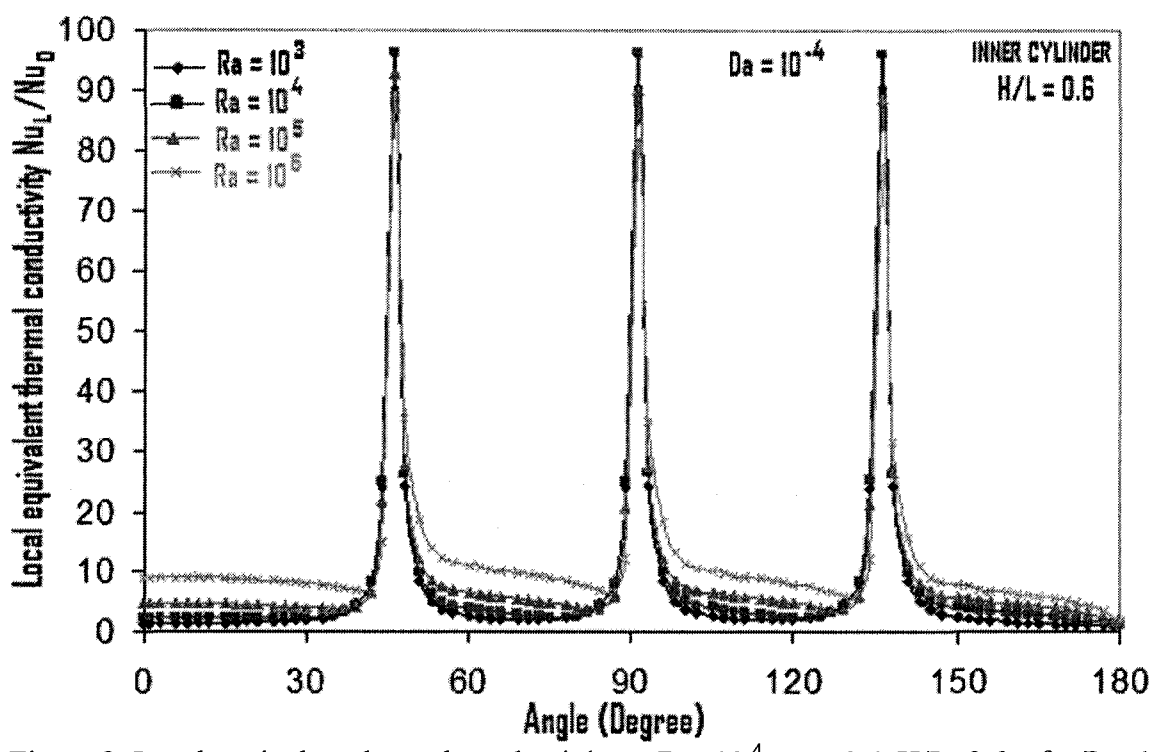


Figure 8: Local equivalent thermal conductivity at Da= $10^{-4}$ ,  $\varepsilon = 0.4$ , H/L=0.6, for Ra= $10^{3}$ , Ra= $10^{4}$ , Ra= $10^{5}$ , and Ra= $10^{6}$ 

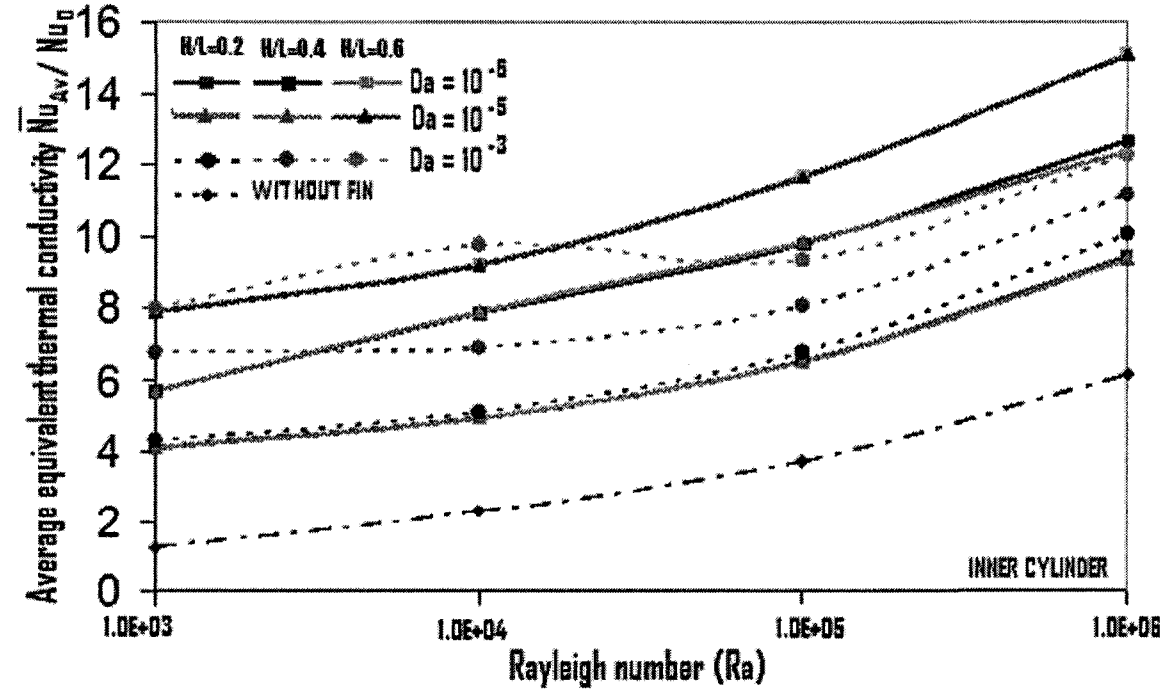
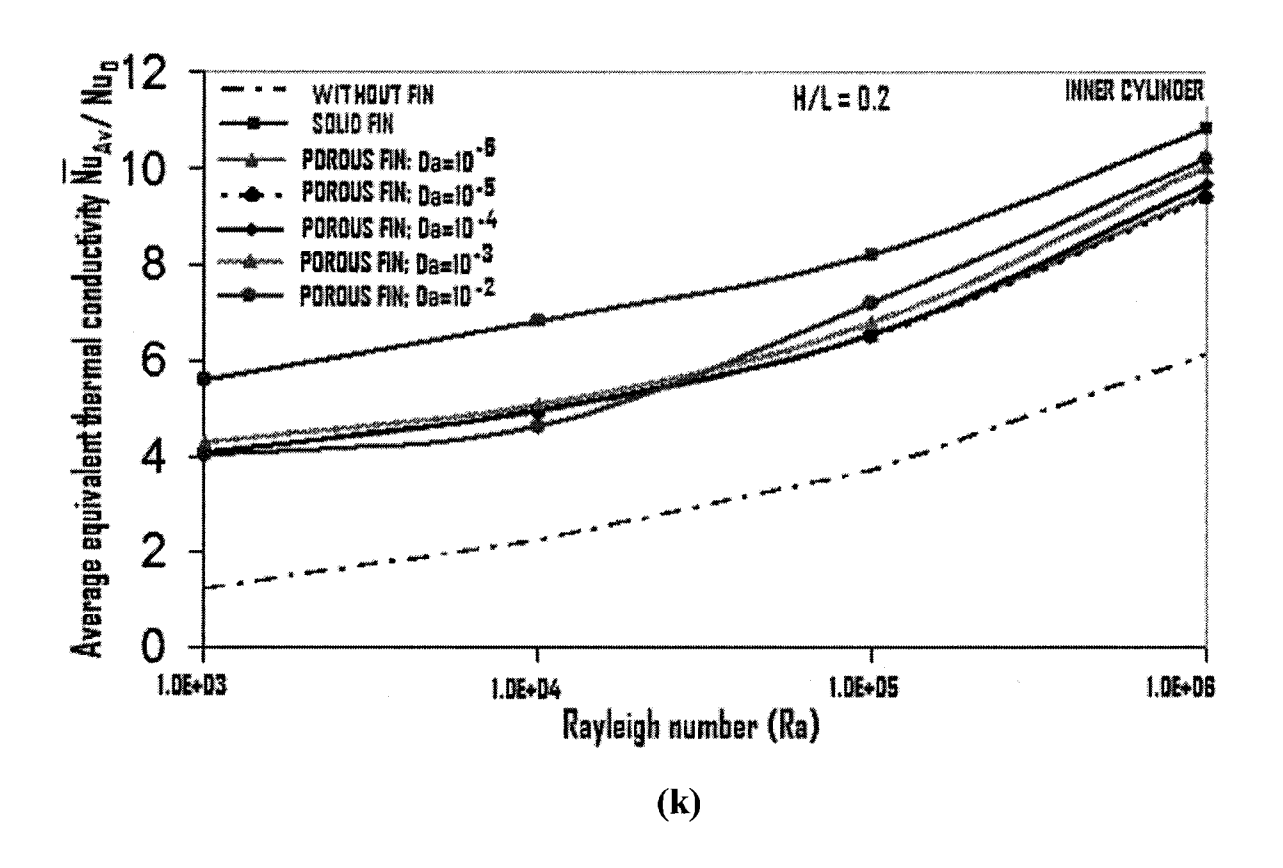
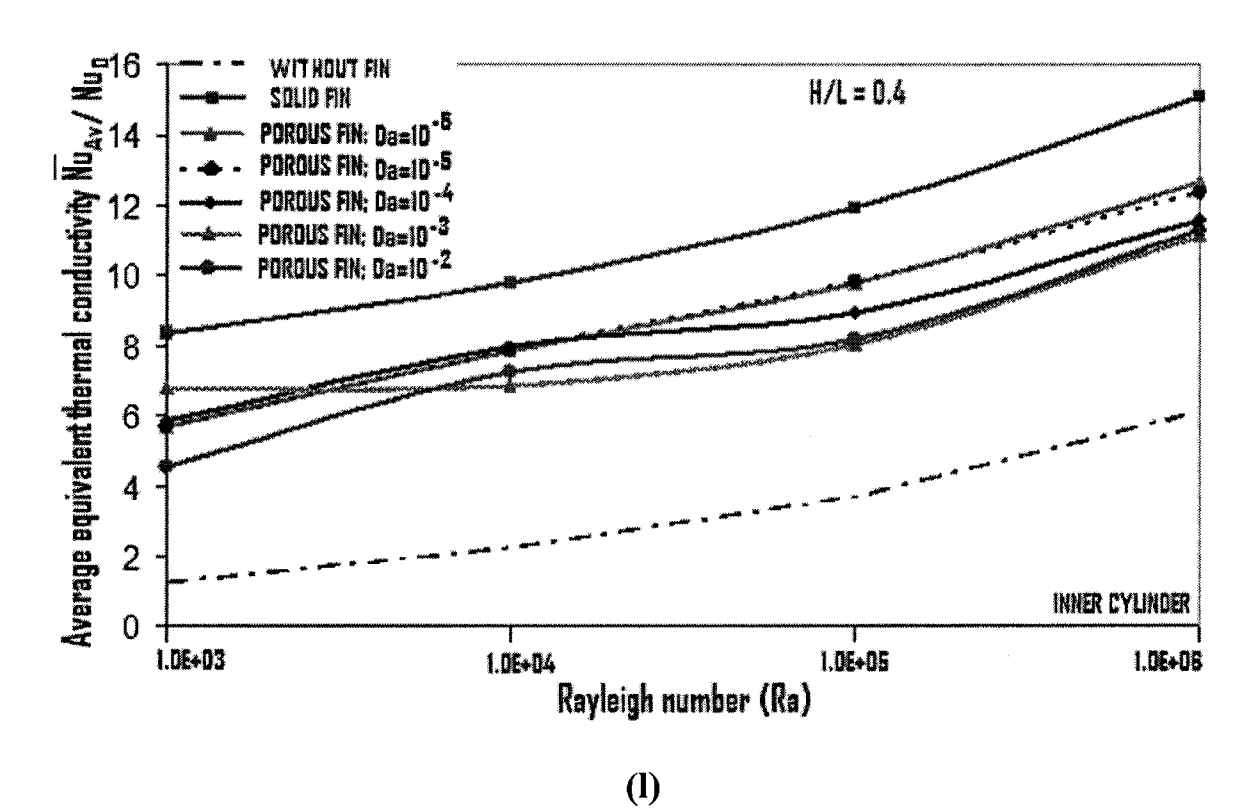


Figure 9: Variation of average equivalent thermal conductivity for various range of Rayleigh number at  $\varepsilon = 0.4$ , H/L=0.2, 0.4, and 0.6 for Da= $10^{-3}$ , Da= $10^{-5}$ , and Da= $10^{-6}$ 

# Comparative study between solid fins and porous fins for the same geometric and flow conditions

Figures 10(k)-10(m) show the change in average equivalent thermal conductivity versus Ra ranging from 10<sup>3</sup> to 10<sup>6</sup>, respectively. The dashed curve indicates the results for a plain cylinder while the solid lines indicate the results for porous and solid fins. The results for the solid fins are taken from the previous chapter [Chapter 1] and are reported here for comparison purposes only. These figures show the comparison for heat transfer of plain cylinder, internally attached solid fins, and internally attached porous fins for the same geometric and flow conditions. The present study of natural convection shows that the heat transfer is enhanced in the case of internally attached solid fins compared to the porous fins [Figs. 10(k)-10(m)], which is not an expected outcome for porous finned surfaces. Irrespective of the Darcy number, it can be seen that the use of solid fins results in a significantly higher heat transfer enhancements over porous fins under the same geometric and flow conditions. For all parametric conditions, for the same fin height, the solid fins show a higher Nusselt number compared to the porous fins. This clearly shows that the solid fins perform the function of increasing the heat transfer rate without the penalty of reduction in heat transfer that results in due to the decrease in the effective thermal conductivity in the case of porous fins. The use of solid fins is an excellent passive method for providing high heat transfer rates for electronic components in a small, light weight, low maintenance, and energy free package. These figures indicate that the use of solid fins is more beneficial when using long fins. Although the convection current is increased near the inner cylinder for porous fins but this increase in convection is overshadowed by the decrease in the effective thermal conductivity of the porous fins compared to the solid fins. It is in such circumstances that the aerodynamic advantages of solid fins become prevalent. The significant increase in solid fin heat transfer compared to that of the porous fins at larger fin heights and high Rayleigh numbers is mainly due to the reduction in the average equivalent thermal conductivity of the fin surfaces of porous fins at suitable combinations of longporous fins and high Rayleigh numbers.





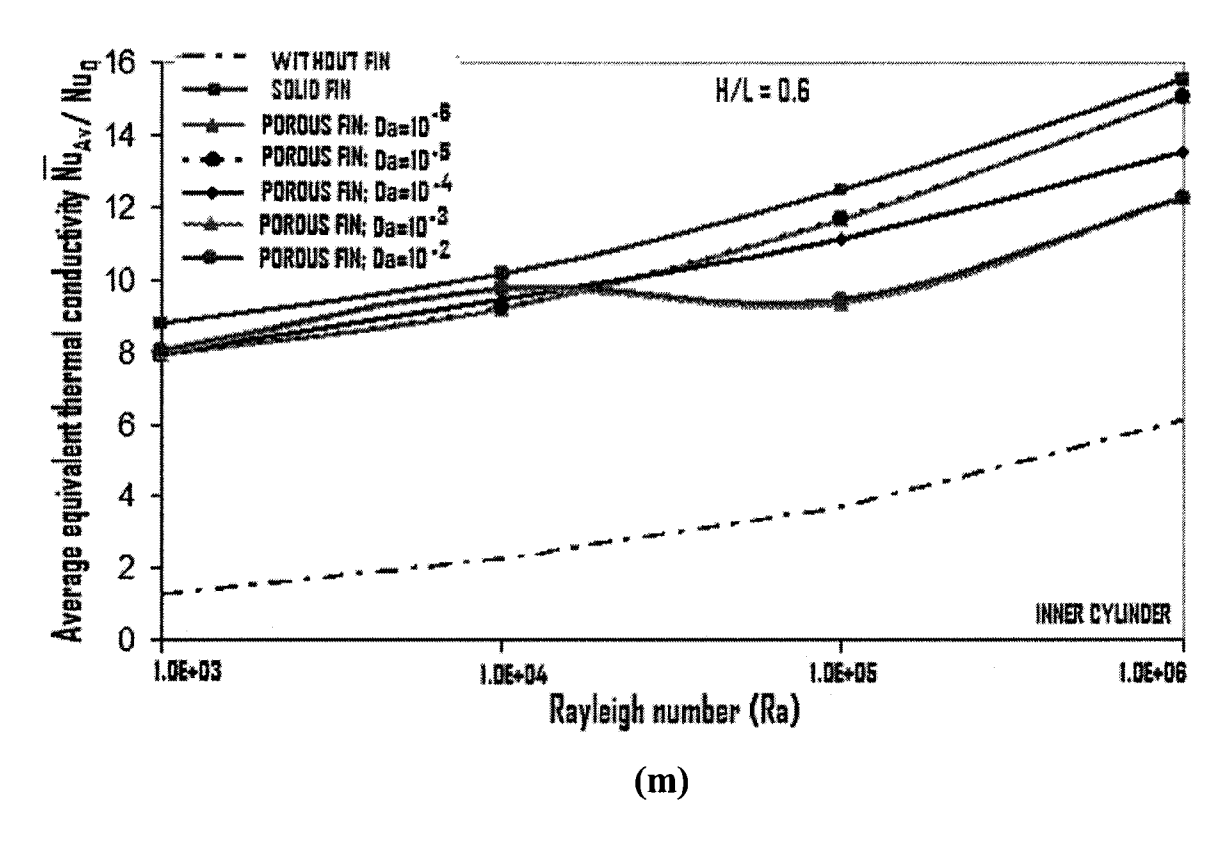


Figure 10: Comparison of average equivalent thermal conductivity with various regions of Rayleigh number between solid fin, porous fin, and without fin. (k) H/L=0.2, Da=  $10^{-6}$ ,  $10^{-5}$ ,  $10^{-3}$ ,  $\varepsilon = 0.4$ ; (l) H/L=0.4, Da=  $10^{-6}$ ,  $10^{-5}$ ,  $10^{-3}$ ,  $\varepsilon = 0.4$ ; (m) H/L=0.6, Da=  $10^{-6}$ ,  $10^{-5}$ ,  $10^{-3}$ ,  $\varepsilon = 0.4$ 

# Effect of porosity of porous fin

The effect of porosity on mean equivalent thermal conductivity is shown in Figure 11. The variation of mean equivalent thermal conductivity on inner cylinder's outer surface at Rayleigh number of 10<sup>6</sup> for various Darcy numbers and different fin heights is seen in Fig. 11. Figure 11 shows a decrease in average Nusselt number for an increase in porosity which in fact shows the existence of lower effective thermal conductivity of the porous fin surface with the increase of porosity. It is observed from this figure, irrespective of the Darcy values, for every fin height the average Nusselt number is reduced along the inner cylinder with the increase of porosity,. It is also seen in this figure that for each fin height the rate of reduction of mean Nusselt number is significantly dependent on Darcy number. For

Da= 10<sup>-6</sup>, and 10<sup>-5</sup>, there is almost no variation of mean equivalent thermal conductivity with porosity for all fin heights but it significantly differs for Darcy number 10<sup>-3</sup>. One reason for such a behavior may be due to the differences in the fluid flow resistance inside the porous fins.

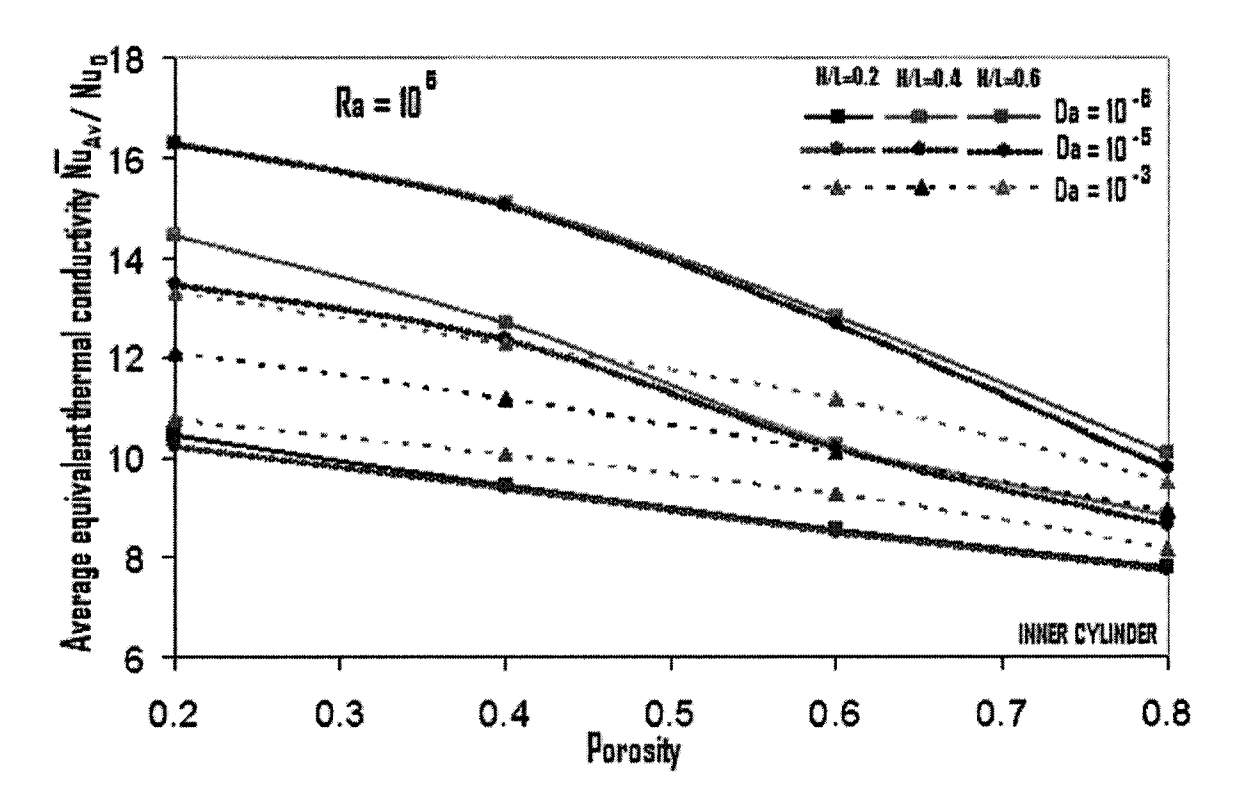


Figure 11: Comparison of average equivalent thermal conductivity with various porosities ( $\varepsilon = 0.2$  to 0.8) at Rayleigh number  $10^6$  for different Darcy values and fin heights

# **Concluding Remarks**

The problem of laminar natural convection heat transfer from a horizontal cylinder with three uniformly spaced longitudinally divergent, round tip porous fins was studied numerically over a range of Rayleigh numbers, Darcy numbers and three different fin heights. The use of porous fins resulted in a much lower Nusselt number values compared to the case of a similar cylinder/fin configuration but with solid fins. Although the convection current is increased near the inner cylinder for porous fins but this increase in convection is

overshadowed by the decrease in the effective thermal conductivity of the porous fins compared to the thermal conductivity of the solid fins. Although a porous finned surface will result in the reduction of weight and material cost, but the present results indicate that solid fins could be more useful in situations which require higher heat transfer rates under laminar natural convection situations. For a cylindrical porous finned surface, the average Nusselt number for the inner cylinder decreases with the increase of porosity due to the reduction of the effective thermal conductivity of the fins

#### **References:**

- [1] Duffin, R., "A variational problem relating to cooling fins", J. Math. Mech., Vol.8, pp.47-56, 1959.
- [2] Jany, P., and Bajan, A., "Ernst Schmidt's Approach to fin optimization: An extension to fins with variable conductivity and the design of ducts for fluid flow", Int. J. Heat Mass Transfer, Vol.31, pp.1635-1644, 1988.
- [3] Snider, A. D., and Kraus, A. D., "The quest for the optimum longitudinal fin profile", ASME HTD, Vol.64, pp.43-48, 1986.
- [4] Irey, R. K., "Errors in the One-Dimensional fin solution", ASME J. Heat Transfer, Vol.90, pp.175-176, 1968.
- [5] Lau, W., and Tan, C. W., "Errors in One-Dimensional Heat Transfer Analysis in straight and annular fins", ASME J. Heat Transfer, Vol.95, pp.549-551, 1973.
- [6] Look, D.C., Jr., "Two-Dimensional fin performance: Bi(Top surface)≥ Bi(Bottom surface)", ASME J. Heat Transfer, Vol.110, pp.780-782, 1988.
- [7] Alkam, M., and Al-Nimr M.A., "Improving the performance of double-pipe heat exchangers by using porous substrates", Int. J. Heat Mass Transfer, Vol.42, pp.3609-3618, 1999.
- [8] Al-Nimr, M. A., and Alkam, A., "A modified tubeless solar collector partially filled with porous substrates", Renewable Energy, Vol.13(2), pp.165-173, 1998.
- [9] Al-Nimr, M. A., and Alkam, A., "Unsteady Non-Darcian forced convection analysis in an annulus partially filled with a porous material", ASME J. Heat Transfer, Vol.119, pp.799-804, 1997.
- [10] Vafai, K., and Kim, S. J., "On the limitations of the Brinkman-Forchheimer-Extended Darcy Equation", Int. J. Heat Fluid Flow, Vol.16, pp.11-15, 1995.
- [11] Abu-Hijleh, B. A., "Natural convection heat transfer from a cylinder with high conductivity permeable fins", Transactions of the ASME, Vol.125, pp.282-288, 2003.

# **Chapter 3**

Laminar Mixed Convention Heat Transfer in a
Concentric Horizontal Cylindrical Annulus for
Aiding and Opposing Flows

# **ABSTRACT**

A numerical study of mixed convective heat transfer (laminar natural and forced convections) of water in the vented annular region between the two concentric horizontal cylinders has been carried out. The forced flow conditions are imposed by providing an inlet (  $\theta_{inlet} = 15^{0}$  ) at the top of the outer cylinder in the upper symmetry plane. The smaller outlet vent  $(\theta_{outlet} = 5^{\circ})$  compared to the inlet vent is at the bottom and is placed diametrically opposite from the inlet. This geometry is suitable as a heat exchanger for solar energy applications. The average and local Nusselt numbers along the inner cylinder are calculated for water as the heat transfer fluid for the outer and inner cylinder diameters ratio of 2.6. The non-dimensional parameters governing the problem are Richardson number (RI) and Reynolds number (Re<sub>D</sub>). Parametric studies are carried out for  $0.0 \le RI \le 2.0$  and  $50 \le \text{Re}_{\text{D}} \le 200$ . The nature and the basic characteristics of the aiding as well as opposing flows are numerically investigated. In the cases studied, the aiding flows are found to have a significant effect in the enhancement of average Nusselt number than opposing flows. For a fixed ReD, with the increase of RI the heat transfer rate increases slowly in case of aiding flows but for opposing flows the heat transfer initially decreases with RI and then slowly increases. For a fixed RI, for both aiding and opposing flows, the heat transfer rate significantly increases with the increase of Re<sub>D</sub>. To get a visual understanding of the mixed convection phenomena in the vented annulus, the velocity vectors, streamlines and isotherms for various cases are also presented.

#### Introduction

For many practical applications, the analysis of the mixed convection heat transfer problem in annuli is important. Mixed convection plays an important role in heat exchangers, electronic boards, combustors, etc.

There have been lots of investigations published in the literature on mixed convective flow in the cavities with many different configurations and combinations of thermal boundary conditions and with various working fluids. Torrance et al. (1972) investigated mixed convection in driven cavities. Cha and Jaluria (1984) studied numerically the effect of buoyancy on the flow and thermal fields in a shallow rectangular reservoir, which can be applied to solar ponds. Kumer and Yuan (1989) presented a numerical study on the laminar, two-dimensional mixed convection flow in a rectangular enclosure with inlet and outlet ports. Papanicolaou and Jaluria (1990, 1992, 1993, 1995) examined various aspects of the mixed convection flow in adiabatic vented enclosures with isothermal sources flushed with the inner walls. For the cooling of electronic components in a package, they examined laminar, transitional, and turbulent flow situations, and obtained optimal locations for the better cooling of the heated objects. Perez-Srgarra et al. (1995) reported the numerical results which combines some of these considerations.

Moallemi and Jang (1992) numerically investigated the mixed convection in a bottom heated square driven cavity and reported on the effect of Prandtl number on the flow and heat transfer processes. They reported that the effects of buoyancy are more pronounced for higher values of Prandtl number. Mohammad and Viskanta (1992) numerically investigated the two and three-dimensional laminar mixed convection flow in a bottom heated lid driven shallow cavity with a working fluid of water having a Prandtl number of 5.84. They found that the lid motion destroys all types of convective cells due to heating from below for finite size cavities. Mohammad and Viskanta (1994) studied experimentally and numerically on mixed convection in shallow rectangular bottom heated cavities filled with a low Prandtl number working fluid liquid Gallium. They reported that the heat transfer rate is rather insensitive to the lid velocity and an extremely thin shear layer exists along the major portion of the moving lid. The flow contour consists of an elongated secondary circulation that occupies a third of the cavity.

Hsu et al. (1997) performed a numerical study on mixed convection in a partially divided rectangular enclosure. Sparrow and Samie (1982) numerically investigated the fluid flow and heat transfer in a vertically oriented cylindrical enclosure with apertures for forced flow in the lower and upper horizontal circular walls, which is very much related with some of the engineering applications, such as the oven of an electric stove, and natural convection recirculation in an attic, etc. In between the enclosure a recirculating flow arises due to the

throughflow stream and natural convection flows are induced because of the temperature difference between the entering stream and the enclosure walls. The strength of the forced and natural convection flows are characterized by the Reynolds and Rayleigh numbers and the aiding and opposing flow depends on the temperature of the entering stream and the enclosure walls. When the through-flow stream is vertically downward with higher temperature than the enclosure walls, the through-flow stream is overpowered by the natural convection, with resulting high values of heat transfer known as aiding flow situation. In case of opposing flow situation, the temperature of the incoming through-flow stream is lower than the temperature of the enclosure walls, where the natural convection opposes the through-flow driven recirculation and this causes in the reduction of the heat transfer.

The major objective of this part of the work is to study numerically the effects of mixed convection on heat transfer in the annulus between two horizontal, concentric cylinders under aiding and opposing flow situations. This study concentrates on the characteristics of both aiding and opposing buoyant flows arising from hot/cold jets impinging from the top of the outer cylinder of the annulus and discharging through the bottom of the outer cylinder. The wall of the inner cylinder is maintained isothermal at the non-dimensional temperature of  $0^0$  which is colder (hotter) compared to the jet temperature and thus give rise to the aiding and opposing the forced flow situations. The outgoing flow is assumed to be hydrodynamically and thermally fully developed. The rest of the outer (except the inlet and outlet) wall of the outer cylinder is insulated. A steady, laminar, two-dimensional flow is assumed. The velocity and temperature profiles are obtained inside the annulus along with the heat transfer rates on the inner cylinder for various Richardson numbers (also called buoyancy parameter or mixed convection parameter), and Reynolds numbers all for a fixed radius ratio of outer cylinder to inner cylinder of 2.6. To the best of author's knowledge, no experimental or numerical work for this flow situation in horizontal concentric cylindrical annulus has been reported in the literature. It is to be noted that converged solutions could not be obtained for higher values of Reynolds number. Thus, the upper limit of the Reynolds number for which the flow stays laminar was not reached in this study. Because of the unavailability of similar studies, the presented results could not be directly compared with any experimental or numerical results from the literature.

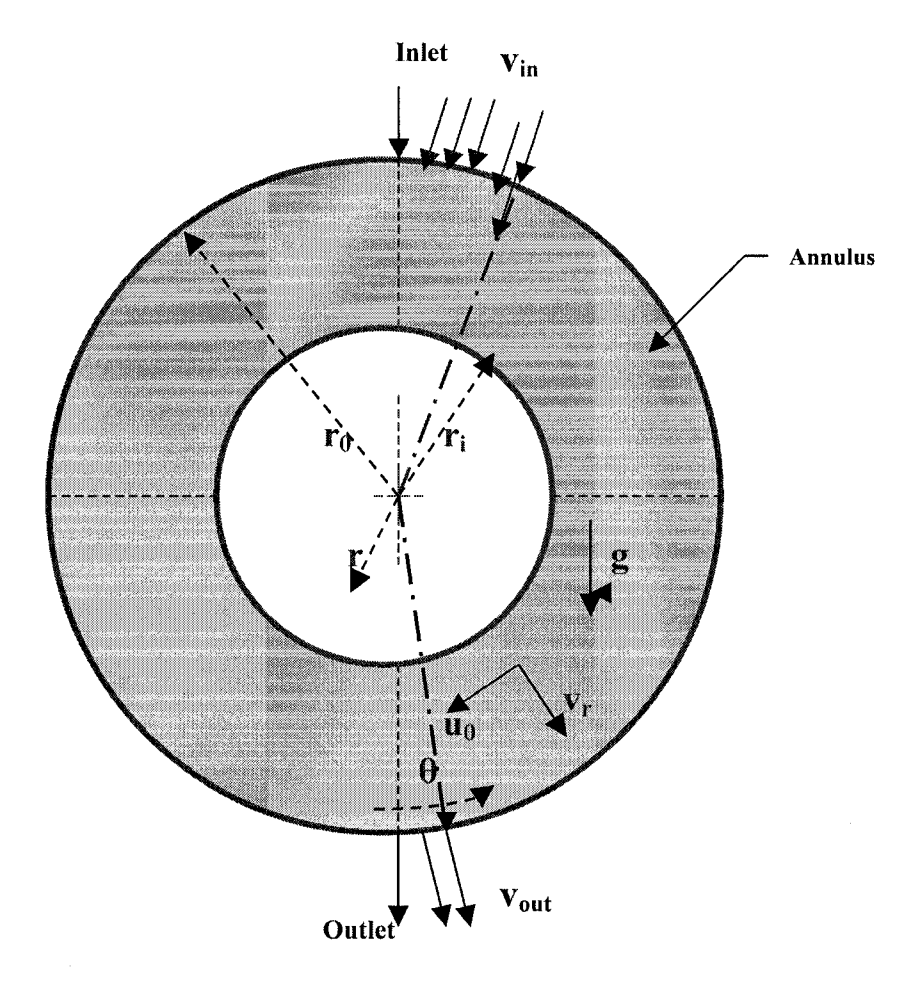


Fig. 1: Schematic diagram of two concentric cylinders with coordinate system

# **Analysis**

The problem to be considered is schematically presented in Fig. 1. Natural convective motion is generated by the Buoyancy in between annulus in the  $(r, \theta)$  plane with radial and angular velocity components. The steady-state, two-dimensionless conservation equations of mass, momentum and energy for a Newtonian fluid in conservative form under laminar mixed convection situation over a cylinder, including the Boussinesq approximation, are given as follows:

Using the Boussinesq approximation, the density term is given by 
$$\rho = \rho_{ref} \left[ 1 - \beta \left( T - T_{ref} \right) \right] ------(1)$$

Continuity:

$$\frac{1}{R}\frac{\partial(RV)}{\partial R} + \frac{1}{R}\frac{\partial U}{\partial \theta} = 0 \qquad -----(2)$$

U-momentum equation:

$$\frac{1}{R} \frac{\partial}{\partial R} (RUU) + \frac{1}{R} \frac{\partial}{\partial \theta} (UV) = \frac{1}{\text{Re} R} \frac{\partial}{\partial R} \left( R \frac{\partial U}{\partial R} \right) + \frac{1}{\text{Re} R} \frac{\partial}{\partial \theta} \left( \frac{1}{R} \frac{\partial U}{\partial \theta} \right) - \frac{1}{R} \frac{\partial P^*}{\partial \theta} + 2 \frac{1}{\text{Re} R^2} \frac{\partial V}{\partial \theta} - \frac{U}{\text{Re} R^2} - \frac{UV}{R} + RI * \phi * \sin \theta$$
(3)

V-momentum equation:

$$\frac{1}{R} \frac{\partial}{\partial R} (RUV) + \frac{1}{R} \frac{\partial}{\partial \theta} (VV) = \frac{1}{\text{Re*}R} \frac{\partial}{\partial R} \left( R \frac{\partial V}{\partial R} \right) + \frac{1}{\text{Re*}R} \frac{\partial}{\partial \theta} \left( \frac{1}{R} \frac{\partial V}{\partial \theta} \right) - \frac{\partial P^*}{\partial R} - 2 \frac{1}{\text{Re*}R^2} \frac{\partial U}{\partial \theta} - \frac{V}{\text{Re*}R^2} - \frac{U^2}{R} - RI * \phi * \cos \theta - \dots (4)$$
Energy equation:

The dimensionless variables (capitalized letters and  $\theta$  ) are defined as:

# **Boundary conditions**

The geometry (the right-half of the annulus is chosen as the solution domain) and the dimensionless boundary conditions corresponding to this problem are presented as follows:

- On the inner cylinder surface, i.e., Ri=1.0; U=V=0.0;  $\phi = 0.0$
- On the outer cylinder surface except inlet and outlet ports, i.e., Ro=2.6; U=V=0.0;  $\frac{\partial \phi}{\partial R} = 0.0$
- Lower plane of symmetry; i.e.,  $\theta = 0$  ; U=0.0;  $\frac{\partial V}{\partial \theta} = \frac{\partial \phi}{\partial \theta} = 0.0$
- Upper plane of symmetry; i.e.,  $\theta = \pi$ ; U=0.0;  $\frac{\partial V}{\partial \theta} = \frac{\partial \phi}{\partial \theta} = 0.0$
- At the inlet port (R<sub>0</sub>=2.6,  $\theta = 165^{\circ}$  to  $\pi$  ); i.e., U=0.0; V= 1.0,  $\phi = 1.0$  for the adding flow and U=0.0; V= 1.0,  $\phi = -1.0$  for the opposing flow.

At the outlet port (R<sub>0</sub>=2.6, 
$$\theta = 0^{\circ}$$
 to  $5^{\circ}$  ); i.e., U=0.0;  $\frac{\partial \phi}{\partial R} = \frac{\partial V}{\partial R} = 0.0$ 

In this study, the Prandtl number of the working fluid water is taken as 6.78. The Richardson numbers considered are 0.0, 0.1, 0.5, 1.0, and 2.0. The Reynolds numbers prescribed are 50, 100, 150, and 200.

The solution procedure approach is similar to that used in Chapter 1. Relative variations of the non-dimensional velocities and temperature by less than 10<sup>-4</sup> over all grid points are adopted as the convergence criterion.

## Local and Average Nusselt number calculations

Non-dimensional Local Nusselt number along the inner cylinder is

$$Nu_{Local\ at\ R=R_i} = -\frac{\partial \phi}{\partial R}\Big|_{R_i=1.0} \tag{7}$$

Circumferential average Nusselt number based on cylinder radius, which gives the net heat transfer rate through the cylinder surface, is calculated as

$$\tilde{N}u \text{ at } r=r_{i} = \frac{\int_{0}^{L} \int_{0}^{\pi} (Nu_{L})_{r=r_{i}} r_{i} d\theta dZ}{\int_{0}^{L} \int_{0}^{\pi} r_{i} d\theta dZ}$$

$$\bar{Nu}_{\text{at R}=R_{i}} = -\frac{1}{\pi} \int_{0}^{\pi} \frac{\partial \phi}{\partial R} d\theta \qquad (8)$$

The Lagrangien interpolation scheme is used to calculate the local Nusselt number results. This interpolation scheme is used to improve the accuracy of the calculations near the solid surfaces because of the non-uniform grid distributions near the inner cylinder wall. The non-uniformity in the grid distributions near the walls is due to the employment of B-type staggered grids. The average Nusselt number is obtained by integrating the local Nusselt number over the inner cylinder, which is numerically calculated using the Simpson-rule of numerical integration of a definite integral.

#### Results and discussion

Flow and temperature fields and heat transfer rates are examined where the Richardson number, RI is varied as 0.0, 0.1, 0.5, 1.0 and 2.0 and the corresponding ranges of Rayleigh numbers (GrxPr) varied from 10<sup>3</sup> to 10<sup>5</sup>, Reynolds number (Re<sub>D</sub>) is varied as 50, 100, 150 and 200, for an inlet angle,  $\theta_{inlet} = 15^{\circ}$  , and an outlet angle,  $\theta_{outlet} = 05^{\circ}$  . The inlet angle ( $\theta_{\it inlet}$ ), outlet angle ( $\theta_{\it outlet}$ ), the outer to inner radius ratio (2.6) of the annulus are kept fixed for a total of 40 different runs. The working fluid is chosen as water with Prandtl number, Pr=6.78. At the exit, the flow is assumed to be fully developed, allowing derivatives of the radial velocity and temperature to be set to zero. Along the solid walls of the cylinder the velocities are zero, while the non-dimensional temperature on the inner cylinder surface is zero and in the inlet port is either positive one (defined as aiding flow) or negative one (defined as opposing flow) depending upon the case modeled. The above are two flow situations that have been employed in the course of this work. The first one, referred to as case I hereafter, involves forcing a hot fluid through the inlet, i.e.,  $\phi = 1.0$  for the inlet fluid and  $\phi = 0.0$  for the inner cylinder wall. The second one, referred to as case II hereafter, involves forcing a cold fluid through the inlet, i.e.,  $\phi = -1.0$  for the inlet fluid and  $\phi = 0.0$  for the inner cylinder wall.

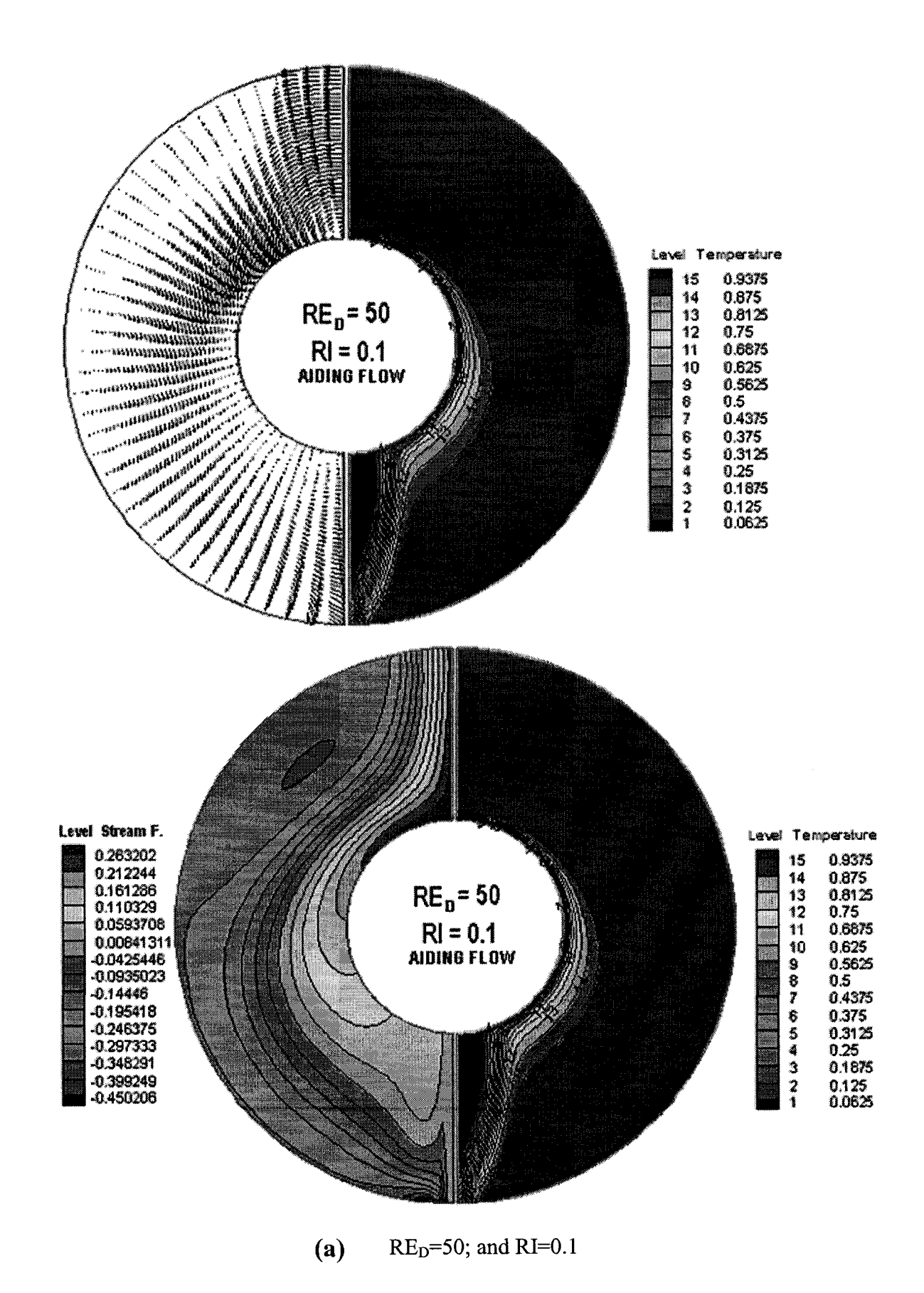
In order to obtain grid independent solution, a grid refinement study is performed for a plain horizontal concentric cylinder on natural convection described in previous chapter [Chapter-1]. It is noticed that a  $82 \times 82$  mesh within the annulus produces grid independent solution and the  $82 \times 82$  mesh is therefore used for all computations reported in this section.

## Case I

First, the predicted velocity, streamlines and isotherms in the annulus for four cases are presented in Figs. 2(a)-2(b), 3(c)-3(d). All are for aiding flow situation for two RI values of 0.1 and 2.0 and for two Reynolds numbers, 50 and 200. Here, RI=0.1 and 2.0 indicate two different regimes of flow; the first one is a forced convection dominated flow and the second

case is a natural convection dominated flow problems. There is a hot fluid flow entering from the top of the annulus, passing through a channel between the cold inner cylinder surface and the insulated outer cylinder surface, and coming out at the exit. The isotherms for a Reynolds number 50 of Figs. 2(a) and 2(b) and for two Richardson numbers 0.1 and 2.0 show large temperature gradients on the upper part of the inner cylinder and the fluid is cooled all along the inner cylinder wall. Clearly, the heat transfer along the inner cylinder wall is mostly carried out by the forced and natural convection. In both cases a thin hydrodynamic and thermal boundary layers are observed near the cold inner cylinder wall. As Reynolds number increases, Figs 3(c) and 3(d) show that the isotherms almost disappear from the upper part of the inner cylinder wall, i.e., after 60°. For Re<sub>D</sub> =200 the velocity profiles show the formation of a reverse flow and the streamlines show a separate convection cell near the outer cylinder wall. In general, the flow field is characterized by a primary clockwise recirculation bubble near the outer cylinder wall where the shear driven flow by the fluid is impacted on the outer wall and forced to move downward. A large recirculation flow is observed at higher Reynolds numbers. With the increase of Re, the fluid flow from the entrance is increased, the higher velocity fluid passes above the upper part of the cooled surface and gets cooled. As a result, the thermal buoyancy force manifests itself only in the lower part of the domain. The isotherms for higher Re show that as Re increases, the role of natural convection becomes negligible, and forced convection plays the dominant role in heat transfer.

For Re<sub>D</sub> =50 there is a small individual convection cell visible, but there is no reverse flow in the annulus. Hence, the heat from the surface is mostly transferred by natural convection by the fluid entering from the inlet and passing through the annulus. The recirculation flow results from natural convection combined with boundary conditions specified at the exit. The velocities, streamlines and the isotherms for Re<sub>D</sub> = 50 and 200; and RI=0.1 and 2.0 show clearly that heat transfer is increased by increasing Re<sub>D</sub> and RI. The strength of the imposed flow plays an important role on the flow patterns and isotherms through creating the larger sizes of recirculation bubble near the outer cylinder wall.



ì

80

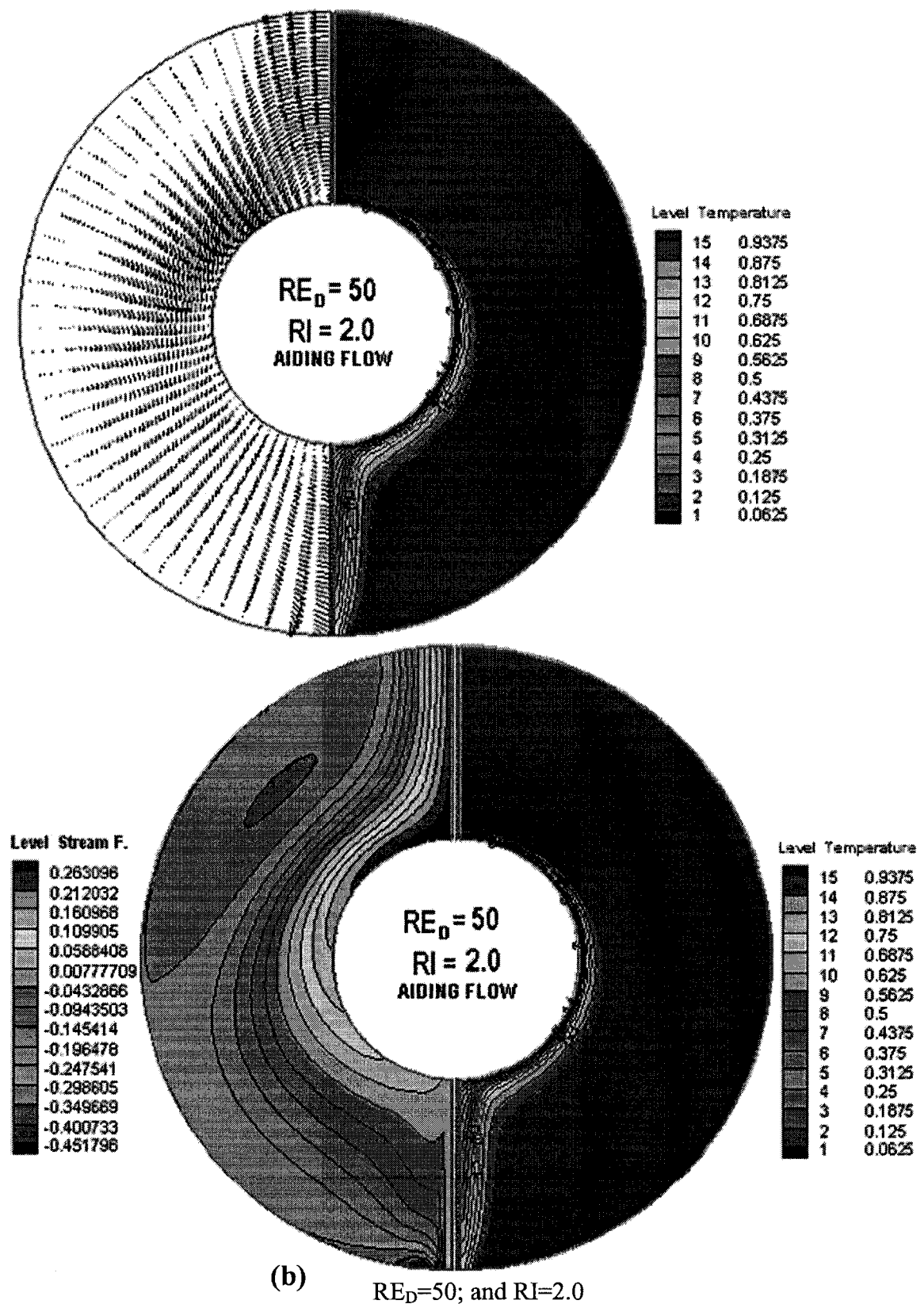
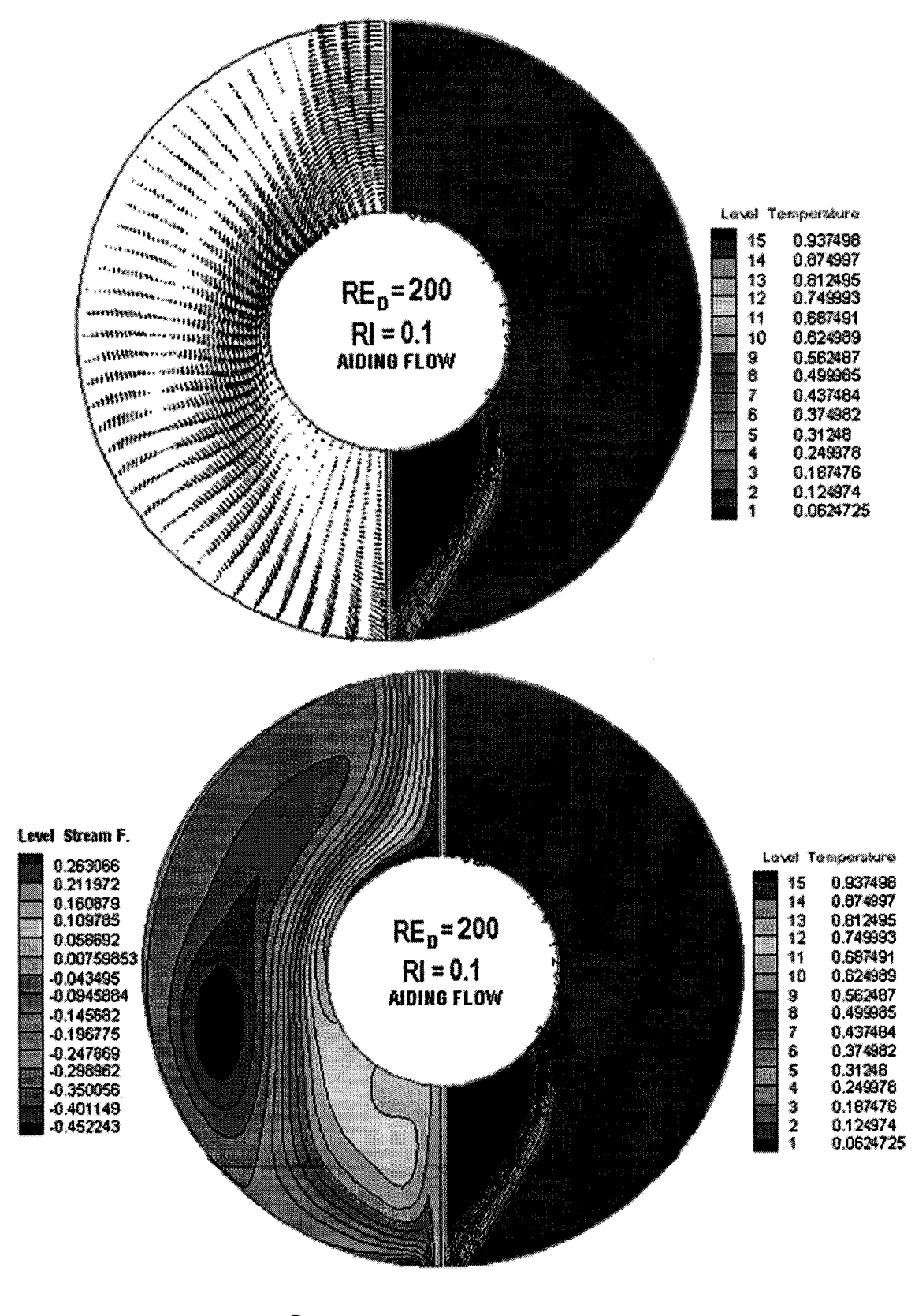


Fig.2: Isotherms and velocity vectors and streamlines for two different Richardson numbers at Reynolds number  $RE_D = 50$ 



 $\mathbb{C}$  RE<sub>D</sub>=200; and RI= 0.1

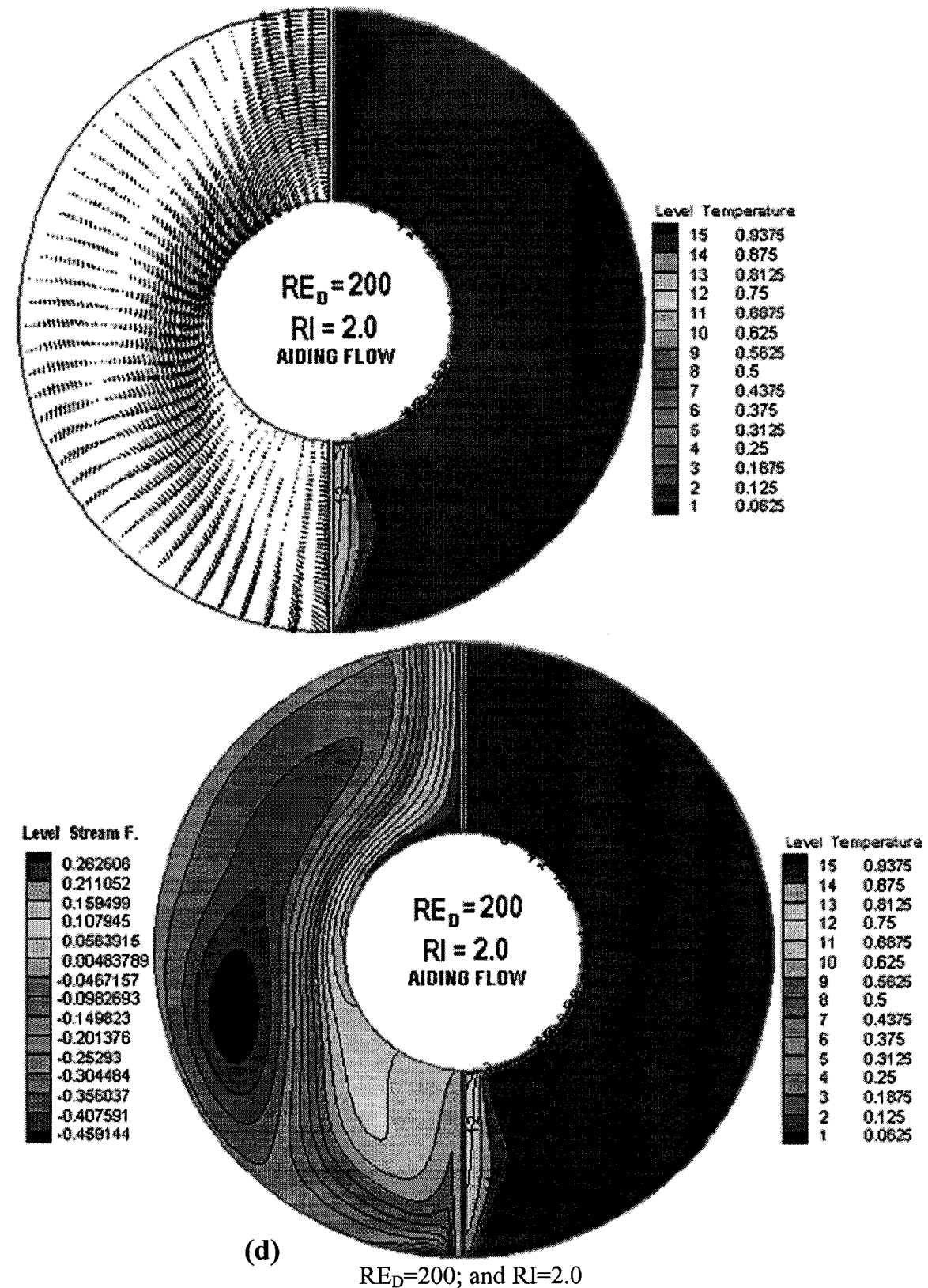
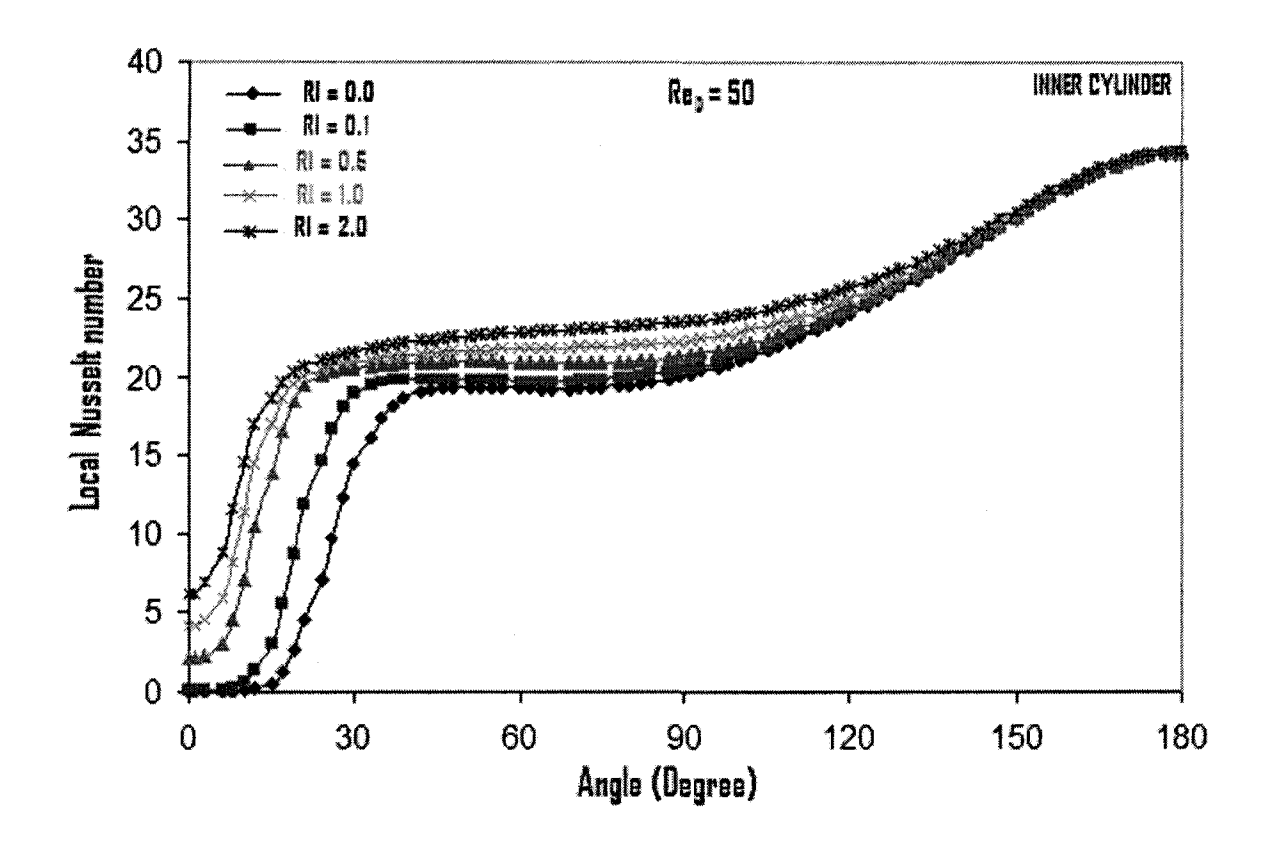
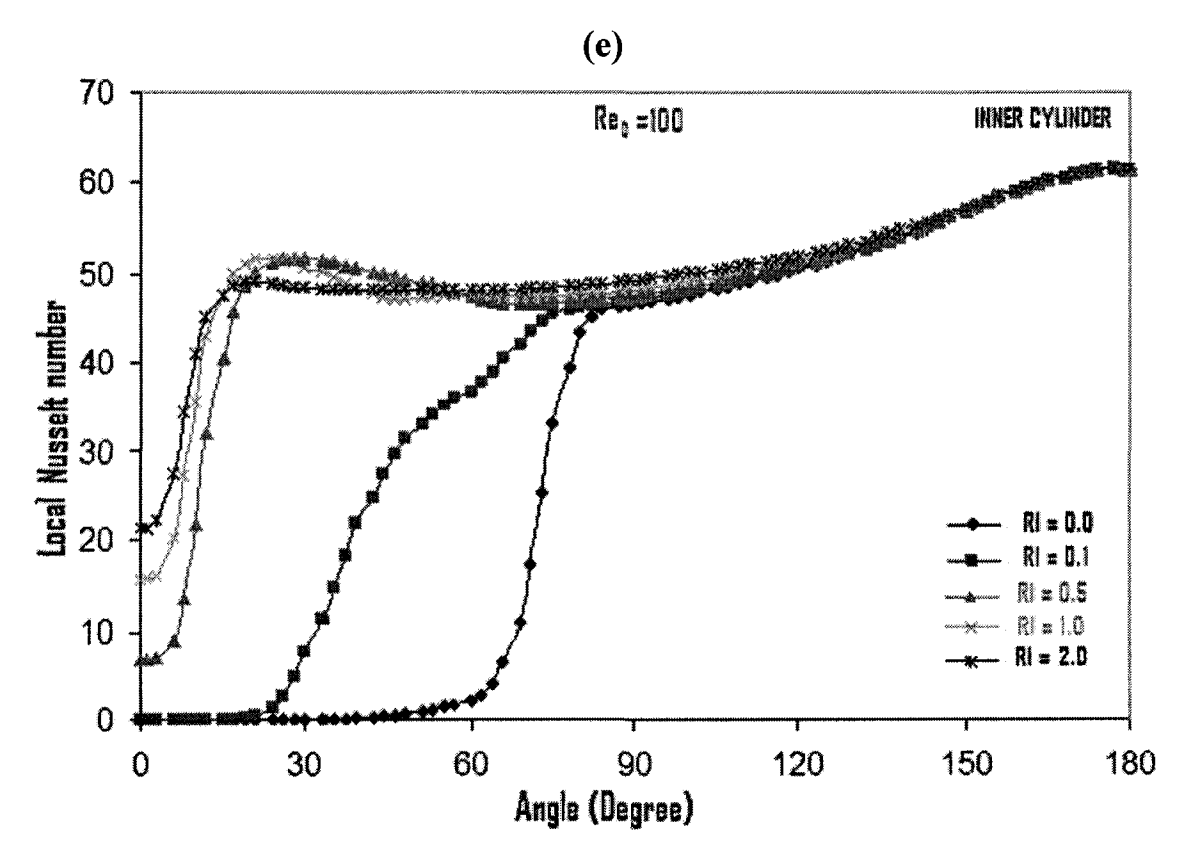


Fig.3: Isotherms and velocity vectors and streamlines for two different Richardson numbers at Reynolds number  $RE_D = 200$ 

#### Local Nusselt number distributions

The distribution of the local Nusselt numbers along the inner cylinder is defined by Eqs. (7) for the same configuration presented in Fig.1 and for four different regimes of flow, viz., purely forced convection, dominating forced convection, mixed convection, and dominating natural convection representing Richardson numbers (RI) = 0.0, 0.1 and 0.5, 1.0, and 2.0, respectively and for four different Reynolds numbers (Re<sub>D</sub>)=50, 100, 150 and 200 are shown in Figs. 4(e), 4(f), 4(g) and 4(h). The intermittent character of the thermal boundary layer can be observed as the local heat transfer is increased at the top of inner cylinder. At different Reynolds numbers and to some extent on the upper part of the inner cylinder, the increment of local Nusselt number is almost the same for four different flow regimes. The influence of RI and Re<sub>D</sub> can be seen later, particularly towards the bottom part of the inner cylinder. As expected, increasing imposed flow enhances the local heat transfer, which is more pronounced on the upper part of the inner cylinder as seen through Figs. 4(e)-4(f). Heat transfer from the lower part of the inner cylinder is mainly due to forced and natural convection and that through the exit is by natural convection with little contribution from forced convection. At RI=0.0 (purely forced convection), local heat transfer is at the lowest level for every Re<sub>D</sub> compared to the dominating forced convection, mixed convection, and dominating natural convection situations. Local heat transfer is almost insignificant at the lower part of the inner cylinder wall for RI = 0 and 0.1 and this insignificancy increases with increasing Re<sub>D</sub>. From Figs. 2(a) and 3(c), it is observed that at RI=0.1, the fluid is vertically downward in the stagnant zone and conduction and natural convection are the principle modes of heat transfer in that zone. In the dominating forced convection flow regimes i.e., RI=0.1, the local heat transfer rate at the lower symmetry plane is negligible due to the weak buoyancy effect. In case of mixed and dominating natural convection flow regimes, the local Nusselt number increases sequentially at the lower symmetry plane with increased imposed flow because of increased natural convective effects. It is seen that Nu<sub>Local</sub> is an increasing function of  $\theta$  with increased RI because the buoyancy force is acting in the imposed flow direction in case of aiding flow situation. As a result, the natural convection effect is enhanced with the increase of RI.





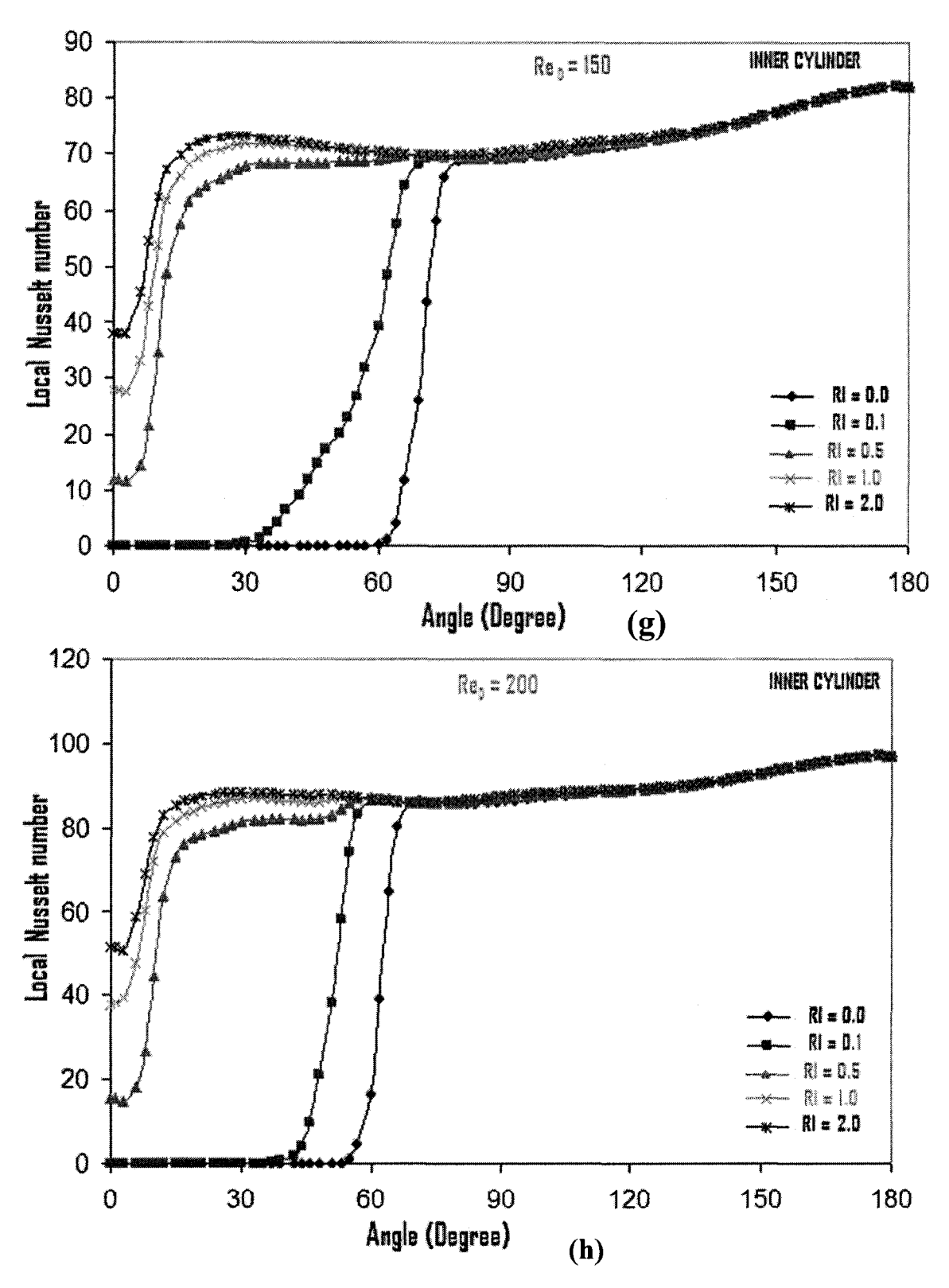
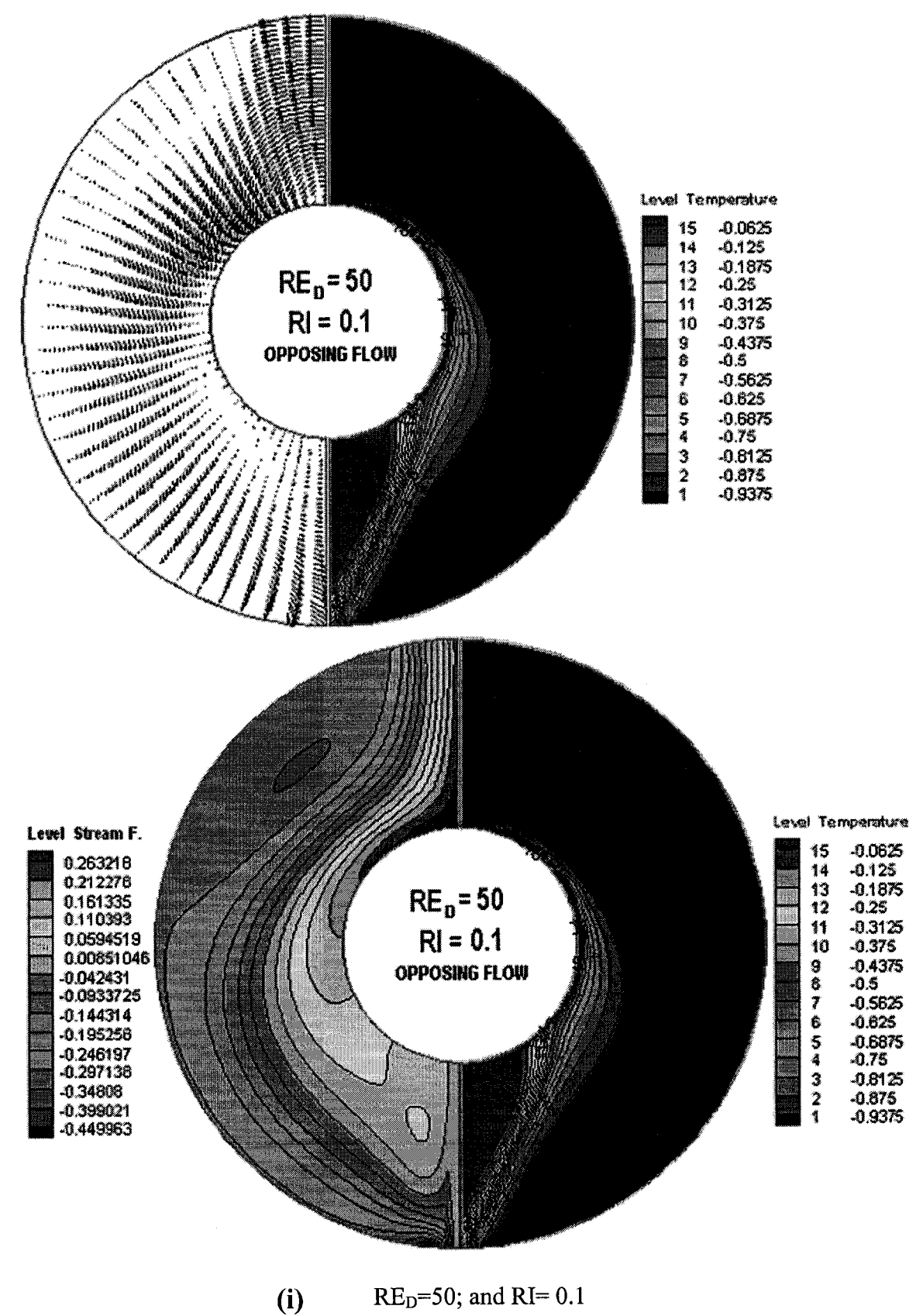


Fig.4: The local Nusselt number on the inner cylinder in case of aiding flow for Richardson numbers (RI=0 means heat transfer without natural convection) at Reynolds number (e) 50, (f) 100, (g) 150, and (h) 200 for inlet angle 15<sup>0</sup> and outlet angle 5<sup>0</sup>

Computed local Nusselt number for various Reynolds numbers over the RI range studied in this part of the study shows that for the isothermal inner cylinder near the outlet the heat flux rate decreases which is evident from Figs. 4(e), 4(f), 4(g) and 4(h). The lowest heat transfer occurs at the dominating forced convection flow regimes. This behavior can be explained from studying the flow and temperature fields in the computed domain. From Figs. 2 and 3 the developments of the thermal boundary layer growth on the inner cylinder and the effect of flow separation on the temperature contours can be seen. Presented temperature contours reveal that the separation angle is a function of both Reynolds and RI numbers. For a fixed RI number, the separation occurs earlier when the Reynolds number is lower. For a higher Reynolds number a significant change of the separation angle from the inlet is observed when RI number varies but for lower Re<sub>D</sub>, there is an insignificant effect on the separation angle for different RI values. For a fixed Reynolds number, the flow separation occurs earlier for smaller values of RI. Due to the difference in the locations of flow separation on the inner cylinder, the extent and strength of the formation of wakes vary which reduce and create different rates of heat flux at the outlet for various Reynolds and RI numbers. Near the outlet, the flow could be unsteady in nature because of the development of the wakes. The present steady state simulation might have not captured correctly the heat and fluid flow phenomena in these regions. For accurate predictions, detail and close examinations of the flow and temperature fields are required in the mixed convection phenomenon.

#### Case II

Here, the results are discussed for an opposing flow situation. In this case there is a cold fluid entering from the top of the annulus, passing through the outer surface of the hot inner cylinder and the insulated inner surface of the outer cylinder, and coming out at the exit. The isotherms, streamlines and velocities for Reynolds number 50 and 200, and two Richardson numbers 0.1 and 2.0 are presented in Figs. 5(i), 5(j); and in Figs. 6(k), 6(l), respectively. For Re<sub>D</sub> =50 and 200 the streamlines and velocities are similar to those of Figs. 2(a), 2(b); and. 3(c), 3(d) except for the predicted isotherms. In the opposing flow case, the isotherms spread out more than the aiding flow case. This indicates that a lower temperature gradient prevails near the inner cylinder in case of opposing flow than aiding flow situations. For an opposing flow, due to the unfavorable manifestations of buoyancy effect, heat transfer rate is decreased in comparison to that of an aiding flow for the same parametric conditions.



 $RE_D=50$ ; and RI=0.1

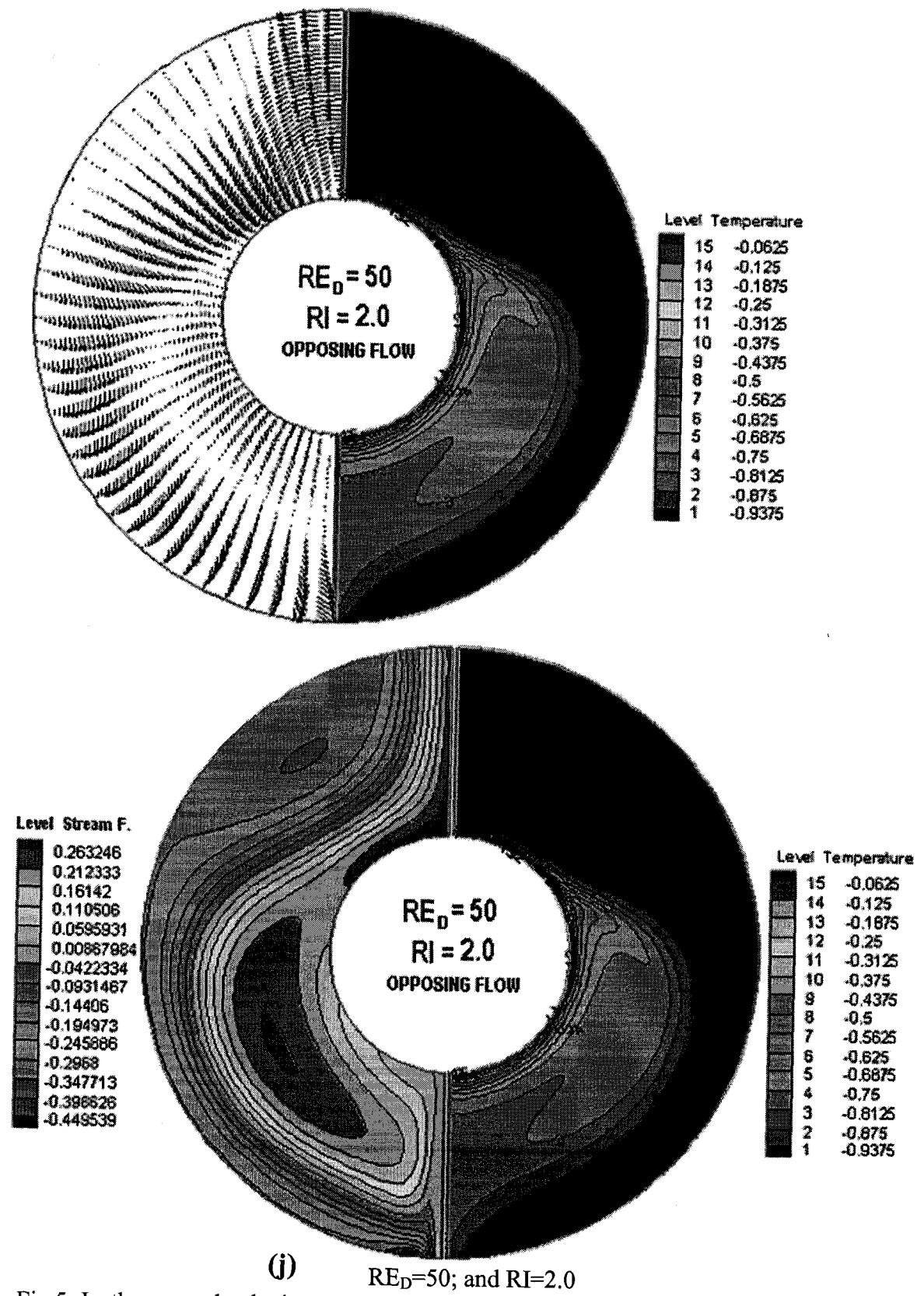
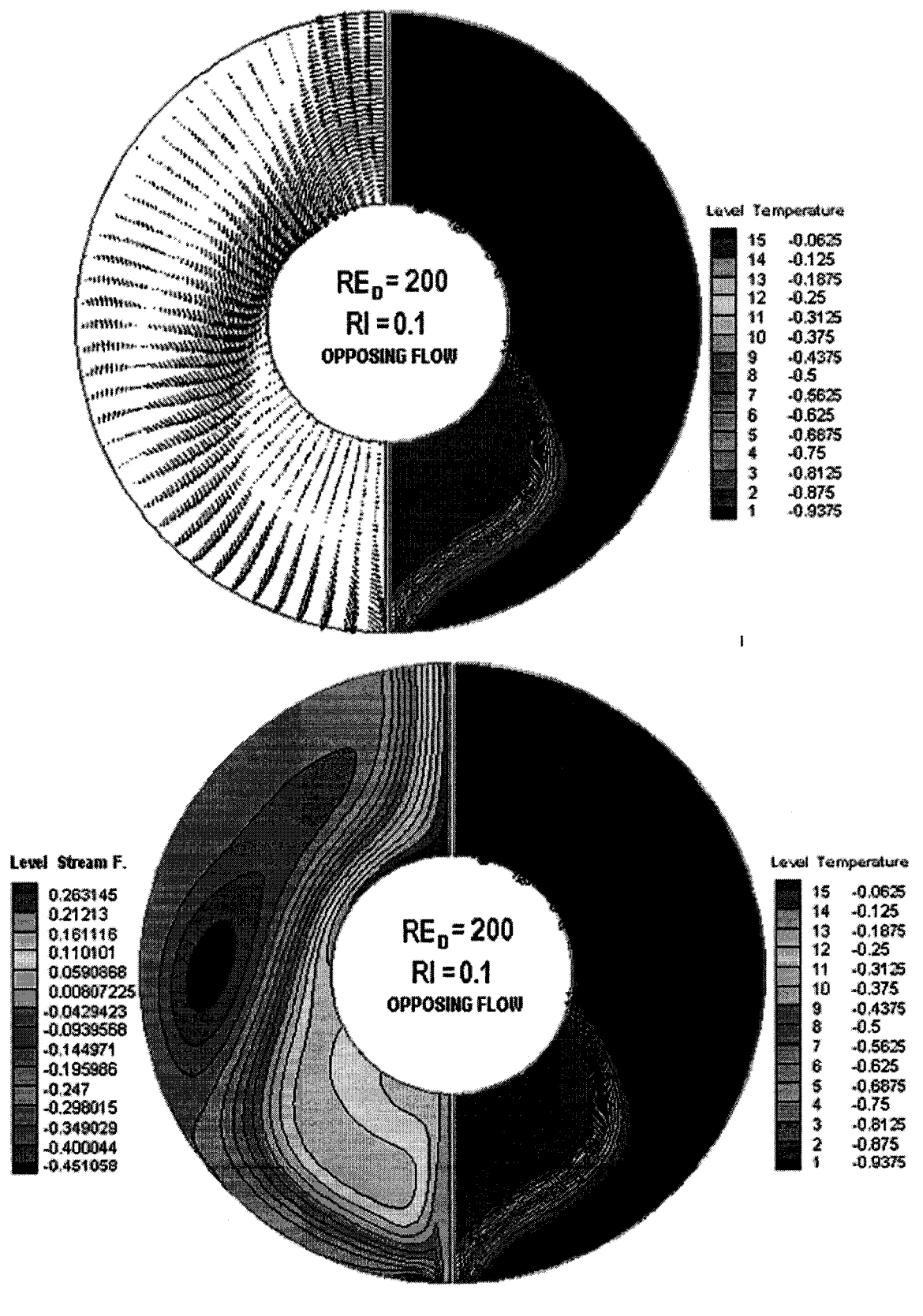


Fig.5: Isotherms and velocity vectors and streamlines for two different Richardson numbers at Reynolds number  $RE_D = 50$ 



(k)  $RE_D=200$ ; and RI=0.1

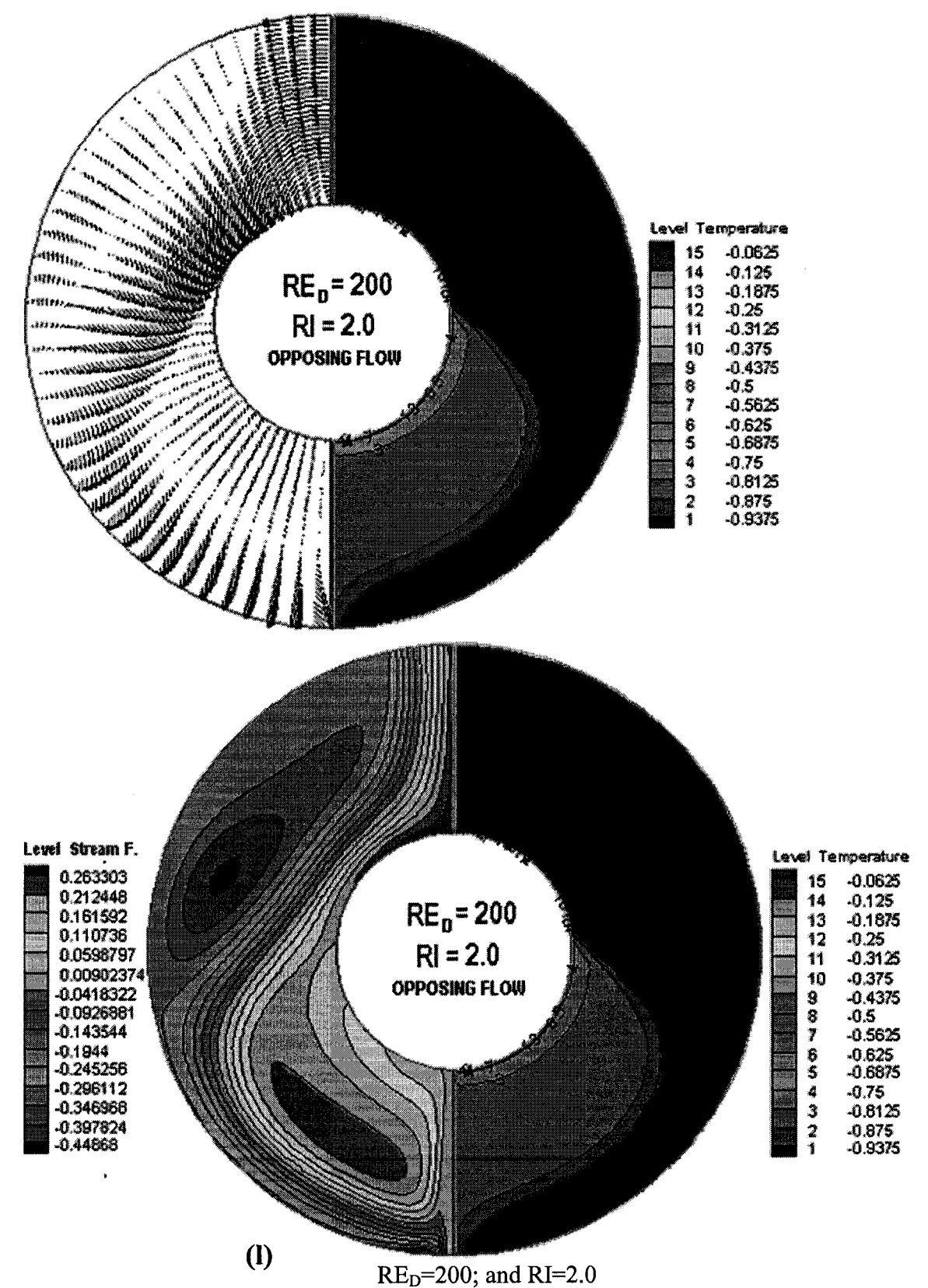
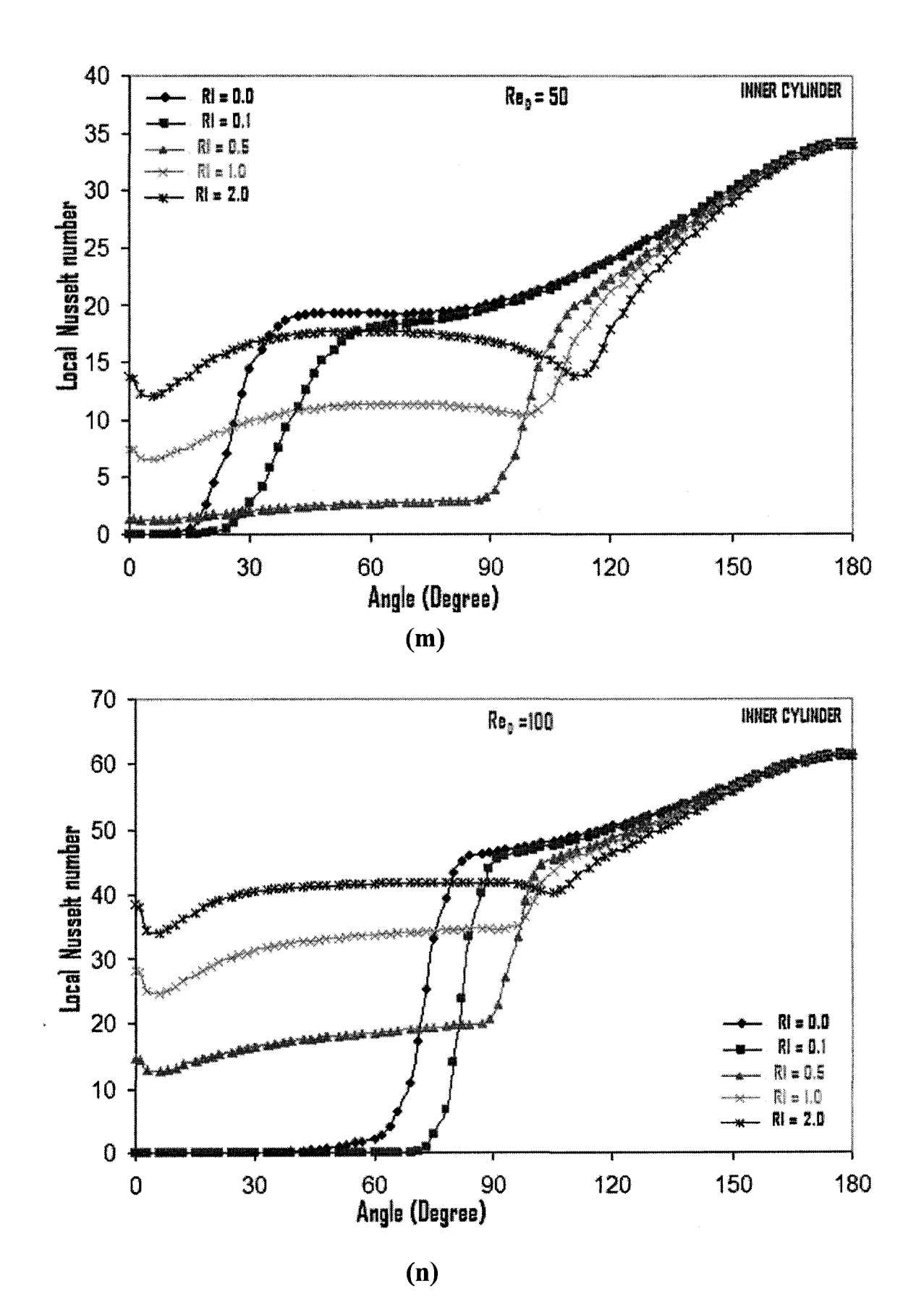


Fig.6: Isotherms and velocity vectors and streamlines for two different Richardson numbers at Reynolds number  $RE_D = 200$ 

## Local Nusselt number distributions

The local Nusselt number along the inner cylinder is calculated for various RI and Re in the opposing flow case. Here, the heat exchange occurs between the hot inner cylinder surface and the cold inlet fluid and the fluid after gaining heat from the inner cylinder they become relatively warmer than the inlet, the warm fluid then comes out through the exit vent. The heat transfer through the upper inner cylinder surface is generally higher for each  $Re_D$  and RI since the influence of forced convection is to increase the heat transfer from the top of the inner cylinder through the cold fluid. In case of pure and dominating forced, mixed, and natural convection flow regimes, it is seen that for opposing flow, at each  $Re_D$ , the local heat transfer rate is generally higher for upto some extent of the upper portion of the inner cylinder wall. From Fig. 6(k), it is observed that at  $Re_D = 200$ , a strong reverse flow occurs and a separate big recirculation cell is formed near the outer cylinder in the lower portion of the domain and this cell is relatively smaller compared to that of the aiding flow situation. An anomalous phenomenon occurs for RI > 0.1, because the buoyancy force opposes the imposed flow in a nonlinear fashion which can be seen in Figs. 7(m)-7(p).

In opposing flow situation, the thermal buoyancy force opposes the momentum of the incoming jet and helps to separate the flow on the inner cylinder earlier compared with aiding flow situation. As a consequence of this, the wake forms earlier from the top which in turns results in inconsistent behavior in this regime. From Figs. 5 and 6, the effects of separation and thermal boundary layer growth on temperature contours can be found. Presented temperature contours reveal that separation angle is a strong function of Reynolds numbers, but it is almost independent of RI numbers. For a fixed RI, the flow separation occurs earlier when the Reynolds number is lower and compared to the aiding flow situation the flow separations occurs faster for a given Re<sub>D</sub> and RI numbers.



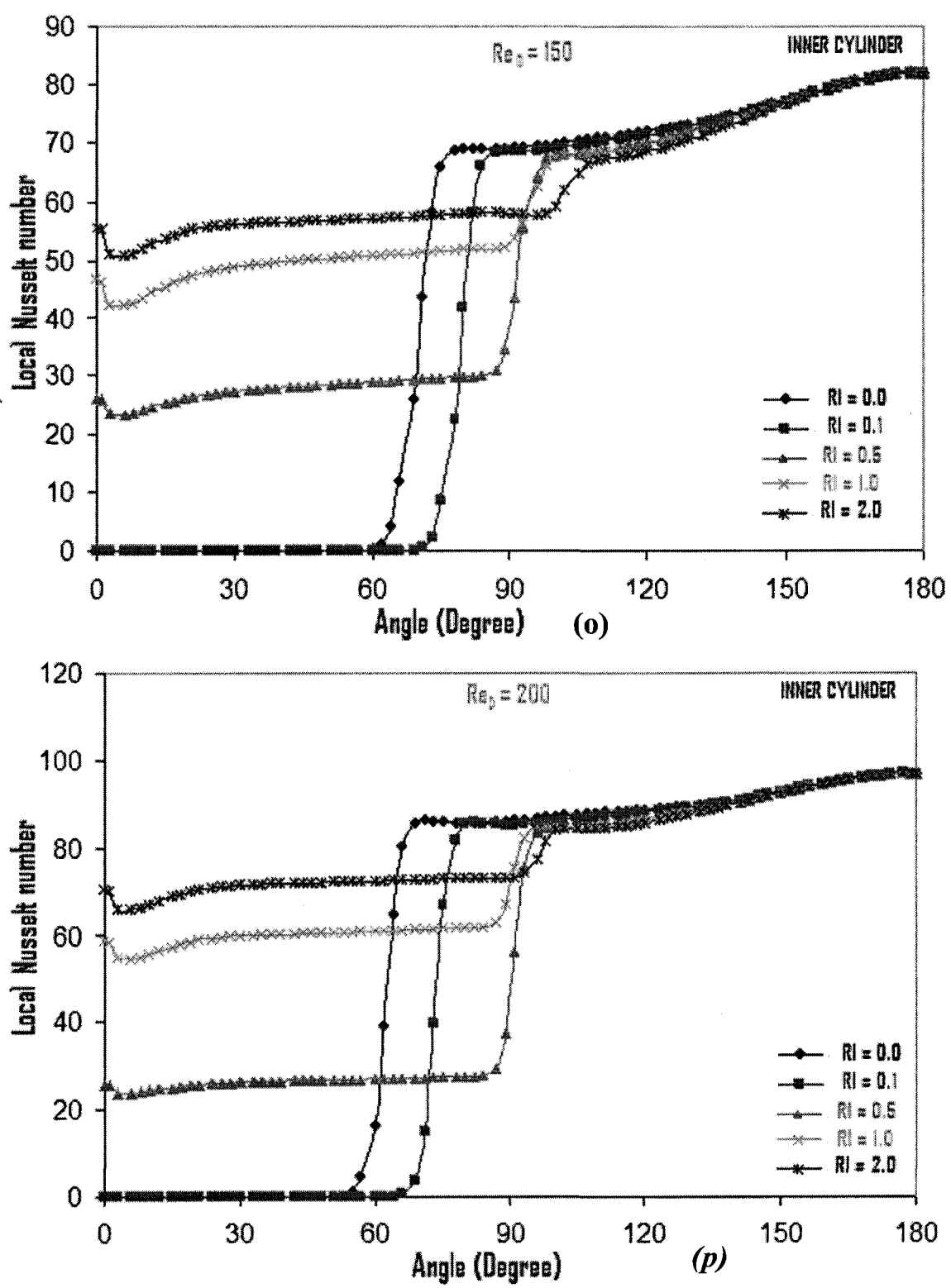


Fig.7: The local Nusselt number on the inner cylinder in case of opposing flow for Richardson numbers (RI=0 means heat transfer without natural convection) at Reynolds number (m) 50, (n) 100, (o) 150, and (p) 200 for inlet angle 15<sup>0</sup> and outlet angle 5<sup>0</sup>

# Average Nusselt number

The effect of the RI on the average Nusselt number is examined for Re<sub>D</sub> =50,100, 150, and 200 when buoyancy forces near the inner cylinder aids and opposes the inlet forced flow. The predicted average Nusselt number results for mixed aiding flow and mixed opposing flow situations are presented through Figs. 8 and 9. From these figures one can see that Nu<sub>Avg</sub> increases with the increase of Re<sub>D</sub> and also enhances with the increase of RI for the aiding flow situations. For opposing flows, Nu<sub>Avg</sub> decreases first and then gradually increases for all Re<sub>D</sub> except for Re<sub>D</sub> =50. At Re<sub>D</sub> =50, for opposing flow the heat transfer rate is maximum when RI=0.0 (purely forced convection). With the increase of RI (for RI≤ 0.5,) Nu<sub>Avg</sub> first deceases but for RI> 0.5, Nu<sub>Avg</sub> gradually increases with the increase of RI but never reaches to the value obtained for pure forced convection. A comparative study of aiding and opposing flow cases was performed and are presented in the form of average Nusselt number as a function of Re for different RI in Figs. 10, 11, 12 and 13. It can be deducted that the average Nusselt number increases with increasing Re<sub>D</sub>. For all RI, the Nu<sub>Avg</sub> is greater for mixed aiding flows compared to mixed opposing flows. For RI=0.1, the Nu<sub>Avg</sub> for the opposing flow is always lower than the purely forced convection situation (Fig. 10). For RI=0.5, the Nu<sub>Avg</sub> for the opposing flow for Re<sub>D</sub> up to about 80, is lower than purely forced convection flow whereas for Re<sub>D</sub> > 80 it is higher. This is due to the fact that the buoyancy force is weaker for RI=0.5. With the increase of Re, the forced flow for this case increases more rapidly.

The data for water in mixed aiding flow situation are correlated using the multi-linear least-squares regression analysis by:

$$Nu_{Av} = 0.7315 (RI)^{0.091} (Re_D)^{0.903}, \quad 0.1 \le RI \le 2.0, \quad 5 \le Re_D \le 200, \quad R^2 = 98.5\%, -----(9)$$

For the opposing flow situation, the correlation is represented by:

$$Nu_{Av} = 0.4059 \; (RI)^{0.116} \; (Re_D)^{0.982}, \quad 0.1 \leq RI \leq 2.0, \quad 5 \; 0 \leq Re_D \leq 200, \quad R^2 = 95.4\% \; ,-----(10)$$

From the above correlations, it is observed that under identical geometric and thermal conditions, the mixed aiding flow leads to a higher heat transfer rate than the mixed opposing flow situation by decreasing the exponents of the Richardson number and Reynolds number, and by increasing the associated coefficient.

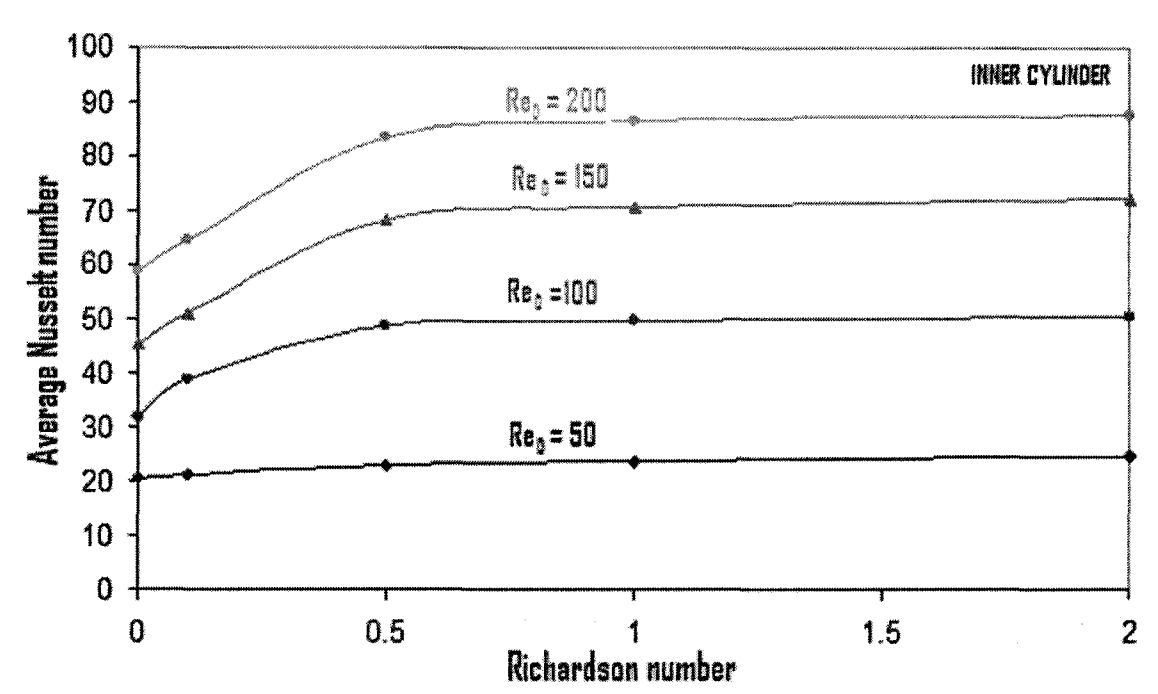


Fig.8: Variation of Average Nusselt number with various Richardson numbers at Reynolds number 50,100,150, and 200 during aiding flow

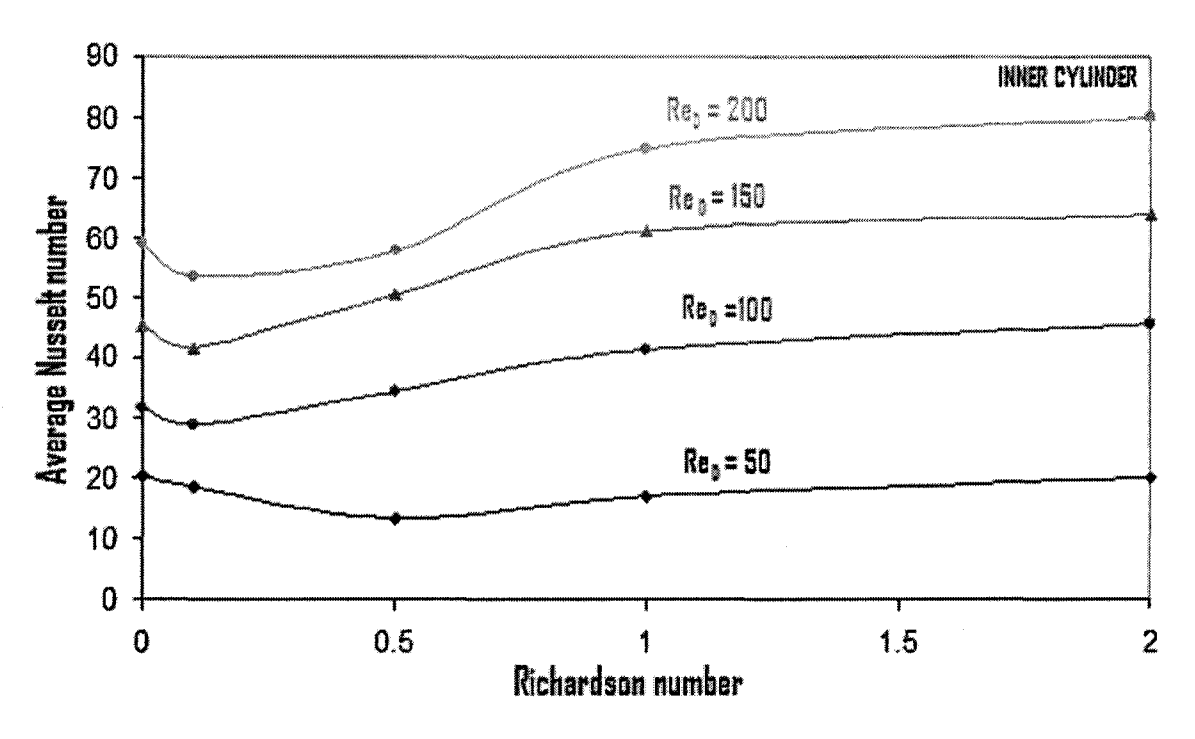


Figure 9: Variation of Average Nusselt number with various Richardson numbers at Reynolds number 50,100,150, and 200 during opposing flow

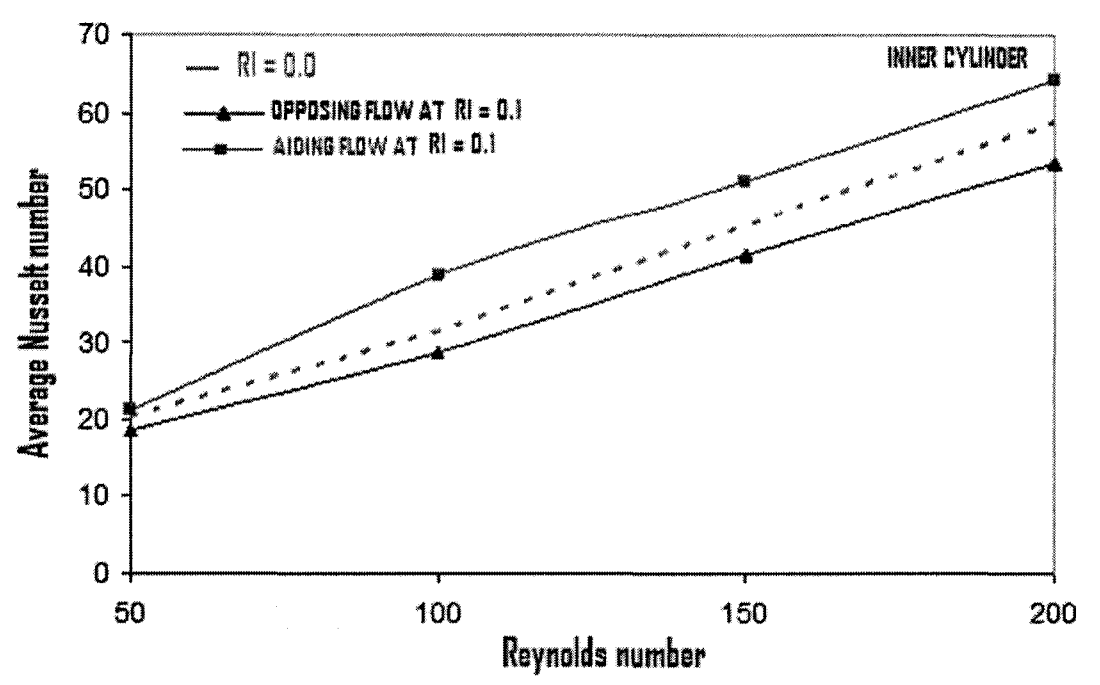


Figure 10: Variation of Average Nusselt number with various Reynolds number at Richardson number 0.1 during opposing, and aiding flow

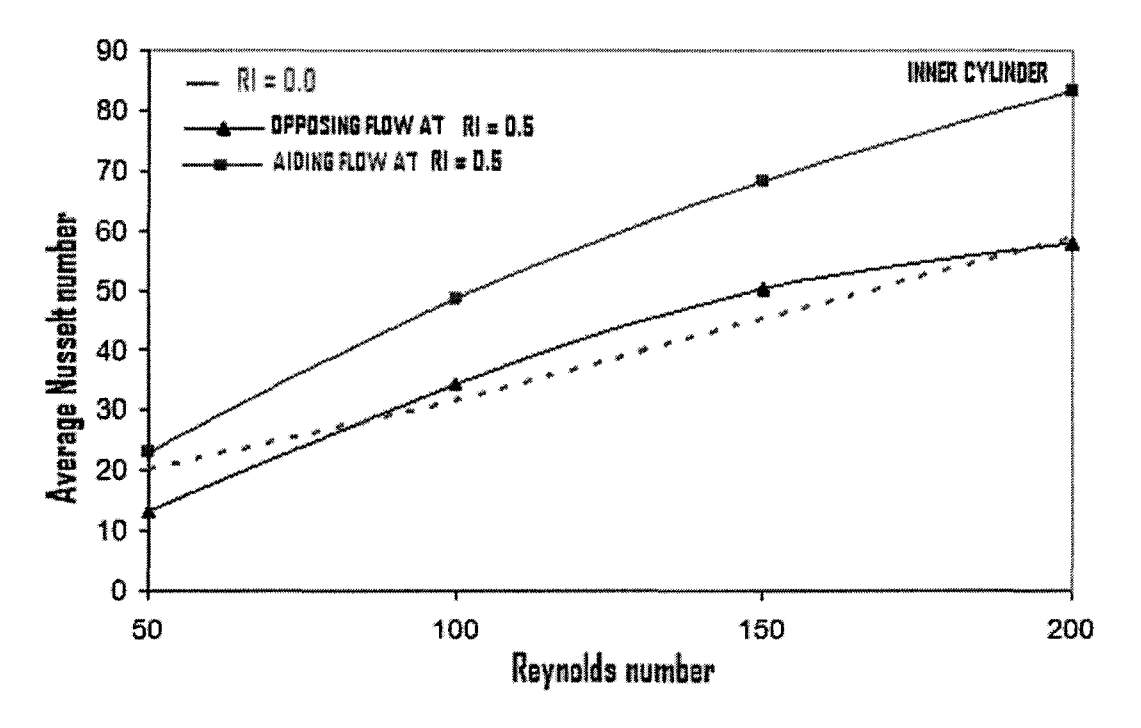


Figure 11: Variation of Average Nusselt number with various Reynolds number at Richardson number 0.5 during opposing, and aiding flow

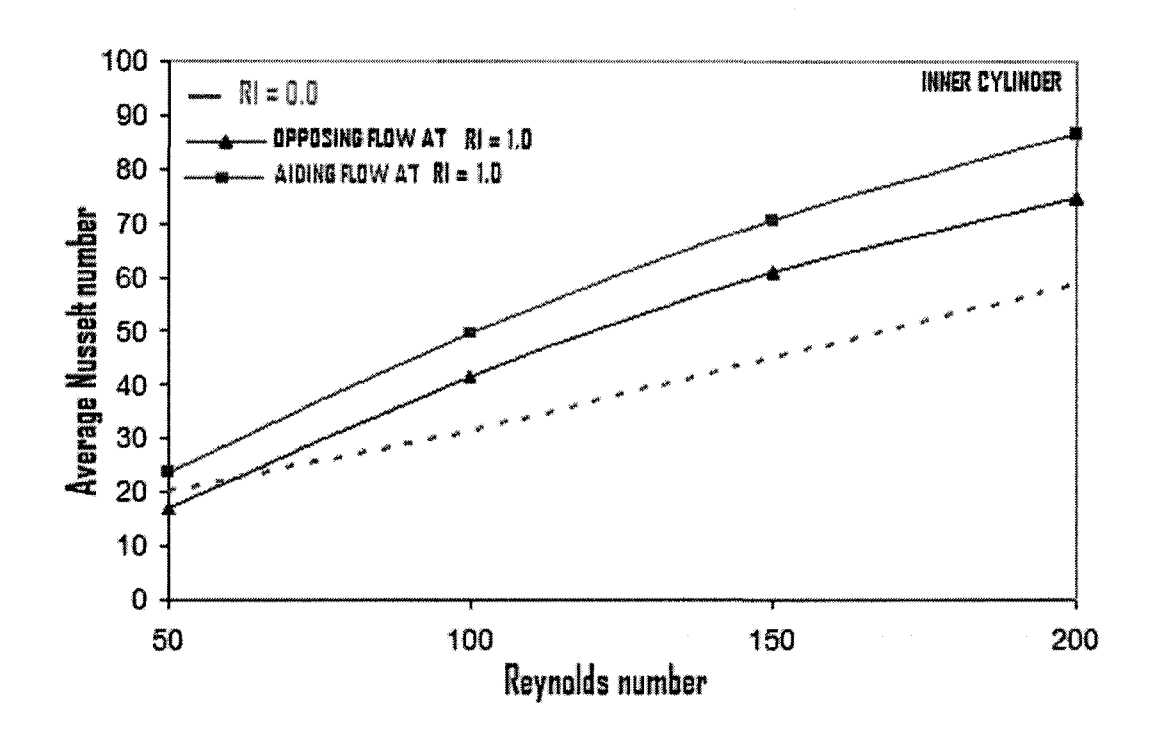


Figure 12: Variation of Average Nusselt number with various Reynolds number at Richardson number 1.0 during opposing, and aiding flow

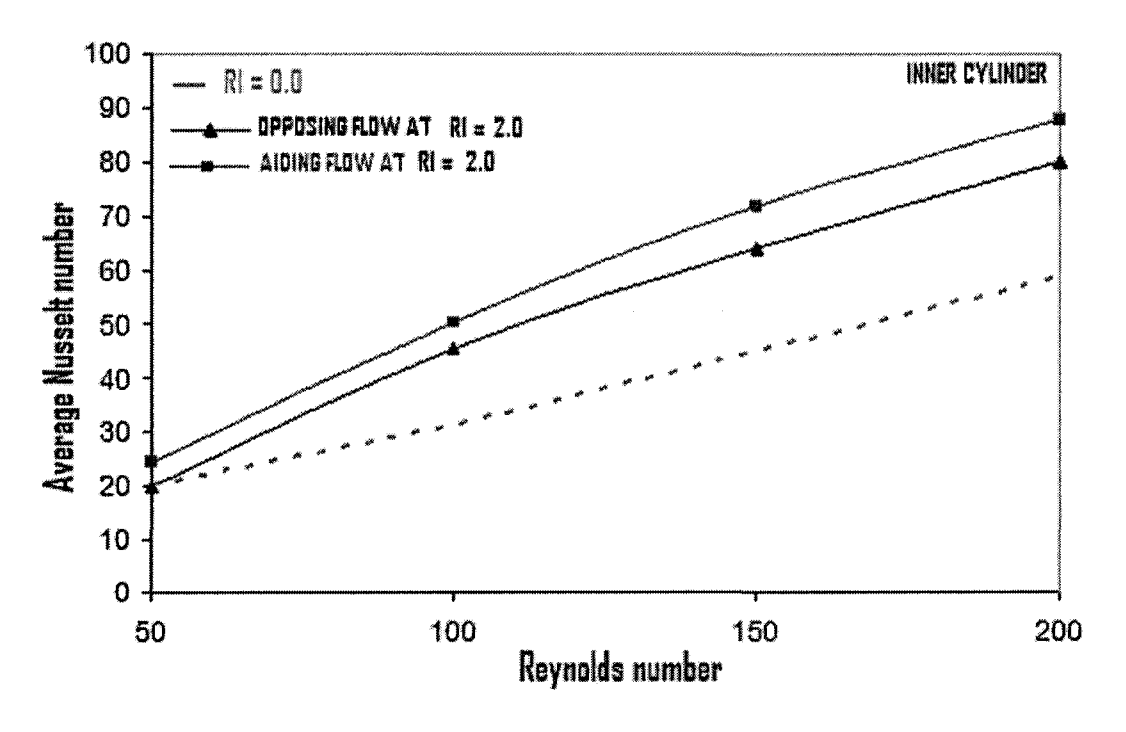


Figure 13: Variation of Average Nusselt number with various Reynolds number at Richardson number 2.0 during opposing, and aiding flow

## **Conclusions**

A numerical study has been carried out on mixed convection heat transfer (laminar natural convection and forced convection) in the annulus between two horizontal concentric cylinders for aiding and opposing flows. It is found that the average Nusselt number is affected considerably by the imposed flow, and the strength of the buoyancy force. Markedly different flow behaviors are observed between two different flow situations. The average Nusselt number increases monotonically with an increasing function of the Richardson number for the aiding flow case while it decreased and then increased with increased Richardson numbers for the opposing flow case. The average Nusselt number is an increasing function of the imposed flow rate for both situations. Since, the imposed flow is stratified (top heated fluid or top cold fluid entering into the annulus), some flow stratification at the bottom regions are observed for all different cases studied. The local Nusselt number at the upper part of the inner cylinder has a high value and it decreases very slowly to some extent along the inner cylinder and this trend is independent of the flow regimes. After the slow decrease along the cylinder, the local Nusselt number then decreases rapidly to a small value at the lower symmetry plane of the annulus for both aiding and opposing flow conditions. At the lower part of the inner cylinder, heat transfer rate is insignificant for RI  $\leq$  0.1, because of the weak buoyancy force effect for both cases. The local Nusselt number near the lower symmetry plane of the inner cylinder exhibits an oscillatory behavior for various ReD and RI numbers. This oscillatory behavior is due to various effects, namely, wake formation, the location of the separation of the flow, the developments of thermal boundary-layer and the presence of weak natural convection. Based on flow visualization, computations predict earlier separation of the flow in case of opposing flow situations compared to the aiding flow situation. This is due to the opposing effects of the thermal buoyancy force on inlet jet. The explanation of the location of separation and formation of wake requires details and more close examination of the flow fields in the domain. For the limited range of parameters studied in this section, it is observed that average Nusselt number is significantly higher for mixed aiding flow than mixed opposing flow. The average Nusselt number correlation is provided separately for aiding and opposing flow situations, which will help in designing horizontal tubular heat exchangers.

### **References:**

- [1] Cha, C.K., Jaluria, Y., "Effect of thermal buoyancy on the recirculating flow in a solar pond for energy extraction and heat rejection", ASME J. Solar Energy Eng., Vol.106, pp.428-437, 1984.
- [2] D. Angirasa, "Mixed convection in a vented enclosure with an isothermal vertical surface", Fluid Dynamics Research, Vol.26, pp.219-233, 2000.
- [3] D.B. Tuft, H. Brandt, "Forced-Convection Heat Transfer in a Spherical Annulus Heat Exchanger<sup>1</sup>", Transactions of the ASME, Vol.104, pp.670-677, 1982.
- [4] George C. Vradis\*, Lara VanNostrand<sup>+</sup>, "Laminar Coupled Flow Downstream of an Asymmetric Sudden Expansion", Journal of Thermophysics and Heat Transfer, Vol.6, pp.288-295, 1992.
- [5] Hsu, T.-H., Hsu, P.-T., How, S.-P., "Mixed convection in a partially divided rectangular enclosure", Numer. Heat Transfer Part A, Vol.31, pp.655-683, 1997.
- [6] Kumer, R., "Yuan, T.D., "Recirculating mixed convection flows in rectangular cavities", AIAA J. Thermophys. Heat Transfer, Vol.3, pp.321-329, 1989.
- [7] M.K. Moallemi, K.S. Jang, "Prandtl number effects on laminar mixed convection heat transfer in a lid-driven cavity", Int. J. Heat Mass Transfer, Vol.35, pp.1881-1892, 1992.
- [8] A.A. Mohammad, R. Viskanta, "Laminar flow and heat transfer in Rayleigh-Benard convection with shear", Phys. Fluids A 4, pp.2131-2140, 1992.
- [9] A.A. Mohammad, R. Viskanta, "Flow structures and heat transfer in a liddriven cavity filled with liquid gallium and heated from below", Exp. Thermal Fluid Sci., Vol.9, pp.309-319, 1994.
- [10] M.A.R. Sharif\*, "Laminar mixed convection in shallow inclined driven cavities with hot moving lid on top and cooled from bottom", Applied Thermal Engineering, Vol.27, pp.1036-1042, 2007.

- [11] Oberkampf, W.L., Crow, L.I., "Numerical study of the velocity and temperature fields in a flow-through reservior", ASME J. Heat Transfer, Vol.98, pp.353-359, 1976.
- [12] Papanicolaou, E., Jaluria, Y., "Mixed convection from an isolated heat source in a rectangular enclosure", Numer. Heat Transfer Part A, Vol.18, pp.427-461, 1990.
- [13] Papanicolaou, E., Jaluria, Y., "Transition to a periodic regime in mixed convection in a square cavity", J. Fluid Mech., Vol.239, pp.489-509, 1992.
- [14] Papanicolaou, E., Jaluria, Y., "Mixed convection from a localized heat source in a cavity with conducting walls: a numerical study", Numer. Heat Transfer Part A, Vol.23, pp.463-484, 1993.
- [15] Papanicolaou, E., Jaluria, Y., "Computation of turbulent flow in mixed convection in a cavity with a localized heat source", J. Heat Transfer, Vol.117, pp.649-658, 1995.
- [16] Patankar, S.V., "Numerical Heat Transfer and Fluid Flow", Taylor & Francis, London, 1980.
- [17] Pérez-Segarra, C.D., Oliva, A., Costa, M., Escanes, F., "Numerical experiments in turbulent natural and mixed convection in internal flows", Int. J. Numer. Meth. Heat Fluid Flow, Vol.5, pp.13-33, 1995.
- [18] S.M., Saeidi, J.M. Khodadadi, "Forced convection in a square cavity with inlet and outlet ports", International Journal of Heat and Mass Transfer, Vol.49, pp.1896-1906, 2006.
- [19] Sparrow, E.M., Samie, F., "Interaction between a stream which passes through an enclosure and natural convection within the enclosure", Int. J. Heat Mass Transfer, Vol.25, pp.1489-1502, 1982.
- [20] Torrance, K., Davis, R., Eike, K., Gill, P., Gutman, D., Hsui, A., Lyons, S., Zien, H., "Cavity flows driven by buoyancy and shear", J. Fluid Mech. Part 2, Vol.51, pp.221-231, 1972.

# Chapter 4

Numerical Investigation of Buoyancy Driven Flow of Nanofluids in a Horizontal Cylindrical Annulus

#### **ABSTRACT**

A steady-state laminar two dimensional model is developed to analyze natural convection heat transfer in an annulus between horizontal circular cylinders holding a nanofluid. It is assumed that the stable nanofluid behaves as a single phase fluid, there is no velocity slip between the base fluid (water) and the nano particles and the base fluid and the nano particles are in thermally equilibrium. For a fixed diameter of the nanoparticles, the parameters governing this problem are: Rayleigh number (Ra), and solid volume fraction  $(\Phi)$ . Simulations are carried out for Cu-water nanofluids. Except for Ra= $10^3$ , the results show that the presence of nanoparticles systematically decreases the natural convective heat transfer coefficient on the inner cylinder, an observation which is in agreement with the recent experimental observations but is in contrast with the previous numerical study for a rectangular cavity. At low Rayleigh numbers, heat transfer is predominantly dominated by conduction and the Nusselt number increases with increasing nanoparticles concentrations. A probable reason for this expected result may be due to the increasing conductivity of nanofluids compared to the base fluid. The maximum reduction in heat transfer is observed at higher Rayleigh numbers and is found to be around 35% for the limited range of parameters of this study. The dispersion effect of nanoparticles might have played an important role in reducing the heat transfer coefficients at higher Rayleigh numbers. Empirical correlations are obtained for the average Nusselt number on the inner cylinder as a function of the annulus gap-based Rayleigh number and volume fraction. The velocity vectors, streamlines and isotherms are also presented to reinforce the heat transfer results.

## Introduction

The buoyancy-induced flows or natural convection, and heat transfer through different geometries with nanofluids, which have much higher thermal conductivity than convectional fluids, are being increasingly studied experimentally and numerically for its many potential applications in the industrial sectors including transportation, power generation, micromanufacturing, chemical and metallurgical industries, as well as cooling, heating, ventilation and air-conditioning industry. Conversely, the nanofluids may help to enhance or reduce the

heat transfer rate, depending on the amount of millimeter and/or micrometer-sized solid particles are present in the nanofluids. Nanofluids with substantially higher conductivities are expected to exhibit superior heat transfer properties compared with conventional heat transfer fluids, such as water, oil, and ethylene glycol mixture which has low thermal conductivity. Nanofluids have a distinctive characteristic, which is quite different from those of conventional solid-liquid mixtures. Small particles (nanoperticles) stay suspended much longer than larger particles and exhibit little or no substantial additional pressure drop when flowing through the small passages. Moreover, when fluid flows through small passages, they are best because nanoparticles behave similar to the liquid molecules.

Choi [1995] is the first who coined the term nanofluids, a fluid with suspended nanoparticles. He reported a 0.3% volume fraction of 10nm diameter copper Cu nanoparticles in ethylene glycol enhanced about 40% of the thermal conductivity of the base fluid. Choi et al. [2002] explained the reasons of enhancement of thermal conductivity by postulating various causes such as nanoparticles clustering, ballistic phonon transport, layering at the solid/liquid interface, etc. The interaction and collision among particles and the increased surface area of the suspended particles also are significant reasons for improvement of the heat transfer of the fluid. From the recent literature on nanofluids, it is observed that a very few investigations have been carried out with nanofluids for natural convection heat transfer. Khanafer et al. [2003] investigated numerically the heat transfer phenomenon of nanofluids in a two-dimensional rectangular enclosure. The nanofluids was assumed to be in a single phase, in thermally equilibrium with the base fluid (water) and there was no velocity slip between base fluid and nanoparticles. They reported that the heat transfer rate increased with the enhancement of the particle concentration at any given Grashof number. Rong-Yuan et al. [2006] numerically analyzed the Khanafer's model for nanofluids and investigated on the heat transfer performance of nanofluids inside an enclosure taking into account the solid particles dispersion. They analyzed various governing parameters, like volume fraction, Grashof number, and aspect ratio of the twodimensional rectangular enclosure. Similar to Khanafer et al. [2003], they also showed that the average heat transfer coefficient increases with the increasing Rayleigh number and volume fraction of nanofluids. Their conclusions are similar to the conclusions of Khanafer

et al.'s. But completely different experimental heat transfer results for nanofluidsh were found by Putra et al. [2003], Nnanna et. al. [2004], and Wen and Ding [2005]. Putra et al. [2003] presented experimental investigation of buoyancy driven flow with nanoparticles CuO (87.3 nm) and Al<sub>2</sub>O<sub>3</sub> (131.2) in water nanofluids inside a horizontal cylinder heated from one end and cooled from the other. They reported a systematic and definite reduction of the natural convective heat transfer, which was dependent on the particle density, concentration, and aspect ratio of the cylinder. The deterioration of heat transfer increased with particle concentration and was more significant for CuO nanofluids than Al<sub>2</sub>O<sub>3</sub> nanofluids. For example, at a Rayleigh number of  $5x10^7$ , they found the average Nusselt number decreased by about 300% and 150% for 4 wt% of CuO and Al<sub>2</sub>O<sub>3</sub> nanofluids, respectively. Wen and Ding [2005] carried out experiments on natural convection of TiO<sub>2</sub> (30-40nm)-water nanofluids in a vessel which composed of two horizontal aluminum discs of diameter 240 mm and thickness 10 mm separated by a 10 mm gap. They investigated transient and steady heat transfer coefficients for various solid volume fractions of nanofluids. They also found that the natural convective heat transfer coefficient deteriorated with particle concentrations and was lower compared to that of pure water. The reduction of the natural convective heat transfer coefficient was also reported by Nnanna et. al.[2004] through experiments with aluminum/water nanofluids. Wen and Ding [2006] found experimentally (by using a different method of formulation of nanofluids) that the presence of nanoparticles in distilled water (Titanium-dioxide nanofluids) systematically decreases the natural convection heat transfer coefficient.

Xuan and Li [2003] experimentally investigated flow and convective heat transfer characteristics of Cu-water based nanofluids by passing the nanofluids through a straight tube and by imposing a constant heat flux on the wall. Results reveal that the nanofluids give a substantial enhancement of heat transfer rate compared to the pure fluid. They also claimed that the friction factor for nanofluids at low volume fraction did not produce any extra penalty in the pumping power. Then, what caused the discrepancy between the numerical results and experimental data regarding natural convection from various investigators of nanofluids is a controversy yet to be revealed. From the available experimental and numerical results it has been clearly seen that the heat transfer behavior of

nanofluids is very complex and the applications of nanofluids for heat transfer enhancement should not be decided only by their key factor, the effective thermal conductivity. Many other factors such as particle size, particle shape, particle distribution, concentration difference, particle-fluid and particle-particle interactions, and modifications of the dispersion properties may have important influence on the heat transfer behavior of nanofluids.

On the basis of the above literature studies, the objectives of this part of the thesis research work are to evaluate numerically the circumferential average and the local Nusselt number along the inner and outer walls utilizing Cu nanoparticles in water inside the annulus of concentric horizontal cylinders. To the best of the author's knowledge, there exist no theoretical or experimental studies concerning natural convection heat transfer in nanofluids around a horizontal cylinder or horizontal annulus. Thus the interaction between the buoyancy stemming from isothermally heated inside cylinder and the cooled outside cylinder with nanofluids is the topic of the current investigation. This geometric arrangement has potential applications in heat exchangers.

The circumferential average Nusselt numbers are useful to the heat exchanger design engineers. The local Nusselt number, which is difficult to obtain experimentally, is presented in this study to gain insights to the heat transfer processes. To the best of author's knowledge, there are no published data investigating the effect of Cu-water nanofluids on heat transfer in laminar natural convection in annular geometry.

The remainder of this paper is divided into two main sections. In the next section, the physical situation and the mathematical formulation of the problem considered is described and this section is followed by the presentation of results and discussion. Finally, some concluding remarks are given.

# Mathematical formulation

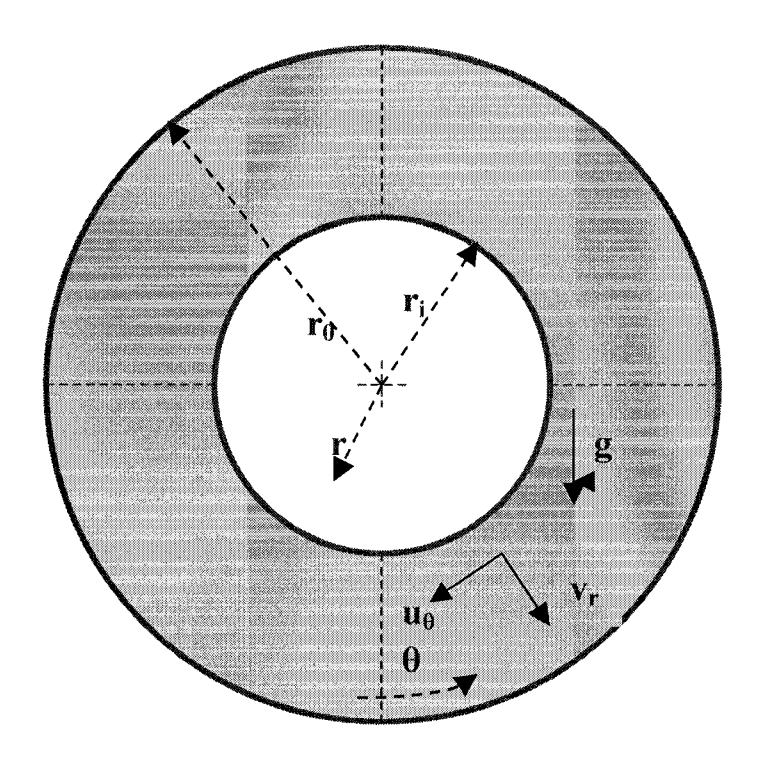


Figure 1: Flow geometry for the physical model

The physical model of the problem is illustrated schematically in Fig. 1. The radius of the inner cylinder is denoted by  $r_i$  while that of the outer cylinder is denoted by  $r_0$ . The inner and outer cylinders are considered to be made of copper and each cylinder has a wall thickness which is equal to one grid distance. The inner and outer cylinders are maintained at temperatures  $T_i$  and  $T_0$  ( $T_0 < T_i$ ), respectively. The cylinders are assumed to be long enough that a two dimensional analysis can be applied. The nanofluids in the annulus are considered as Newtonian and incompressible, and the flow is laminar. The nanoparticles are assumed to have a uniform shape and size. It is assumed that both the fluid phase and nanoparticles are in thermal equilibrium state and they flow at the same velocity. Due to symmetry, the computations are carried on only half the physical domain, making use of the vertical symmetry plane passing through the center of the cylinder. The thermo-physical properties of the nanofluids are temperature-independent, except for the density, for which the Boussinesq approximation is applicable. Viscous dissipation, compressibility effects, radiation, particle shape, particle distribution, concentration difference, particle-fluid and particle-particle interactions, and modifications of the dispersion properties are neglected.

The dimensionless, initial and boundary conditions for the present investigation are given as

- $\bullet$  U=V= $\phi$ =0
- On the inner cylinder surface, i.e., Ri=1.0; U=V=0.0;  $\phi_i = 1.0$
- On the outer cylinder surface, i.e., Ro=2.6; U=V=0.0;  $\phi_0 = 0.0$
- Lower plane of symmetry; i.e.,  $\theta = 0$  ; U=0.0;  $\frac{\partial V}{\partial \theta} = \frac{\partial \phi}{\partial \theta} = 0.0$
- Upper plane of symmetry; i.e.,  $\theta = \pi$ ; U=0.0;  $\frac{\partial V}{\partial \theta} = \frac{\partial \phi}{\partial \theta} = 0.0$

The dimensionless variables (capital letters) are then defined as

$$R = \frac{r}{r_i} \; ; \quad U = \frac{u}{\alpha/r_i} \; ; \quad V = \frac{v}{\alpha/r_i} \; ; \quad \phi = \frac{T - T_{ref}}{T_i - T_0} \; ; \quad Ra = \frac{r_i^3 \beta g (T_i - T_0)}{v \alpha}$$

$$P^* = \frac{\rho (r_i \operatorname{Pr})^3}{\mu^2} \left[ P + \left( \rho_{ref} (1 - \beta T_{ref}) - \frac{\operatorname{Pr}^2 \rho^3 \beta T_{ref}}{\mu} \right) gr \cos \theta \right]$$

The effective density of the nanofluids at a reference temperature is given by

$$\rho_{nf} = (1 - \Phi)\rho_f + \Phi\rho_s \quad ---- \qquad (4)$$

where,  $\rho_f$ ,  $\rho_s$ , and  $\Phi$  are the density of water, density of the nanoparticles—and the volume fraction of the of the nanoparticles, respectively. According to Brinkman [1952] the effective viscosity of a fluid of viscosity  $\mu_f$  containing a dilute suspension of small rigid spherical particles is given as

$$\mu_{eff} = \frac{\mu_f}{(1 - \Phi)^{2.5}} \tag{5}$$

The heat capacity of the nanofluid can be presented as

$$(\rho C_{\rm P})_{nf} = (1 - \Phi)(\rho C_{\rm P})_f + \Phi(\rho C_{\rm P})_s - \dots$$
 (6)

Wasp [1977] introduced the effective stagnant thermal conductivity of the solid-liquid mixture as follows

$$\frac{\left(k_{eff}\right)_{stagnant}}{k_{f}} = \frac{k_{s} + 2k_{f} - 2\Phi(k_{f} - k_{s})}{k_{s} + 2k_{f} + \Phi(k_{f} - k_{s})}$$
 (7)

This equation is only applicable for two-phase mixture containing micro-sized particles. Due to unavailability of any convenient formula for the calculations of the stagnant thermal conductivity of nanofluids, Eq. (6) is applied here to get a reasonable estimation of the natural convection heat transfer coefficient.

The effective thermal conductivity of the nanofluids can be written as:

$$k_{eff} = (k_{eff})_{stagnant} + k_d \qquad (8)$$

Due to thermal dispersion, the enhancement in the thermal conductivity is gives as:

$$k_d = C(\rho C_{\rm P})_{nf} |\overline{V}| \Phi d_{\rm P} \qquad (9)$$

Where,  $|\overline{V}| = \sqrt{u^2 + v^2}$  and C is an unknown constant which should be determined by matching experimental data. The steady-state, laminar two-dimensional conservation equations of mass, momentum and energy for a Newtonian fluid in the conservative form in cylindrical coordinates, including the Boussinesq approximation, can be written in non-dimensional form by incorporating the dimensionless parameters from Eq. (3)

Using Boussinesq approximation, the density term is given by

$$\rho = \rho_{ref} \left[ 1 - \beta \left( T - T_{ref} \right) \right] \qquad (10)$$

Continuity:

$$\frac{1}{R}\frac{\partial(RV)}{\partial R} + \frac{1}{R}\frac{\partial U}{\partial \theta} = 0 \qquad (11)$$

U-momentum equation:

$$\frac{1}{R}\frac{\partial}{\partial R}(RUU) + \frac{1}{R}\frac{\partial}{\partial \theta}(UV) = \frac{1}{(1-\Phi)^{2.5}\left[\Phi\frac{\rho_s}{\rho_f} + (1-\Phi)\right]\sqrt{Gr}}\left[\frac{1}{R}\frac{\partial}{\partial R}\left(R\frac{\partial U}{\partial R}\right) + \frac{1}{R}\frac{\partial}{\partial \theta}\left(\frac{1}{R}\frac{\partial U}{\partial \theta}\right)\right]$$

$$-\frac{1}{R}\frac{\partial P^*}{\partial \theta} + 2GAMA\frac{Pr}{R^2}\frac{\partial V}{\partial \theta} - Pr\frac{U}{R^2} - GAMA\frac{UV}{R} + \lambda\phi\sin\theta \qquad (12)$$

V-momentum equation:

$$\frac{1}{R \partial R} (RUV) + \frac{1}{R \partial \theta} (VV) = \frac{1}{(1-\Phi)^{2.5}} \left[ \Phi \frac{\rho_s}{\rho_f} + (1-\Phi) \right] \sqrt{Gr} \left[ \frac{1}{R \partial R} \left( R \frac{\partial V}{\partial R} \right) + \frac{1}{R \partial \theta} \left( \frac{1}{R \partial \theta} \frac{\partial V}{\partial \theta} \right) \right] 
- \frac{\partial P^*}{\partial R} - 2GAMA \frac{\Pr}{R^2} \frac{\partial U}{\partial \theta} - \Pr \frac{V}{R^2} - GAMA \frac{U^2}{R} - \lambda \phi \cos \theta \right]$$
where, 
$$GAMA = \frac{1}{\left[ (1-\Phi)^{2.5} \left\{ \Phi \frac{\rho_s}{\rho_f} + (1-\Phi) \sqrt{Gr} \right\} \right]} \quad \text{and} \quad \lambda = \frac{\beta_{\text{nf}}}{\beta_{\text{f}}}$$

Energy equation:

$$\frac{1}{R^2} \frac{\partial}{\partial R} (RV\phi) + \frac{1}{R} \frac{\partial}{\partial \theta} (U\phi) = \frac{1}{\Pr{\sqrt{Gr}}} \left[ \frac{1}{R} \frac{\partial}{\partial R} \left( \varepsilon * R \frac{\partial \phi}{\partial R} \right) + \frac{1}{R} \frac{\partial}{\partial \theta} \left( \varepsilon * \frac{1}{R} \frac{\partial \phi}{\partial \theta} \right) \right] - \dots (14)$$

where, 
$$\varepsilon = \left[ \frac{\frac{\left(k_{eff}\right)_{stagnant}}{k_f}}{\left(1 - \Phi\right) + \Phi \frac{\left(\rho C_{\rm p}\right)_s}{\left(\rho C_{\rm p}\right)_f}} + C\Phi \frac{d_{\rm p}}{H} \Pr \sqrt{Gr} \sqrt{U^2 + V^2} \right]$$

# Average and local Nusselt number calculations

For presenting the results two quantities are used. These are circumferential average equivalent thermal conductivity ( $\bar{K}_{eq_{inner}}$ ) and local equivalent thermal conductivity  $K_{eq}$  along the inner cylinder.

$$\overline{K}_{eq_{inner}} = \frac{\overline{Nu_{avg}}}{Nu_0}$$
 and  $K_{eq} = \frac{Nu_L}{Nu_0}$ 

 $\overline{Nu_{avg}}$  = circumferential average Nusselt number based on cylinder radius, is calculated as

$$\overline{Nu}_{avg} \underset{\text{at } r=r_i}{\text{at } r=r_i} = \frac{\int_0^L \int_0^\pi (Nu_L)_{r=r_i} r_i d\theta dZ}{\int_0^L \int_0^\pi r_i d\theta dZ}; \text{ and } Nu_{L \text{ at } r=r_i} = \frac{h(\theta)r_i}{k}; \text{ where, } h(\theta) = \frac{q_w}{T_w - T_{ref}};$$

$$q_{w \text{ at } r=r_i} = -k \frac{\partial T(r_i, \theta)}{\partial r}$$

 $Nu_0$  = Nusselt number for conduction between the annuli. The subscript o indicates Nusselt number for conduction heat transfer in the annulus. This is obtained by solving the one-dimensional conduction equation at steady state which is given by

$$\frac{1}{r}\frac{\partial}{\partial r}\left(kr\frac{\partial T}{\partial r}\right) = 0 \tag{15}$$

The Nusselt number for conduction is evaluated as

$$Nu_0 = \frac{1}{\ln \frac{R_0}{R_i}}$$

A Lagrangien interpolation scheme is used to calculate the local Nusselt number results because of the non-uniform grid distributions near the walls. And the average Nusselt numbers are obtained by integrating the local Nusselt numbers along the inner cylinder, which are numerically calculated using the Simpson rule for a definite integral.

### Results and discussion

Natural convection flow and temperature fields in a horizontal cylindrical annulus with nanofluids are examined. The numerical code developed in the present study is used to carry out a number of simulations for a wide range of the controlling parameters, namely Ra and  $\Phi$ . The ranges of Ra and  $\Phi$  for this investigation are varied between  $10^3 \le \text{Ra} \le 10^6$  and  $0 \le \Phi \le 20\%$ , respectively. The thermo-physical properties of fluid and the solid phases are shown in Table-1. The results are presented next.

Table 1: Thermophysical properties of different phases

Property	Fluid phase (water)	Solid phase (copper)
C <sub>P</sub> (J/kgK)	4179	383
$\rho  (\text{kg/m}^3)$	997.1	8954
k(W/mK)	0.6	400
$\beta$ (K <sup>-1</sup> )	2.1X10 <sup>-4</sup>	1.67X10 <sup>-5</sup>

To test and assess the grid independence of the present solution scheme, numerical simulations are compared with the literature values for cylindrical annulus and are discussed in Chapter-1 and will not be repeated here. These simulations show that an equally spaced B-Type staggered grid mesh of 82x82 is adequate to describe the flow and heat transfer processes correctly. Further increase in the number of grid points produced the same results. The validation of presently used in-house numerical code is performed against the results generated by other authors for pure fluids and are discussed in detail in Chaper-1.

The velocity vectors, streamlines and temperature contours for a solid volume fraction of 20% for various Rayleigh numbers are presented in Figs. 2(a)-2(d). The inner cylinder wall is at a higher temperature compared to the outer cylinder as a result at and near the inner cylinder wall the nanofluids are moving upward while at the outer cylinder wall the nanofluids move downward due to the buoyancy effects. As can be seen from Figs. 2(a)-2(d), there is a single recirculation zone and the recirculation is clockwise and the fluid motion is mainly dictated by the imposed Rayleigh number. The formation of the thermal boundary layer on the inner and outer cylinder walls can be noticed. As Rayleigh number increases, the heat transfer increases as the thermal boundary layers are getting thinner near the inner cylinder walls. The isotherms spread outs more in the flow direction with increased Ra because of the increased natural convection strength. When  $\Phi=0$ , i.e., for the base fluid and for the increased  $\Phi$ , up to 0.2, i.e., for the nanofluids, there is no significant effects on the velocity vectors, streamlines and isotherms and this is true for different Rayleigh numbers. It means, the flow pattern characteristics are almost similar for  $0 \le \Phi \le 15\%$ shown in Figs. 3(e)-3(h). For a fixed Rayleigh number, there is a considerable change in the local Nusselt number profile around the inner cylinder with the solid volume fraction of nanoparticles which can be observed in Figs. 6-9.

For Ra>10<sup>3</sup>, the pattern is similar for all values of  $\Phi$ . It decreases monotonically with the increase of  $\Phi$ . Figure 9 shows that at Ra=10<sup>3</sup>, Nu<sub>L</sub> has a sudden increase for higher values of  $\Phi$  after 90<sup>0</sup> from the lower part of the inner cylinder. This behavior is very logical because here the flow is conduction dominated and buoyancy force is very small and the effective thermal conductivity of nanofluids is higher with the increase of solid volume fraction. In this investigation the effective thermal conductivity is calculated as follows:

$$K_{eff} = (1 - \Phi)K_f + \Phi K_s$$

where,  $K_S$  is the conductivity of the solid particles and is much higher than the conductivity of the base fluid  $K_f$ . With this formulation, for increasing of  $\Phi$ ,  $K_{eff}$  increases rapidly. But in case of higher Rayleigh number, i.e.,  $Ra > 10^3$  the  $Nu_L$  decreases with the increase of  $\Phi$  because of the increased buoyancy and shear forces. As the solid volume fraction enhances, with higher Rayleigh number irregular and random movements of the particles increases the frictional loss between the wall and solid particles and consequently decreases energy exchange rate in the fluid. For this reason may be the thermal dispersion in the flow of nanofluids decreases. In addition, the velocity at the upper part of the annulus for a higher Rayleigh number is large compared to that at the inner cylinder wall boundary where the fluid is moving at lower velocities. At the higher velocity regions, the friction between the particles may play a significant role in reducing the natural convective heat transfer coefficient for increasing of  $\Phi$ . Moreover, the results presented here are in the form of local Nusselt number ( $Nu_L$ ) as the function of the product of the Grashof number (Gr) and Prandtl number (Gr), which are defined on the basis of pure fluid properties as

$$Nu_{L \text{ at } r=r_i} = \frac{h(\theta)r_i}{k_f}$$
,  $Pr = \frac{\upsilon_f}{\alpha}$ ;  $\alpha = \frac{\kappa_f}{\rho_f C_{Pf}}$ ;  $\upsilon_f = \frac{\mu_f}{\rho_f}$ ;  $Gr = \frac{g\beta\Delta T(r_0 - r_i)^3}{\upsilon_f^2}$ 

Where,  $r_i$ =inner cylinder radius,  $K_f$  the thermal conductivity of the fluid,  $v_f$  the kinematic viscosity of the fluid,  $\alpha$  the thermal diffusivity of the fluid,  $\rho_f$  the density of the fluid,  $C_{Pf}$  the fluid thermal capacity and  $\mu_f$  fluid dynamic viscosity.

From the above mathematical terms it can be seen that for a fixed fluid Pr and Gr, when  $\Phi$  increases the density of the nanofluids increases, which may lead to a disproportionate thermal diffusivity and kinematic viscosity of the nanofluids in some specific regions and it is also probable that the nanofluids becomes non-Newtonian in rheological characteristics in some regions. As a consequence of the above causes, the actual Prandtl number of the nanofluids may be decreased compared to the pure fluid which may lead to the formation of thicker thermal boundary layer near the wall compared to the pure fluid and as a result the temperature gradient i.e., the heat transfer rate has decreased. This may be one of the causes in the reduction of the natural convective heat transfer with the increased particle volume fractions.

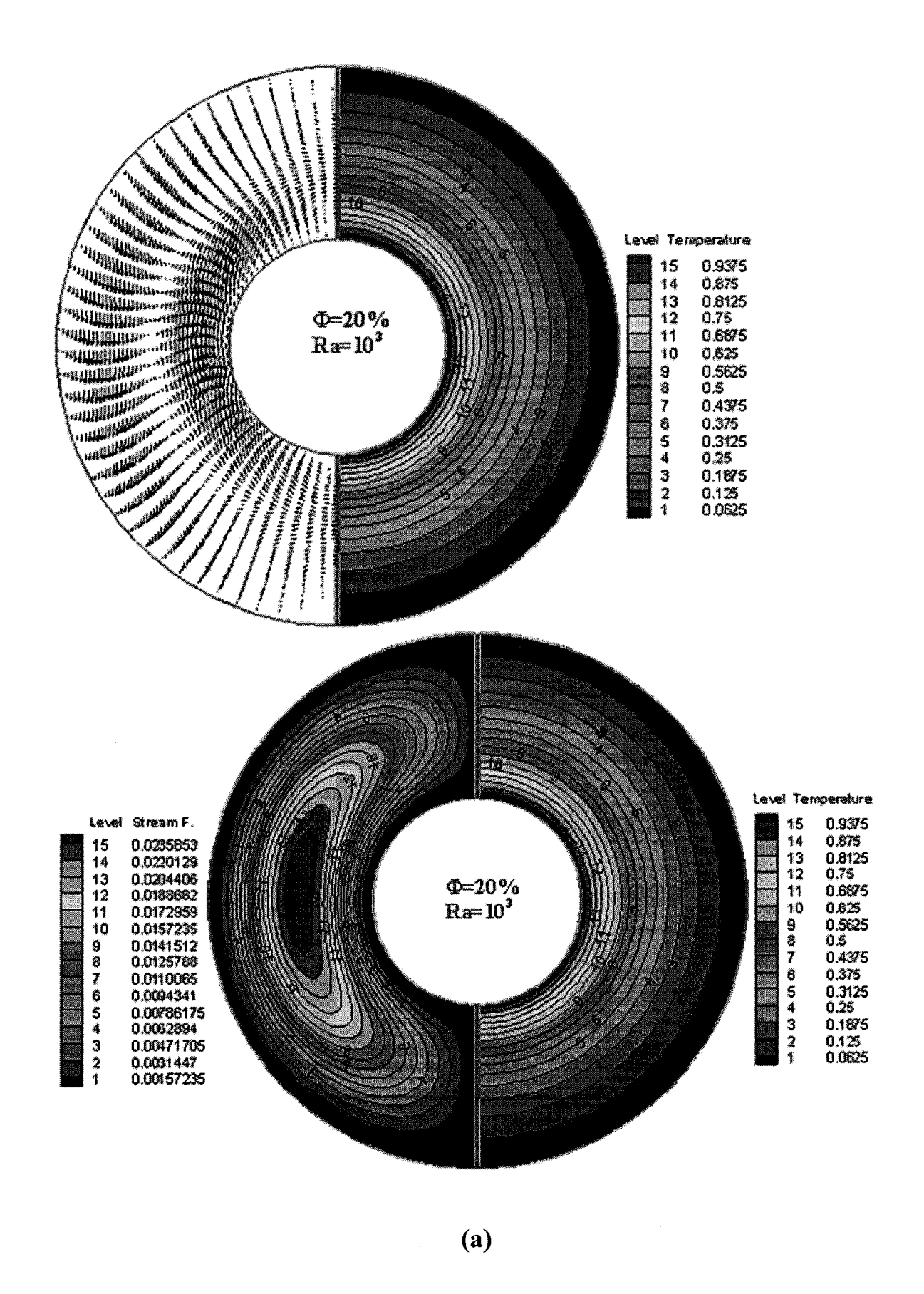
In Figs.10-11, a comparison of the local Nusselt number between nanofluids at  $\Phi$ =0.05, and 0.2 and the conventional fluid is conducted for various Rayleigh numbers. The figures clearly show the impact of the presence of natural convective strength. For a clear fluid, the local Nusselt number for Ra>10<sup>3</sup> is always higher than in nanofluids. It is expected that the local heat transfer coefficient will be increased with the increase of Ra, the predicted results have shown this trend in Figs.10-11. But for Ra=10<sup>3</sup>, the local heat transfer coefficients of nanofluids is slightly above the pure water results.

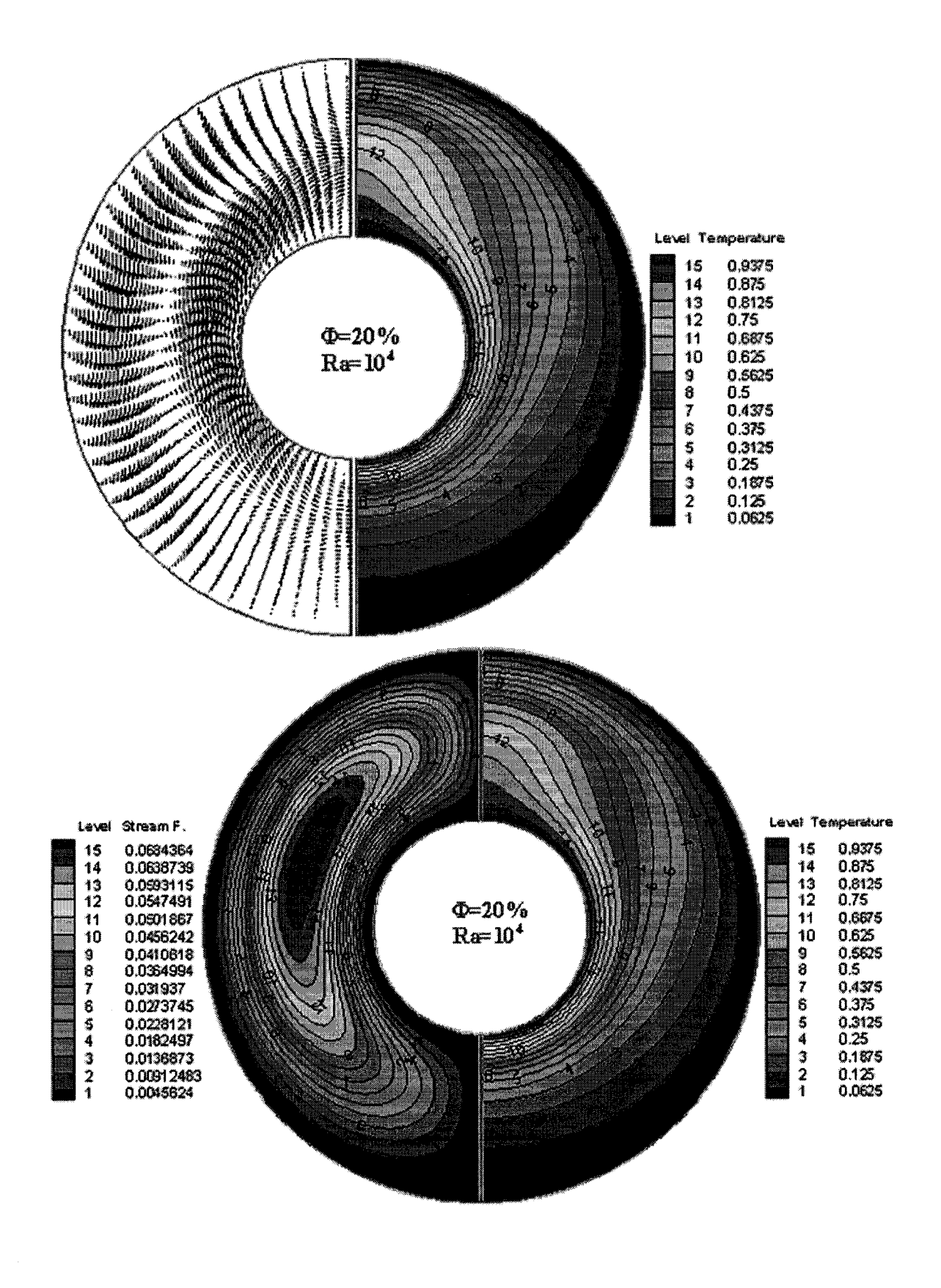
The average Nusselt number versus solid volume fractions for the inner and outer cylinders are shown in Figs. 4-5. As solid volume fraction increases, the average Nusselt number has decreased in both inner and outer cylinder walls for all Ra values except for Ra= $10^3$ . The variations in the average Nusselt number are nonlinear with solid volume fraction ( $\Phi$ ). For Ra= $10^6$ , there is a substantial decrease in the average Nusselt number on the inner cylinder as solid volume fraction is increased above 5%. When  $\Phi$  is 0.05, the decrease is approximately 6%. But when  $\Phi$  is 0.10, 0.15, or 0.20, the decrease is approximately 13%, 21%, and 26%, respectively compared to the base fluid. It is found that in the natural convection regime for  $\Phi$ =20% and Ra= $10^3$ , the heat transfer rate increases on the inner cylinder by about 3% and for all other cases heat transfer reduces considerably compared to the base fluid. The reductions are 35%, 24%, and 26% compared to the pure fluid for Ra= $10^4$ , Ra= $10^5$ , and Ra= $10^6$ , respectively.

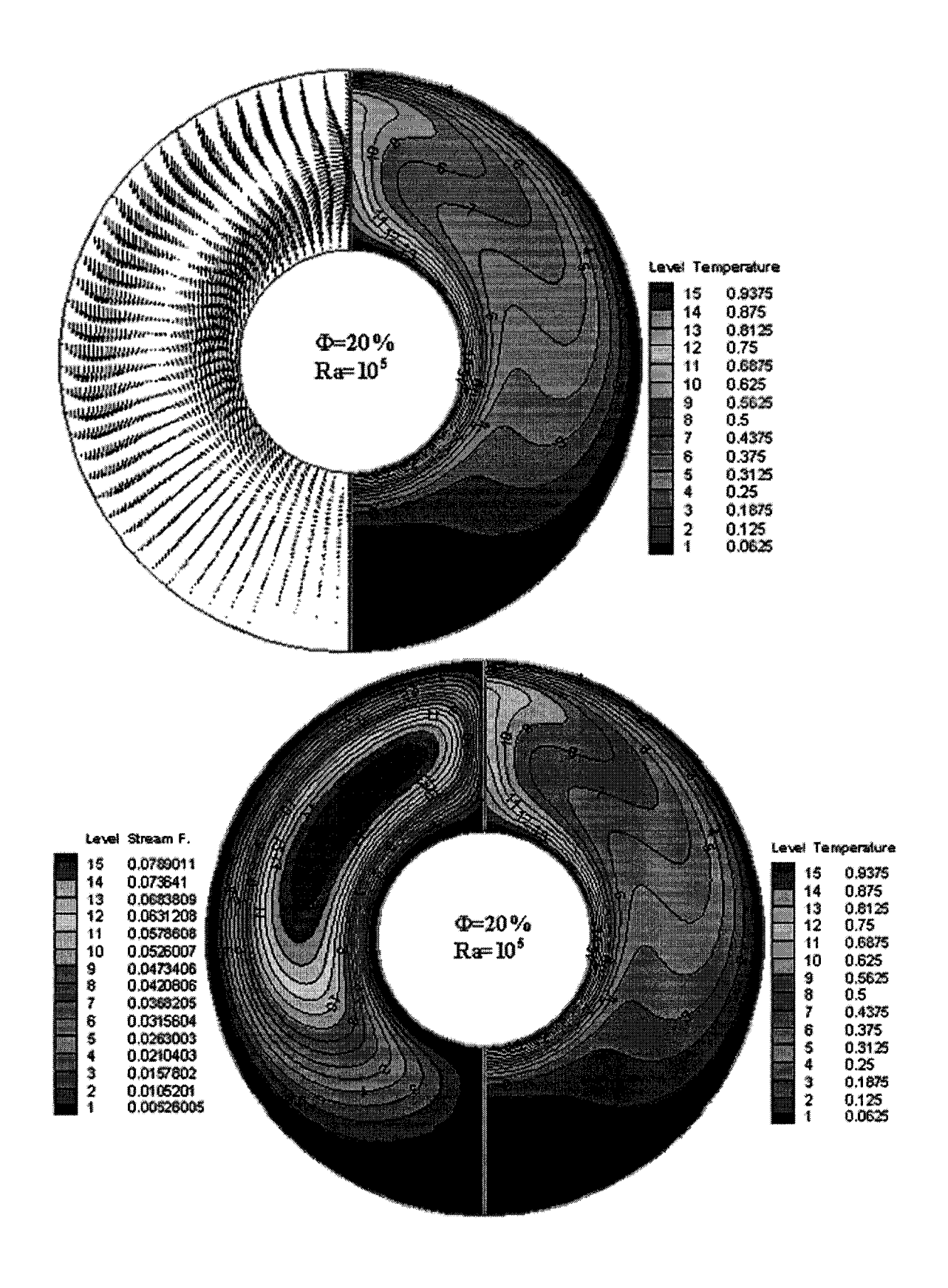
The average Nusselt numbers along the inner cylinder surface are correlated in terms of the Rayleigh number and the particles volume fraction. Using the results from the present simulations for Cu-nanofluids with 10 nm diameter nanoparticles, the following correlation is obtained using the multi-linear least-squares regression analysis:

$$\overline{Nu}_{inner} = 0.1743 (0.4436 + \Phi^{1.0809})^{-0.75} (Ra)^{0.2119} - (15)$$

The above correlation is valid for,  $10^3 \le \text{Ra} \le 10^6$ ;  $0 \le \Phi \le 20\%$  and  $r_o/r_i = 2.6$ . where the confidence coefficient of the above correlation is determined as  $R^2 = 99.07\%$ . This correlation of average Nusselt number for Cu nanoparticles in pure water can be considered for designing the tubular heat exchangers.







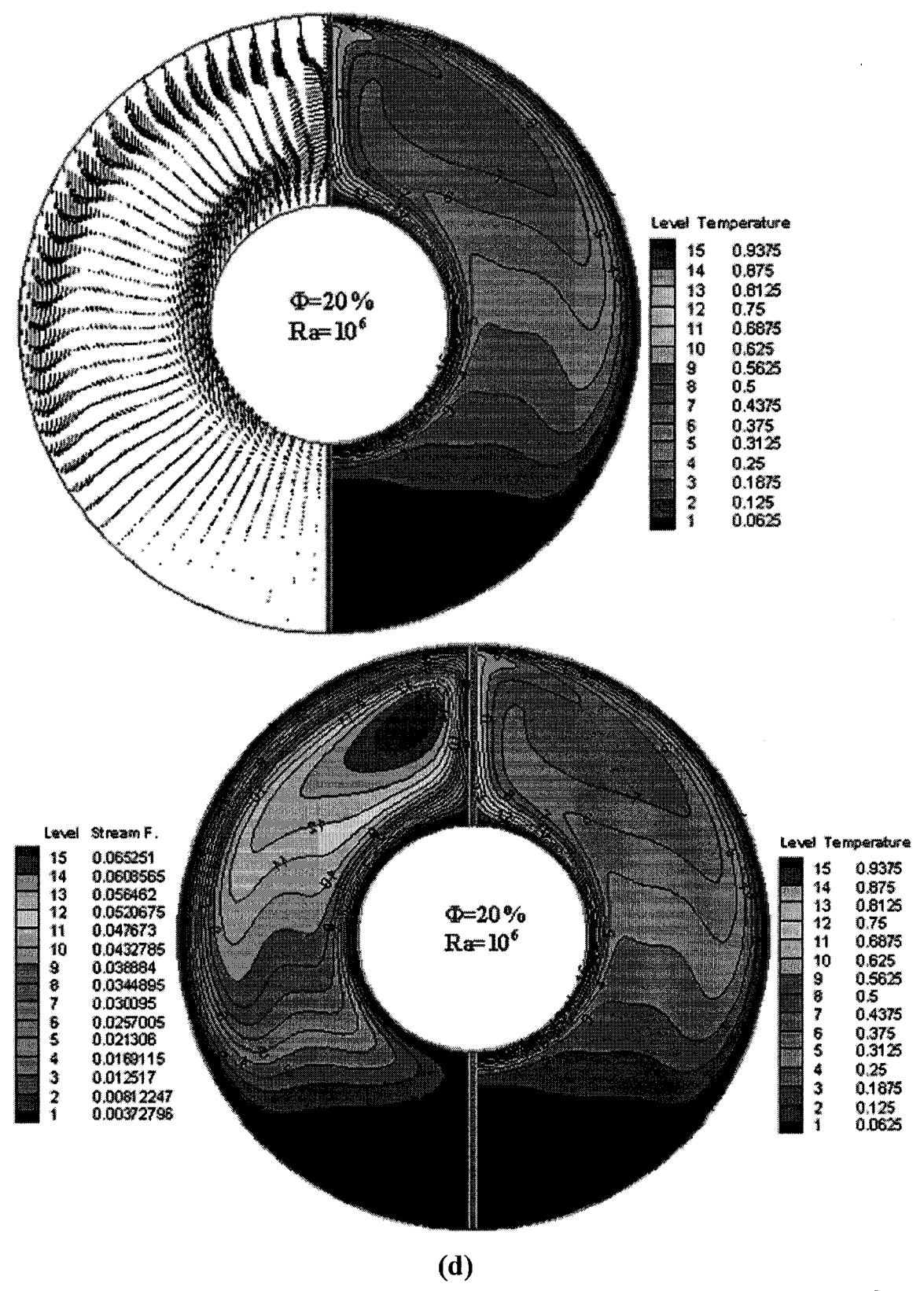
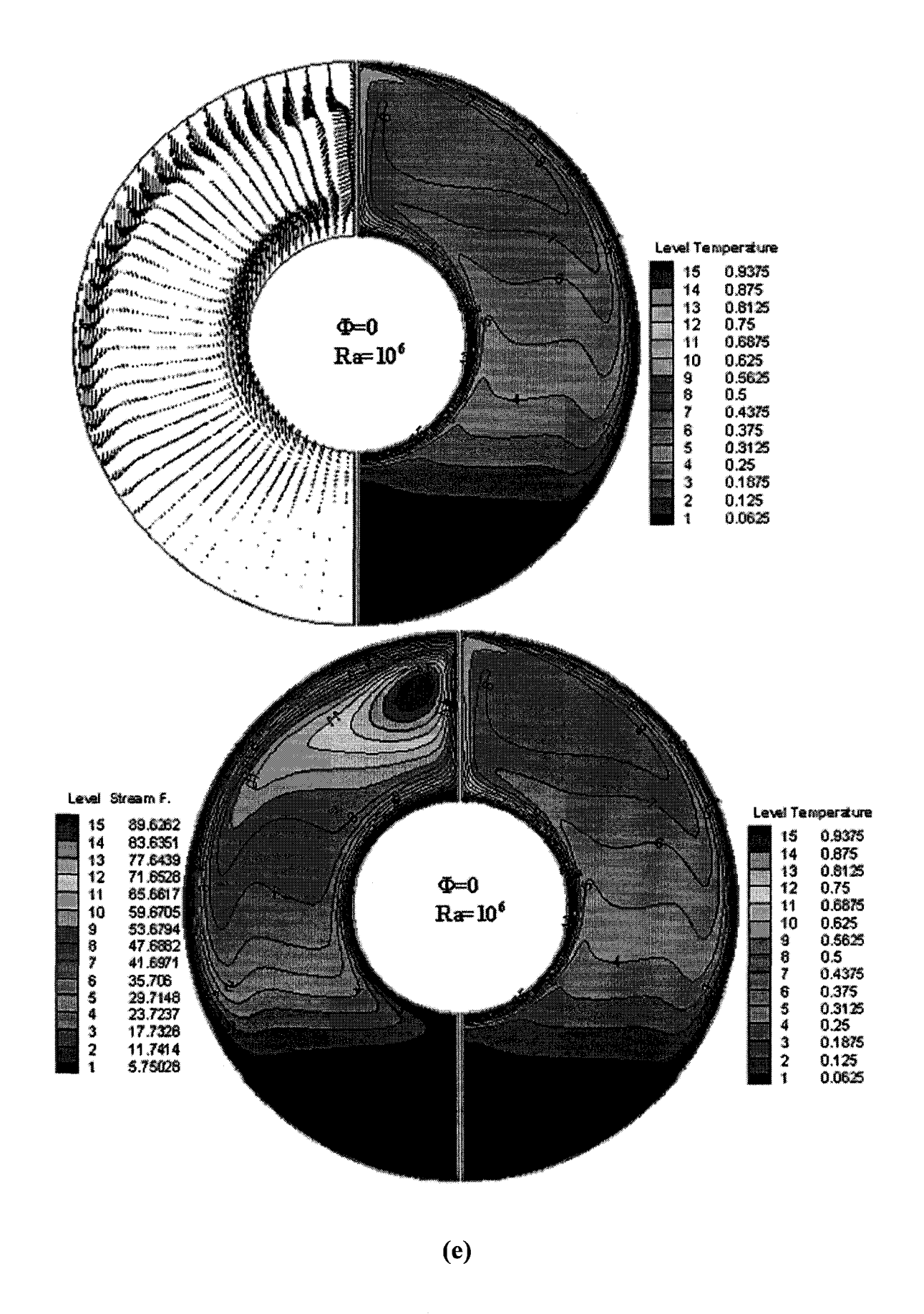
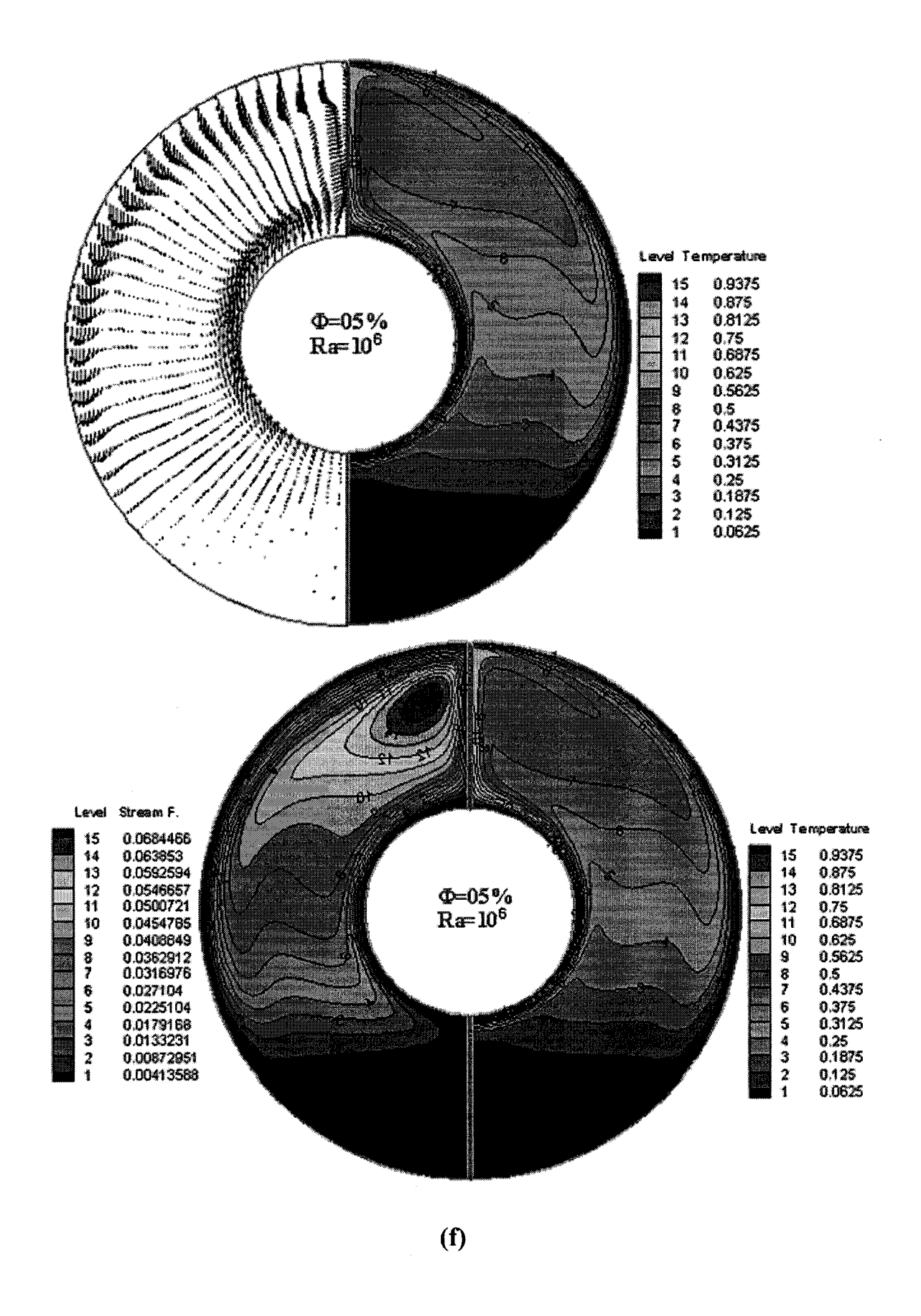
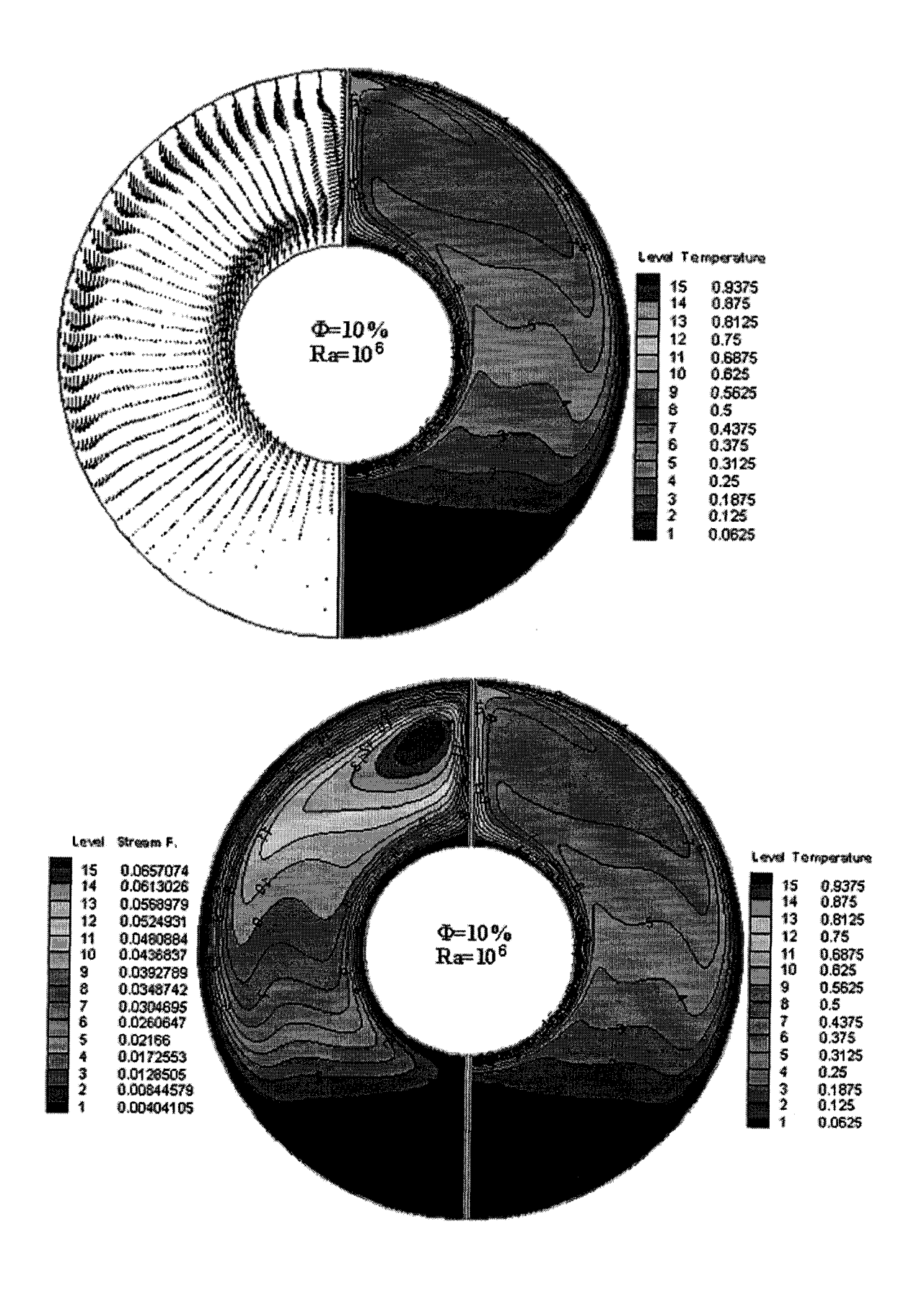


Figure 2: Velocities and isotherms, Streamlines and isotherms for  $\Phi$ =0.2: (a) Ra=10<sup>3</sup>, (b) Ra=10<sup>4</sup>, (c) Ra=10<sup>5</sup>, (d) Ra=10<sup>6</sup>







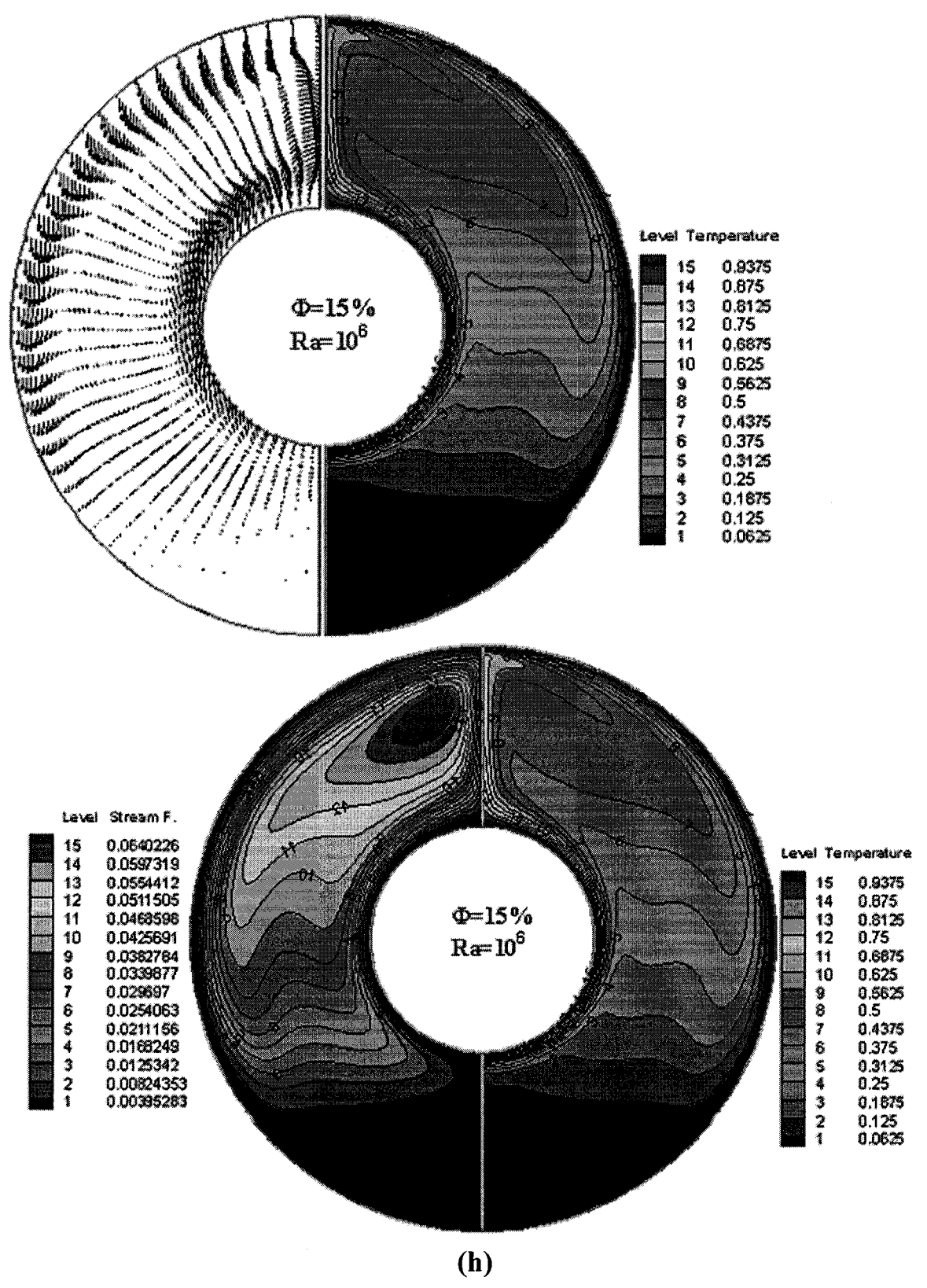


Figure 3: Velocities and isotherms, Streamlines and isotherms for Ra= $10^6$ : a)  $\Phi$ =0.0, (b)  $\Phi$ =5%, (c)  $\Phi$ =10%, (d)  $\Phi$ =15%

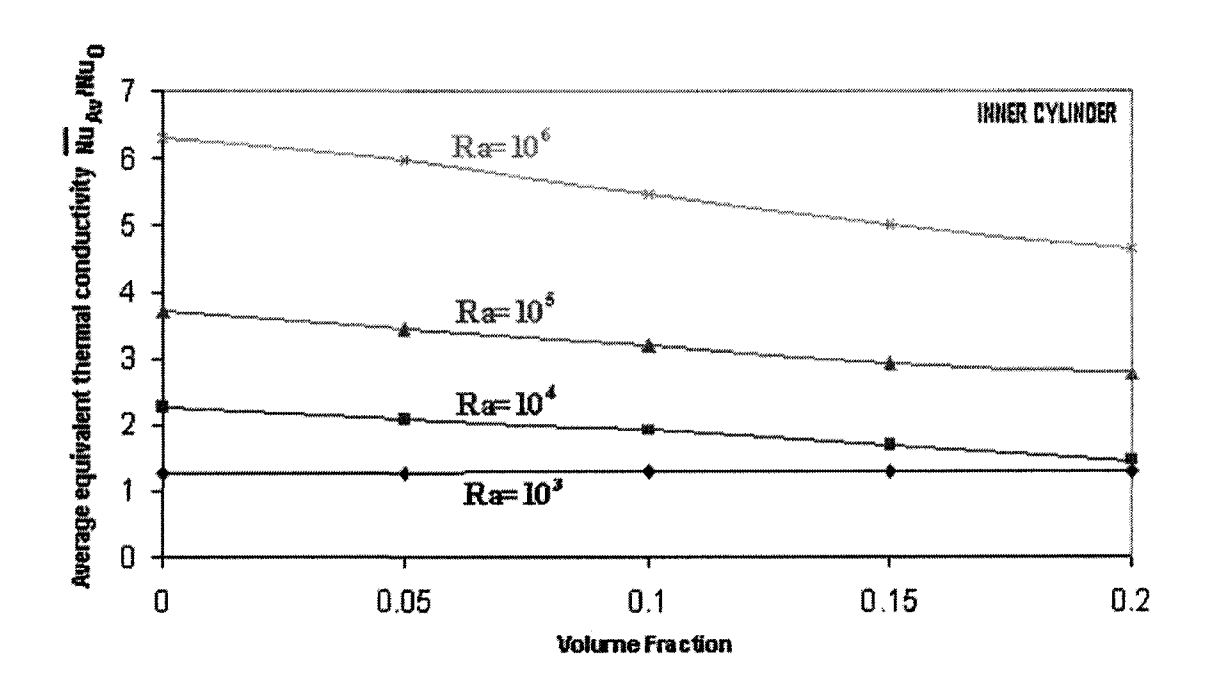


Figure 4: Comparison of the average Nusselt number at different volume fraction on the inner cylinder for various Rayleigh number

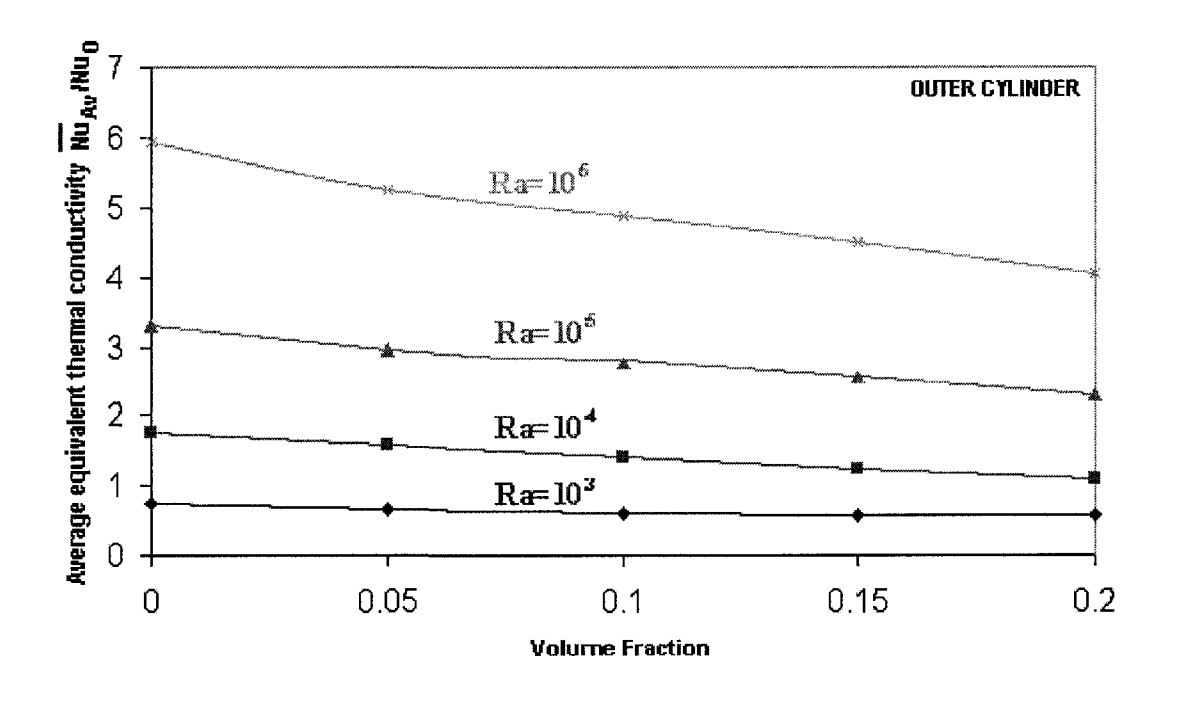


Figure 5: Comparison of the average Nusselt number at different volume fraction on the outer cylinder for various Rayleigh number

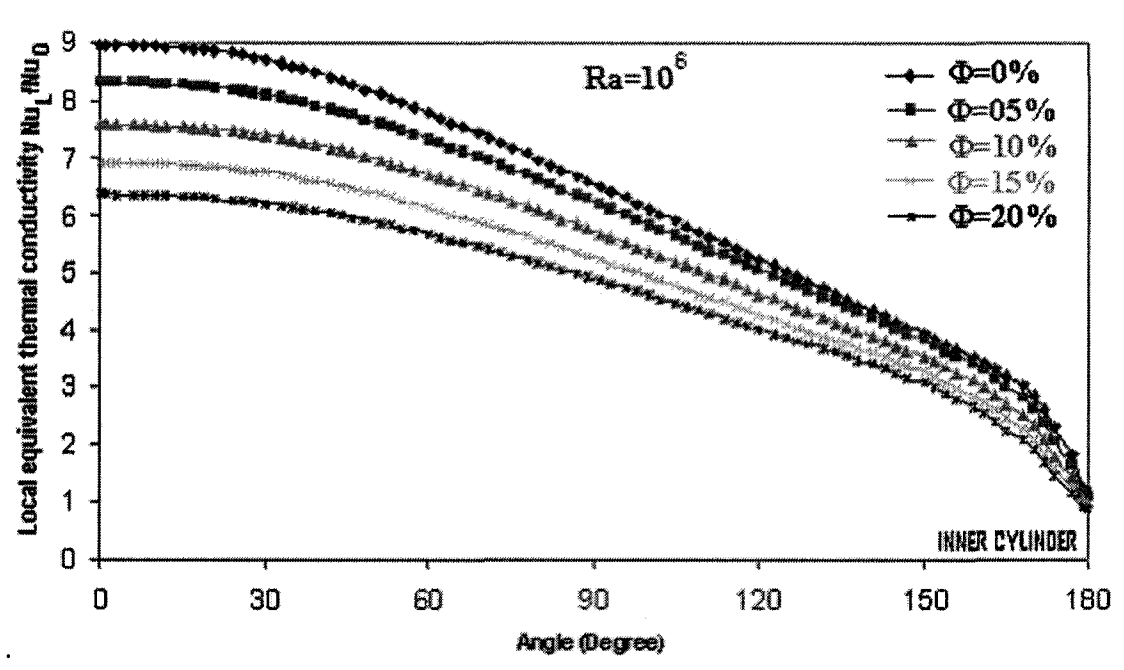


Figure 6: Comparison of the local Nusselt number along the inner cylinder between different volume fractions at Rayleigh number 10<sup>6</sup>

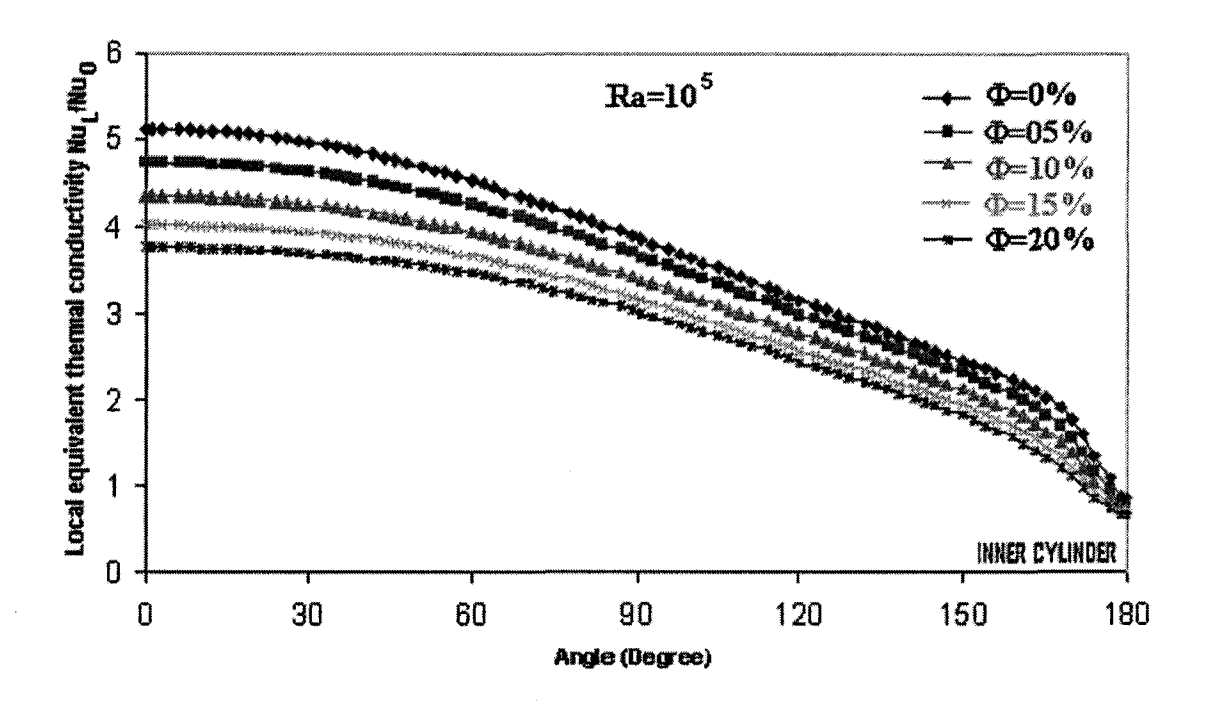


Figure 7: Comparison of the local Nusselt number along the inner cylinder between different volume fractions at Rayleigh number 10<sup>5</sup>

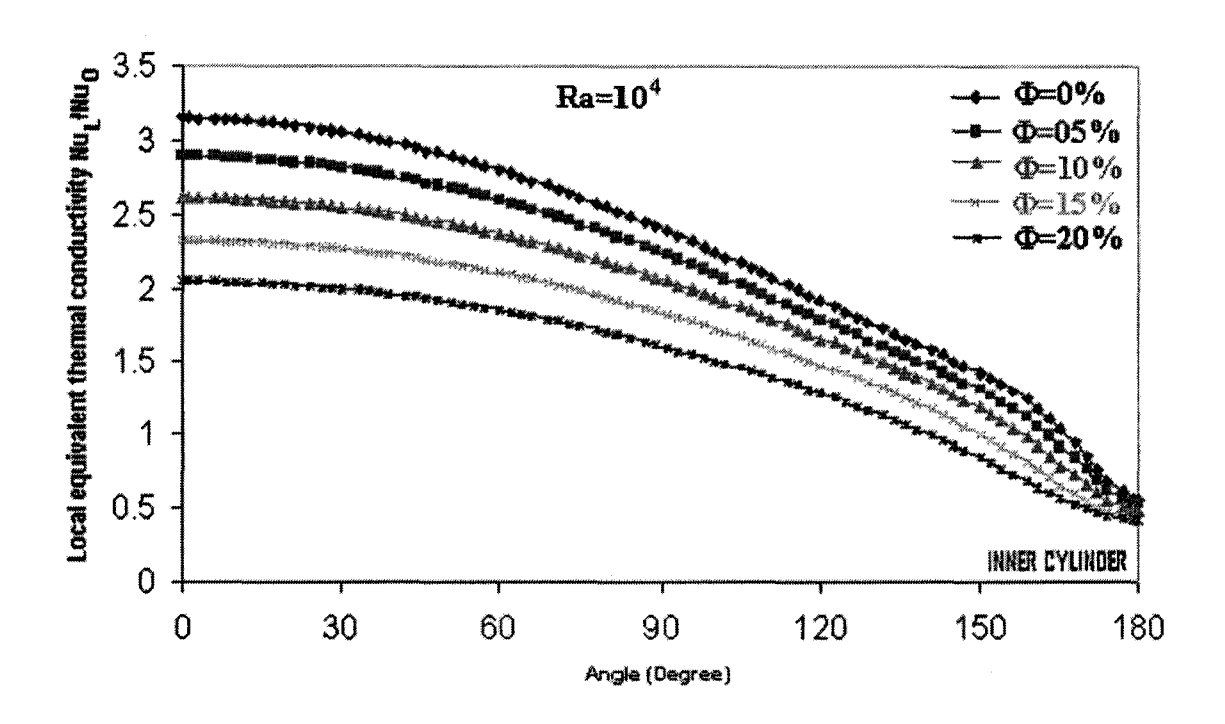


Figure 8: Comparison of the local Nusselt number along the inner cylinder between different volume fractions at Rayleigh number 10<sup>4</sup>

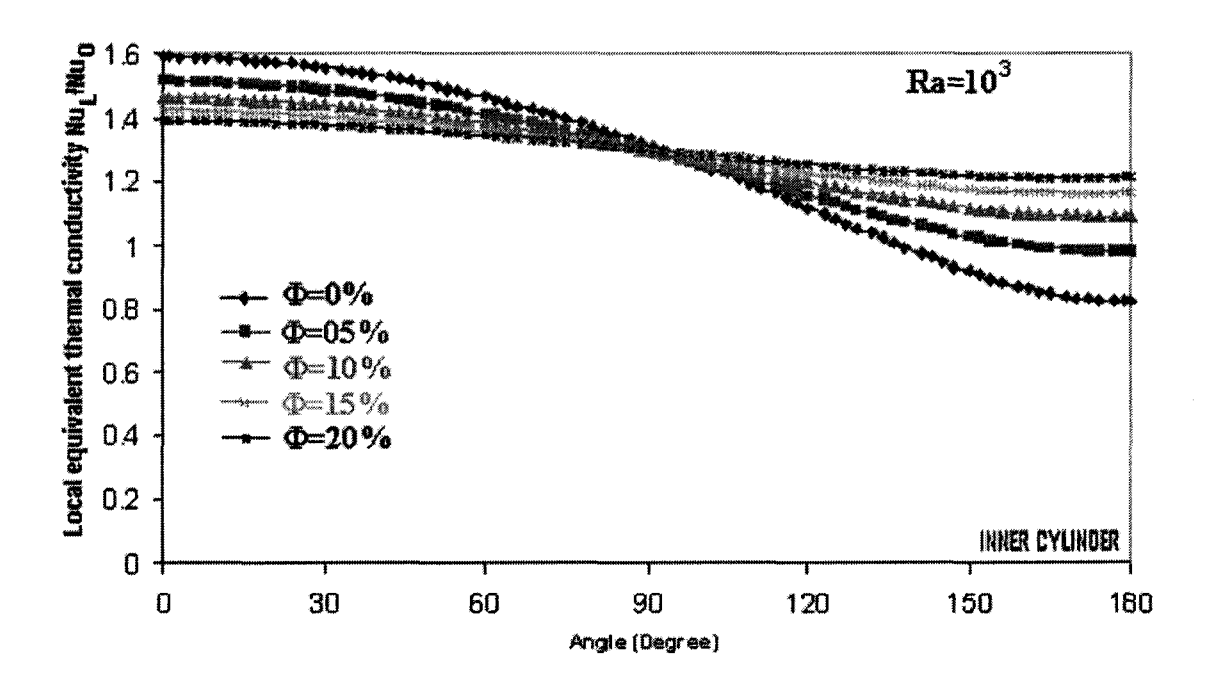


Figure 9: Comparison of the local Nusselt number along the inner cylinder between different volume fractions at Rayleigh number 10<sup>3</sup>

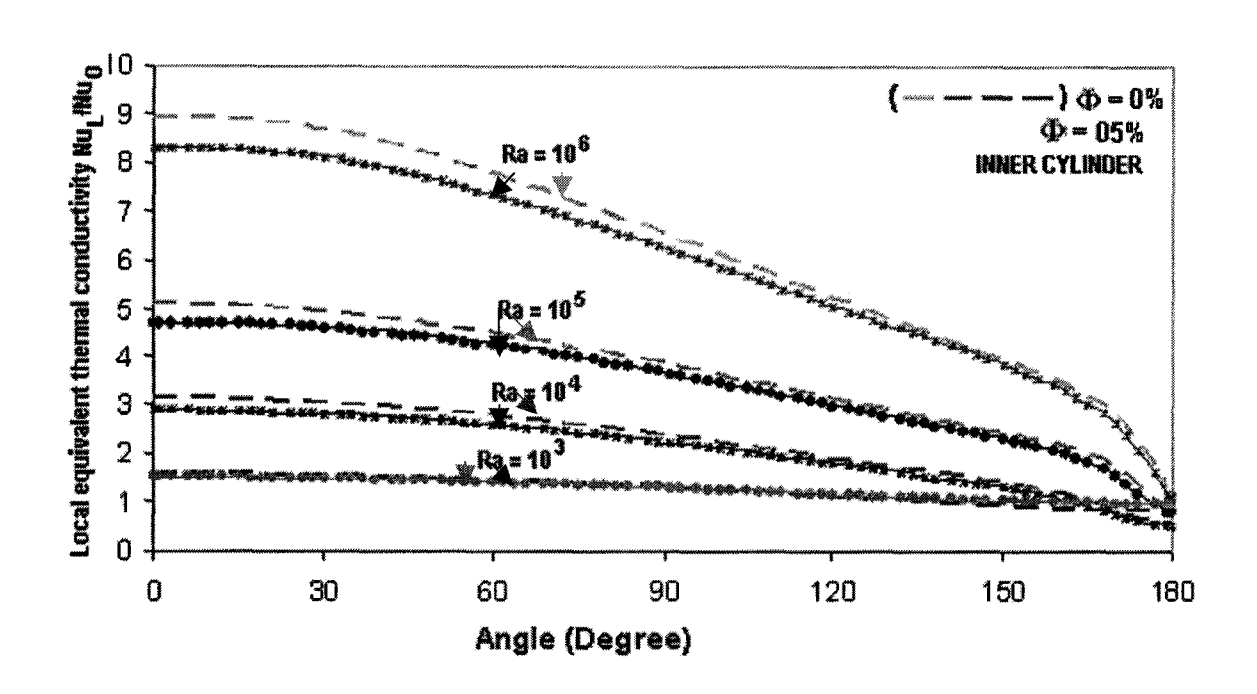


Figure 10: Local Nusselt number on the inner cylinder at different Rayleigh number for pure fluid ( $\Phi$ =0) and nanofluid at  $\Phi$ =0.05

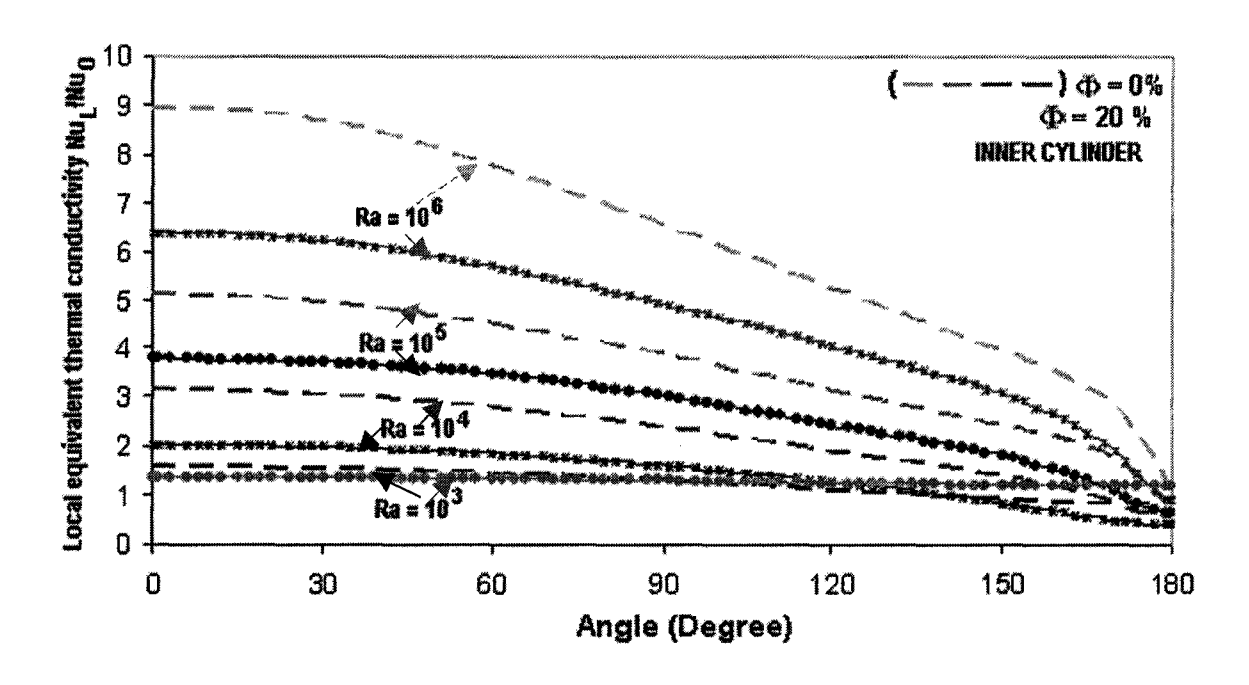


Figure 11: Local Nusselt number on the inner cylinder at different Rayleigh number for pure fluid ( $\Phi$ =0) and nanofluid at  $\Phi$ =0.2

## **Conclusions**

This present study brings about the heat transfer characteristics of water-Cu nanofluids under natural convection inside a horizontal cylindrical annulus wherein the inner cylinder is isothermally heated and the outer cylinder is kept at a lower but constant temperature. Unlike conduction or forced convection, a systematic and definite deterioration in natural convective heat transfer coefficient has been found to occur with the increase of solid volume fraction of nanoparticles  $\Phi$ , which is consistent with the recent experimental findings on natural convection by Wen and Ding [2006]. But this observation contrasts with previous expectations. The deterioration in heat transfer rate seems to be dependent in a complex manner on the thermal conductivity and viscosity of the nanofluids. However, the role of the particle-fluid slip and sedimentation may be important which will require more closer investigations in the future. The present theoretical findings are important due to the fact that the nanofluids are being considered as alternative heat transfer fluids. As stated earlier, very little work exists in the literature concerning natural convection in nanofluids in cavities other than rectangular enclosures. In this regard, the present study offers a useful contribution to the field. This study also indicates that a much needed detailed investigation is required for understanding the physical phenomenon completely before using these fluids in practical cooling applications.

### **References:**

- [1] S.U.S. Choi, "Enhancement thermal conductivity of fluids with nanoparticles in: D.A. Siginer, H.P. Wang(Eds.), Developments and Applications of Non-Newtonian flows", ASME, New York, Vol.FED-231/MD-66, pp.99-105, 1995.
- [2] S.U.S. Choi, et. al. "Mechanisms of heat flow in suspensions of nano-sized particles (nanofluids)", Int. Heat Mass Transfer, Vol.45, pp.855-863, 2002.
- [3] K. Khanafer et. al. "Buoyancy-driven heat transfer enhancement in a two-dimensional enclosure utilizing nanofluids", International Journal of Heat and Mass Transfer, Vol.46, pp.3639-3653, 2003.
- [4] N. Putra, et. al. "Natural convection of nano-fluids", Heat and Mass Transfer, Vol.39 (8-9), pp.775-784, 2003.
- [5] D.Wen, Y. Ding, "Formulation of nanofluids for natural convective heat transfer applications", International Journal of Heat and Fluid Flow, Vol.26(6), pp. 855-864, 2005.
- [6] D.Wen, Y. Ding, "Formulation of nanofluids and its application in natural convective heat transfer conditions", in proc. 6<sup>th</sup> World Conf. Experiments. Heat Transfer, Fluid Mech, Thermodynam, Matsushima, Japan, 2005.
- [7] D.Wen, Y. Ding, "Natural convective heat transfer of suspensions of Titanium Dioxide Nanoparticles (Nanofluids)", IEEE Transactions of Nanotechnology, Vol.5, No.3, pp. 220-227, 2006.
- [8] Y. Xuan and Q. Li, "Investigation on convective heat transfer and flow features of nanofluids", J. Heat Transfer (Trans. ASME), Vol.125, pp.151-155, 2003.
- [9] Rong-Yuan Jou, et. al., "Numerical research of nature convective heat transfer enhancement filled with nanofluids in rectangular enclosures", International Communications in Heat and Mass Transfer, Vol.33, pp.727-736, 2006.
- [10] A. G. A. Nnanna, et. al., "Thermal transport phenomena in buoyancy-driven nanofluids", in proc. ASME Int. Mech. Eng. Congress RD&D Expo., IMECE2004-62059, Anaheim, CA, pp.1-8, Nov.2004.